



**INSTITUTO POTOSINO DE INVESTIGACIÓN
CIENTÍFICA Y TECNOLÓGICA, A.C.**

POSGRADO EN CIENCIAS APLICADAS

**Estudios Estructurales de C60 Polimerizado
Usando Dinámica Molecular Clásica**

Tesis que presenta

Jaime Enrique Pérez Terrazas

Para obtener el grado de

Maestro en Ciencias Aplicadas

En la opción de

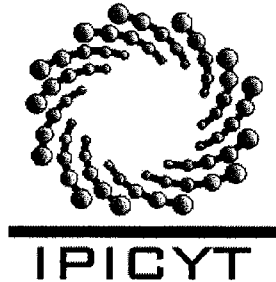
Nanociencias y Nanotecnología

Codirectores de la Tesis:

Dr. Mauricio Terrones Maldonado

Dr. Aldo Humberto Romero Castro (CINVESTAV)

San Luis Potosí, S.L.P., Septiembre de 2005.



Instituto Potosino de Investigación Científica y Tecnológica, A.C.

Acta de Examen de Grado

COPIA CERTIFICADA

El Secretario Académico del Instituto Potosino de Investigación Científica y Tecnológica, A.C., certifica que en el Acta 012 del Libro Primero de Actas de Exámenes de Grado del Programa de Maestría en Ciencias Aplicadas en la opción de Nanociencias y Nanotecnología está asentado lo siguiente:

En la ciudad de San Luis Potosí a los 5 días del mes de septiembre del año 2005, se reunió a las 11:00 horas en las instalaciones del Instituto Potosino de Investigación Científica y Tecnológica, A.C., el Jurado integrado por:

Dr. Mauricio Terrones Maldonado	Presidente	IPICYT
Dr. José Luis Rodríguez López	Secretario	IPICYT
Dr. Aldo Romero Castro	Sinodal externo	CINVESTAV
Dr. Florentino López Urías	Sinodal	IPICYT
Dr. Ricardo Guirado López	Sinodal externo	UASLP

a fin de efectuar el examen, que para obtener el Grado de:

**MAESTRO EN CIENCIAS APLICADAS
EN LA OPCIÓN DE NANOCIENCIAS Y NANOTECNOLOGÍA**

sustentó el C.

Jaime Enrique Pérez Terrazas

sobre la Tesis intitulada:

Estudios Estructurales de C60 Polimerizado Usando Dinámica Molecular Clásica

que se desarrolló bajo la dirección de

Dr. Mauricio Terrones Maldonado
Dr. Aldo Humberto Romero Castro (CINVESTAV)

El Jurado, después de deliberar, determinó

APROBARLO

Dándose por terminado el acto a las 13:15 horas, procediendo a la firma del Acta los integrantes del Jurado. Dando fé el Secretario Académico del Instituto.

A petición del interesado y para los fines que al mismo convengan, se extiende el presente documento en la ciudad de San Luis Potosí, S.L.P., México, a los 5 días del mes septiembre de 2005.




Mtra. Ma. Elisa Lucio Aguilar
Jefa del Departamento de Asuntos Escolares

San Luis Potosí, S.L.P. a 17 de Agosto del 2005

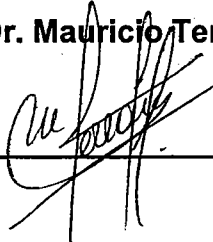
Dr. Emilio Muñoz
Coordinador de la opción de
Nanociencias y Nanotecnología del
Posgrado en Ciencias Aplicadas
IPICyT
PRESENTE.

Por medio de la presente le informamos que, después de haber revisado el trabajo de Tesis de Maestría del estudiante Jaime Enrique Pérez Terrazas, no encontramos inconveniente alguno para que pueda llevarse a cabo el Examen de Grado ante un jurado.

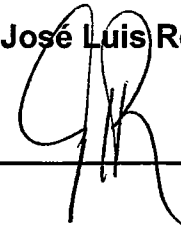
Atentamente,

Comité Tutorial

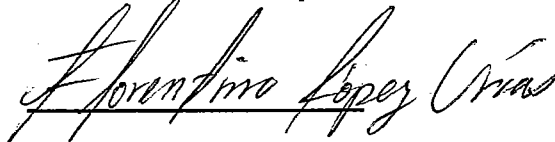
Dr. Mauricio Terrones



Dr. José Luis Rodríguez

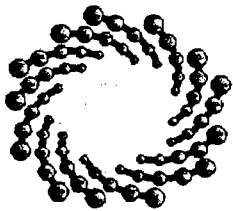


Dr. Florentino López



Recibido 18/08/05
[Handwritten signature]

ccp Mba. Elisa Lucio



IPICYT



DEPARTAMENTO DE
ASUNTOS ESCOLARES

IPICYT

Instituto Potosino de Investigación Científica y Tecnológica, A.C.

Acta de Examen de Grado

COPIA CERTIFICADA

El Secretario Académico del Instituto Potosino de Investigación Científica y Tecnológica, A.C., certifica que en el Acta 012 del Libro Primero de Actas de Exámenes de Grado del Programa de Maestría en Ciencias Aplicadas en la opción de Nanociencias y Nanotecnología está asentado lo siguiente:

En la ciudad de San Luis Potosí a los 5 días del mes de septiembre del año 2005, se reunió a las 11:00 horas en las instalaciones del Instituto Potosino de Investigación Científica y Tecnológica, A.C., el Jurado integrado por:

Dr. Mauricio Terrones Maldonado	Presidente	IPICYT
Dr. José Luis Rodríguez López	Secretario	IPICYT
Dr. Aldo Romero Castro	Sinodal externo	CINVESTAV
Dr. Florentino López Urías	Sinodal	IPICYT
Dr. Ricardo Guirado López	Sinodal externo	UASLP

a fin de efectuar el examen, que para obtener el Grado de:

**MAESTRO EN CIENCIAS APLICADAS
EN LA OPCIÓN DE NANOCIENCIAS Y NANOTECNOLOGÍA**

sustentó el C

Jaime Enrique Pérez Terrazas

sobre la Tesis intitulada

Estudios Estructurales de C60 Polimerizado Usando Dinámica Molecular Clásica

que se desarrolló bajo la dirección de

Dr. Mauricio Terrones Maldonado
Dr. Aldo Humberto Romero Castro (CINVESTAV)

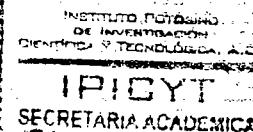
El Jurado, después de deliberar, determinó

APROBARLO

Dándose por terminado el acto a las 13:15 horas, procediendo a la firma del Acta los integrantes del Jurado. Dando fé el Secretario Académico del Instituto.

A petición del interesado y para los fines que al mismo convengan, se extiende el presente documento en la ciudad de San Luis Potosí, S.L.P., México, a los 5 días del mes septiembre de 2005.

Marcial Bonilla
Dr. Marcial Bonilla Marín
Secretario Académico



Elisa Lucio Aguilar
Mtra. Ma. Elisa Lucio Aguilar
Jefa del Departamento de Asuntos Escolares

Acknowledgments

Many people contributed to this work, most of them from the Advanced Materials Department. In particular, I am grateful to my advisors; Aldo Romero and Mauricio Terrones. They guided me through this project, in such a fantastic way that every single advice made notably better each piece of work. Besides, they were also concerned about the person, not only about the student. I am especially grateful by that.

I want to thank to: José Luis Rodríguez and Humberto Terrones by their advices, attention and fruitful discussions; Samuel Baltazar and Felipe Valencia, by their constant and precise technical support (Linux, Trocadero, Xmgrace, etc.); and Eduardo Hernández that gave me permission to use the main tool for this work: the Molecular Dynamics code “Trocadero”.

I am grateful to my parents, for their love and infinite confidence in me ; to my brother, Efrén, by walking with me on the scientific road; to my son, Rafael, by sharing with me his beautiful smile and his happiness. However, there is only one person on whom completion of this project totally depended – my wife. We shared many hours of loneliness to make this a reality. Lovely, thank you.

*To my wife, Dulce,
and my son, Rafael.*

Contents

1	Introduction	1
1.1	Background	1
1.1.1	The beginning: Fullerene Discovery, Crystal Structure and Properties	1
1.1.2	Crystalline Polymerized Fullerite Phases	4
1.1.3	Superhard Phases of Polymerized C_{60} Molecules	8
1.1.4	Intermolecular Bonding Schemes Between C_{60} Molecules	11
1.2	Motivation	12
1.3	Aims of this work	14
2	Theoretical Background	19
2.1	Molecular Dynamics Simulations	19
2.1.1	Why Molecular Dynamics Simulations?	19
2.1.2	Classical Molecular Dynamics Simulations: Fundamentals	21
2.1.3	Simulating non-microcanonical ensembles	29
2.2	Atomic interaction schemes	35
2.2.1	Tersoff Classical Potential	37
2.2.2	Tight-Binding scheme	38
2.2.3	Non-orthogonal tight-binding	42
2.3	The TROCADERO code	44
2.3.1	Code Structure	44
2.3.2	Capabilities of TROCADERO	47
3	Molecular Dynamics Studies of C_{60} Under Pressure	51

3.1	Different crystalline arrangements	51
3.1.1	Face Centered Cubic Structure	52
3.1.2	Rhombohedral Structure	56
3.1.3	Tetragonal Structure	58
3.1.4	Orthorhombic Structure	59
3.1.5	Brief discussion	62
3.2	Temperature and pressure Effects	62
3.2.1	Intermolecular connections between C_{60} molecules	63
3.2.2	Dynamical characterization	66
3.3	Additional Simulations	70
4	Statical studies	74
4.1	C_{60} Dimers	74
4.2	A formation mechanism for the rhombohedral, tetragonal and orthorhombic C_{60} polymerized phases	80
4.3	1-D Polymerized Structures	88
4.4	2-D Polymerized Structures	93
4.4.1	Tetragonal Structures	93
4.4.2	Rhombohedral Structures	95
4.5	3-D Polymerized Structures	97
4.5.1	Simple Cubic Structures	98
4.5.2	BCO Structures	99
5	Concluding Remarks and future work	110
5.1	Conclusions and Contributions	110
5.2	Summary of contributions	111
5.3	Future research	112
A	Intermolecular C_{60} links	114
B	Tables of intermolecular connections appeared in our simulations for systems at high pressure and temperature	122

List of Tables

3.1	Number of intermolecular links formed	65
4.1	Total energies for relaxed dimers	80
4.2	Properties of the structures studied	107
B.1	Intermolecular connections for the simulations performed under 2 GPa	123
B.2	Intermolecular connections for the simulations performed under 4 GPa	124
B.3	Intermolecular connections for the simulations performed under 6 GPa	125
B.4	Intermolecular connections for the simulations performed under 8 GPa	126
B.5	Intermolecular connections for the simulations performed under 10 GPa	127
B.6	Intermolecular connections for the simulations performed under 12 GPa	128
B.7	Intermolecular connections for the simulations performed under 14 GPa	129
B.8	Intermolecular connections for the simulations performed under 16 GPa	130

List of Figures

1.1	Fullerite crystal	2
1.2	Cycloaddition 2+2 between double bonds	5
1.3	Polymerized C_{60} phases	6
1.4	Sketches of the formation of Polymerized C_{60} phases	7
1.5	Paths for obtaining polymeric C_{60} phases	9
1.6	Intermolecular link: the 2+2 cycloaddition between single bonds . . .	12
1.7	Intermolecular link: 6+6 cycloaddition	13
1.8	Intermolecular link: 4+4 cycloaddition	13
2.1	Periodic conditions scheme.	24
3.1	Initial orientations for room temperature studies	53
3.2	Preferential orientations for the fcc phase	54
3.3	Typical thermal stability found in our simulations as a function of time for the fcc arrangement	54
3.4	Ordered C_{60} crystal obtained after applying pressure	55
3.5	Phase ordered proposed by Guo <i>et. al.</i>	56
3.6	Unitary cell and conventional cell for the rhombohedral lattice	57
3.7	First new cycloaddition found in this work	57
3.8	Typical temperature stability for C_{60} cages in a rhombohedral ar- rangement	58
3.9	Typical temperature behavior for the tetragonal arrangement used (5 GPa)	60
3.10	Phase transition observed from the tetragonal configuration to a closer packing	60

3.11	Typical temperature behavior experienced by the orthorhombic arrangement	61
3.12	Temperature stability for a C_{60} crystal under 16 GPa and 1300 K . .	67
3.13	Average volume <i>vs</i> average pressure behavior observed for C_{60} phases under high temperature and high pressure	68
3.14	Average distance between centers of neighboring C_{60} molecules, calculated at 16 GPa and 1300 K	69
3.15	Average C_{60} molecule radius at at 16 GPa and 1300 K	70
4.1	The most common interconnections found in HPHT simulations . . .	76
4.2	Dimer using a 3-bonds intermolecular connection	77
4.3	Dimer connected by the 14h14h link	78
4.4	Dimer linked by the 4link(sd) connection	79
4.5	Metastable dimers found	81
4.6	Scheme of the proposed polymerization mechanism	83
4.7	Different paths for the synthesis of the tetragonal C_{60} polymerized phase	86
4.8	Simulated XRD pattern for 1-D polymerized structures using different intermolecular connections	91
4.9	Density of states for the C_{60} orthorhombic 1-D polymerized structures using different intermolecular connections	92
4.10	Simulated XRD patterns for 2-D polymerized structures using a tetragonal arrangement	95
4.11	Density of states for C_{60} tetragonal 2-D polymerized structures using different intermolecular connections	96
4.12	Simulated XRD patterns for rhombohedral 2-D polymerized structures using different intermolecular connections	97
4.13	Density of states for C_{60} rhombohedral 2-D polymerized structures using different intermolecular connections	98
4.14	Simulated XRD patterns for cubic 3-D polymerized structures using different intermolecular connections	100

4.15	Density of states for C_{60} simple cubic 3-D polymerized structures using different intermolecular connections	101
4.16	Orientation of the molecules in the 564bc structure	102
4.17	Detail of the 564bc structure	102
4.18	Detail of the bcca structure	103
4.19	Detail of the bccb structure	104
4.20	Detail of the bccm structure	105
4.21	Simulated XRD patterns for bco 3-D polymerized structures using different intermolecular connections	106
4.22	Density of states for C_{60} bco 3-D polymerized structures using differ- ent intermolecular connections	106
A.1	65 unit	115
A.2	66 unit	115
A.3	65r unit	116
A.4	66r unit	116
A.5	13h unit	117
A.6	13p unit	117
A.7	14h unit	118
A.8	3link unit	120
A.9	3link extra unit	120
A.10	4link unit	121

Chapter 1

Introduction

1.1 Background

1.1.1 The beginning: Fullerene Discovery, Crystal Structure and Properties

Since the discovery and identification of the C_{60} molecule by Kroto and coworkers¹, numerous groups have carried out fullerene research, looking for applications in a variety of fields such as energy storage, catalysis, medicine and advanced materials. The structural properties of C_{60} are fascinating. The molecule exhibits a high symmetry, possessing sixty equivalent carbon atoms with a point group I_h (truncated icosahedron), and it can be easily identified because of its similarity to a soccer ball. C_{60} was also named buckminsterfullerene, in honor of Richard Buckminster Fuller, a famous architect that used hexagonal and pentagonal shapes to construct giant geodesic domes. It is noteworthy that C_{60} is a three dimensional carbon molecule without sp^3 hybridized bonds. This 60-atoms molecule also exhibits an outstanding theoretical bulk modulus (717 GPa)² caused by the presence of sp^2 hybridized bonds; which are stiffer than sp^3 hybridized bonds. Such a value is higher than that of diamond (443 GPa), and suggests new possible applications in material science. The hardness and symmetry of C_{60} will be of fundamental interest in the present study, because we will study the polymerization of C_{60} molecules using Classical Molecular Dynamics simulations.

A crucial event in fullerene science occurred when Kräestchmer and coworkers found in 1991 a way of producing macroscopic quantities of C_{60} ³. They successfully crystallized C_{60} molecules and found that the molecules follow a fcc structure at ambient conditions, with a lattice parameter of approximately 14.2 Å (see Figure 1.1). This crystal is called fullerite. This breakthrough allowed to fully characterize the new molecular material. Several researches confirmed the icosahedral symmetry of C_{60} molecules, and determined the crystal packing of these molecules using nuclear magnetic resonance (NMR) and X-ray powder diffraction studies respectively.

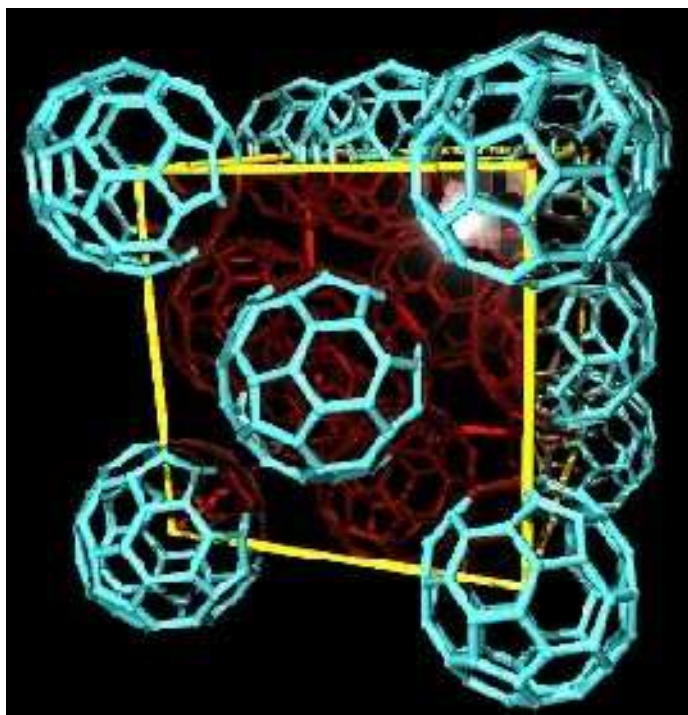


Figure 1.1: Molecular model of a conventional cell of Fullerite. C_{60} molecules are packed in a fcc structure. Image courtesy of Prof. Humberto Terrones

In 1991, Heiney *et. al.* found that below 249 K, C_{60} molecules suffer a "freezing" effect, which causes the molecules to stop rotations, observed under ambient conditions. This process involves a phase transition that results in a new ordered crystal⁴. The transition occurs in such a way that in the new phase, the C_{60} molecules arrange in a simple cubic crystal structure, containing a total of 240 carbon atoms

per unit cell. This orientational order was explained by a structure commensurate with the $\text{Pa}\bar{3}$ space group, in which electrostatic repulsions between C_{60} molecules are minimized⁵. In the same year, Ruoff and Ruoff suggested that compressed fullerite could show a bulk modulus greater than that of diamond^{6,7}. They calculated bulk modulus of C_{60} molecules using macroscopic and atomic elastic models; they predicted that the bulk modulus of a single C_{60} cage might be in the 800-970 GPa range. They proposed that by applying a high pressure treatment to fullerite, the bulk modulus of the crystal should approximate that of the individual cages. Thus opening the possibility of obtaining a material harder than diamond. They calculated the bulk modulus of the C_{60} crystal between 623 and 720 GPa, which is 200 GPa. larger than that of diamond. Subsequently, O'keeffe proposed a theoretical C_{60} crystalline structure formed by C_{60} cages in a bcc array, in such a way that all carbon atoms were fourfold-coordinated by covalent bonds⁸. Such structure was the first approach to 3D structures consisting of highly polymerized C_{60} molecules.

One of the first attempts to measure the bulk modulus of C_{60} was reported by Duclos and coworkers⁹. They carried out various experiments on fullerites at room temperature and pressures up to 20 GPa. In the regime where pressure could be regarded as hydrostatic, they found a smooth curve for the Equation of State, suggesting that cages were not broken during the process. However, they found a different behavior when the applied pressure was non-hydrostatic. In fact, a transition to another crystallographic structure of lower symmetry was observed. Duclos and coworkers also reported that such sample exhibit planes of diffraction parallel to the applied stress, suggesting that fullerite could support uniaxial stress. Subsequent studies reported that the behavior of fullerites under hydrostatic pressure is very different from that presented under non-hydrostatic conditions².

Moshary *et. al.*¹⁰ searched for a possible insulator-to-metallic transition for fullerite under pressure, and also for the extreme mechanical properties of fullerite that were suggested by Ruoff and Ruoff. Instead of such properties, the authors found an irreversible phase transition that lead to a transparent insulator phase

occurring between 17 and 25 GPa (non-hydrostatic pressure) at room temperature. Raman studies revealed that this phase was a new type of amorphous carbon. Later, Hodeau *et. al.*¹¹ reported that by treating C_{60} fullerene with 6-7 GPa (hydrostatic) and 1300 K, black and electrically conducting samples were obtained. Such samples were composed by a mixture of hexagonal AB graphite and rhombohedral ABC graphite. These authors also reported that between 15 and 25 GPa (non-hydrostatic pressure) and room temperature, the samples were transparent and insulators, and their best structural fit with XRD corresponded to polycrystalline mixture of fcc diamond and hexagonal diamond (strong sp^3 character). Samples in other studies presented combinations of different amorphous phases, and sometimes they seem to be almost featureless. In general, some trends were found, samples made under hydrostatic pressure were mainly black and amorphous with a strong sp^2 character; whereas samples obtained by non-hydrostatic pressures were mainly transparent, insulators and polycrystalline, exhibiting a sp^3 character^{2,12}.

1.1.2 Crystalline Polymerized Fullerite Phases

Experiments using high pressures at room temperature resulted in amorphous phases due to the breaking of C_{60} cages. This suggested that different experimental conditions should be tried. When using high temperature or light excitation unexpected structures formed by polymerized C_{60} molecules are observed. The first experimental report of C_{60} polymerization was conducted by Rao *et. al.*¹². They reported the photopolymerization of C_{60} thin films (less than 5000 Å) using either visible or ultraviolet light. The mass spectrograph shown peaks located at masses corresponding to C_{60} , C_{120} , C_{180} ... C_{60n} , thus demonstrating the polymerization process; the vibrational spectra also suggested that C_{60} cages were joined covalently. Rao proposed [2+2] cycloaddition photochemical reaction between double bonds in order to explain how these C_{60} molecules were linked (see Figure 1.2). This intermolecular link is well known in organic chemistry¹³ for photoinduced reactions, but also it is known that this kind of reactions are more difficult to occur using thermal treatments. The final structure has a common four side ring, with 90° angles. Such [2+2] scheme has

been the main intermolecular connection used for explaining the characteristics of C_{60} polymers. Subsequently, Ywasa *et. al.* reported C_{60} polymerization under High Pressure and High Temperature treatments (HPHT)¹⁴. They found two polymeric phases of C_{60} using HPHT; the first one showed the best fitting in XRD with an fcc model; the second one displayed the best fit with a rhombohedral model ($R\bar{3}m$ spatial group). In both cases Infrared (IR) and Raman studies revealed a broadening of peaks, as well as the presence of new peaks with respect to pristine C_{60} fcc. In addition, these new phases were not soluble. It suggested that C_{60} molecules were joined by covalent bonds. Both phases reverted to the pristine fcc phase when heat was applied (more than 250 °C) at normal pressure. This means that the C_{60} cages remained after de-polymerization.

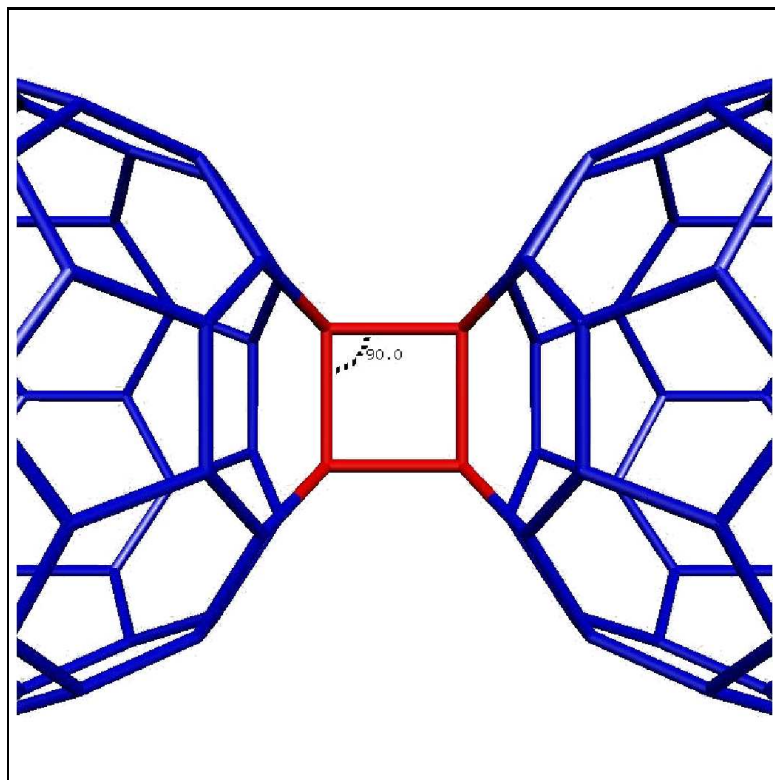


Figure 1.2: Cycloaddition 2+2 between double bonds in two adjacent C_{60} fullerenes.

Nuñez-Regueiro *et. al.*, reported additional phases obtained under HPHT with less than 750 °C and pressures up to 4 GPa.¹⁵ They found samples containing a mixture of rhombohedral ($R\bar{3}m$) and tetragonal ($Immm$) phases of polymerized C_{60}

molecules. They also reported an orthorhombic phase and proposed polymerized structures in layers or chains using the [2+2] cycloaddition between double bonds. An orthorhombic phase can be obtained by polymerizing the cages along the $\langle 110 \rangle$ direction in the original fcc lattice. The rhombohedral structure could be formed by polymerization on the (111) plane of the fcc lattice, and tetragonal phase by polymerization along the (001) plane (see figures 1.3 and 1.4). Such structures have been used in subsequent studies in order to find the better fits of experimental results and for studying the mechanical and electronic properties from a theoretical point of view². Xu and Scuseria¹⁶ used a tight-binding potential, and found that the polymerized structures proposed by Nuñez-Regueiro *et. al.* were stable and could be semiconductors with a gap close to 1.1 eV. The relaxed structures also exhibit a distance between nearest neighbors C_{60} centers close to 9.17 Å, in agreement with experimental observations.

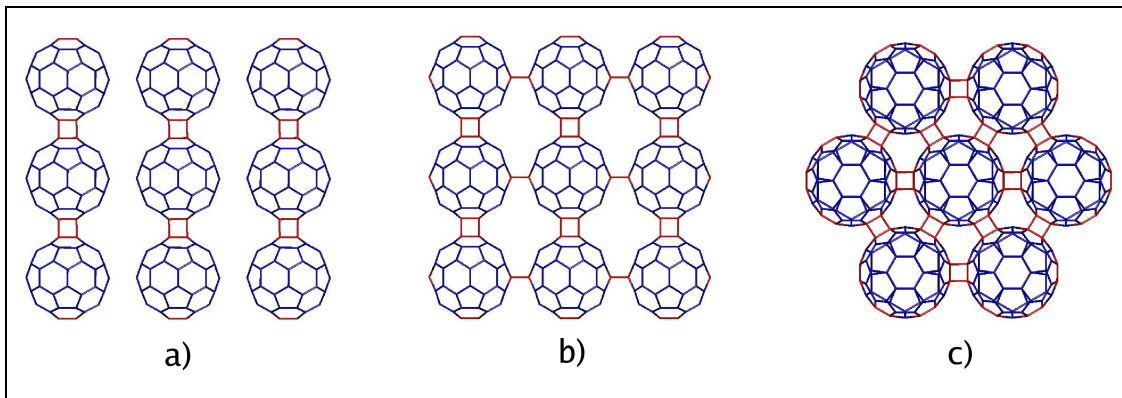


Figure 1.3: Representative sections of a) Orthorhombic 1D, b) Tetragonal 2D and c) Rhombohedral 2D polymerized C_{60} phases. Red has been used to stress the intermolecular bonds

Several studies on the properties of C_{60} polymers have been performed by looking at the vibrational spectra and electronic properties^{17–20}. Vibrational Raman spectra of polymerized C_{60} shows some general trends, like a clear downshift from 1469 cm^{-1} to approximately 1458 cm^{-1} , being sometimes used like a parameter to determine when a sample is polymerized. Also it has been noted that polymerization breaks the symmetry, and produces new peaks in the spectra, arising from degen-

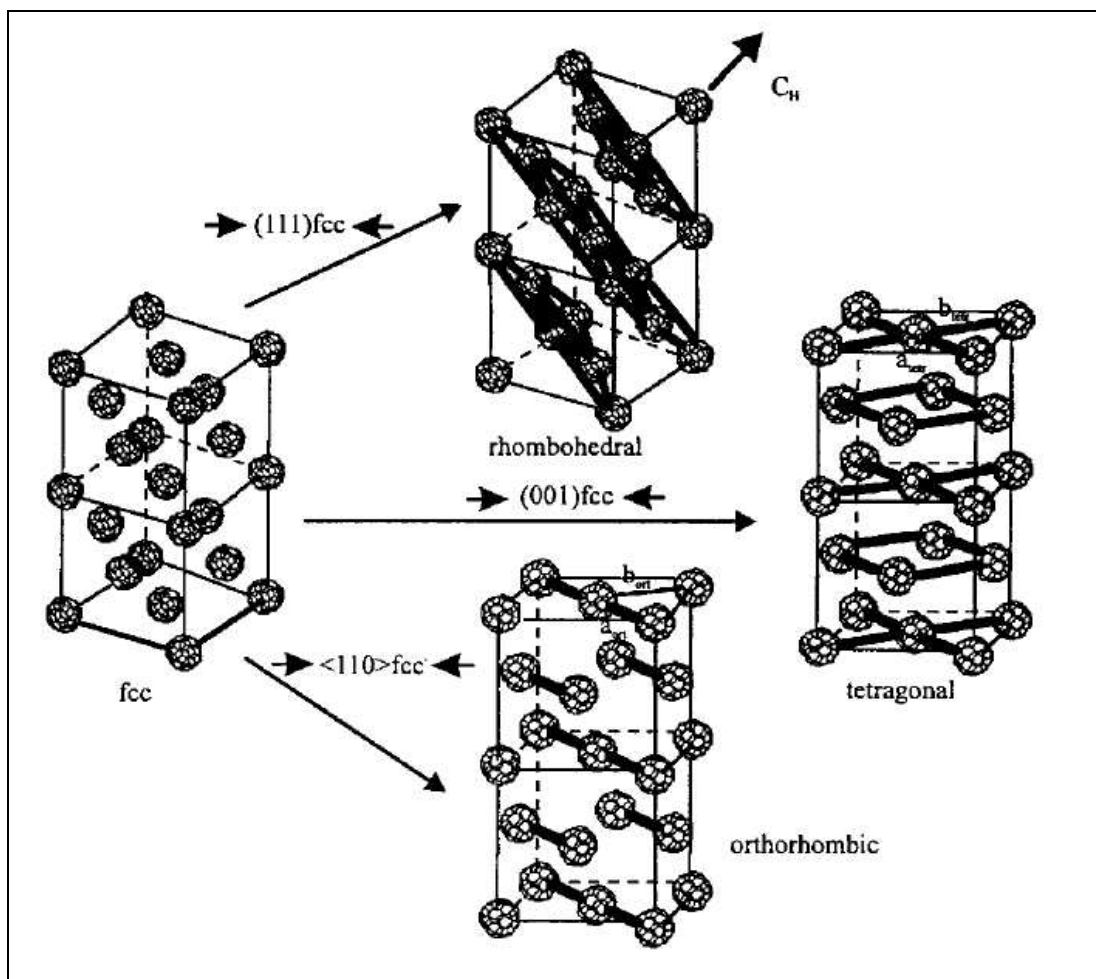


Figure 1.4: Sketches of how Orthorhombic 1D, Tetragonal 2D and Rhombohedral 2D polymeric C_{60} structures are formed from the pristine fcc C_{60} . The molecules are intentionally reduced in size with respect to the lattice in order to clearly see the lattice distortions originated by the different polymer types. Image courtesy of Prof. Leonel Marques from L. Marques *et. al.*, *Molec. Mater* **8**, 49 (1996)

erated modes in pristine C_{60} . There are sharp lines obtained by Laser Desorption Mass Spectroscopy corresponding to C_{60} , C_{120} , \dots C_{60n} (n up to 12), demonstrating that C_{60} cages have not been broken. From the theoretical point of view, using an empirical tight-binding method, Belavin *et. al.*¹⁹ reported that polymerized C_{60} cages exhibit a semiconductor behavior for all phases proposed by Nuñez-Regueiro; a 2.18 eV gap for the chain, a 1.852 eV gap for tetragonal 2-D phase and a 0.577 eV gap for the hexagonal 2-D system. Okotrub *et. al.* proposed a novel rhombohedral 2-D phase using [2+2] cycloadditions, created between a double and a single bond²⁰.

With this structure they found a metallic in-plane conductivity, showing that the connection used for linking C_{60} cages could strongly affect the electronic properties of the material.

Experimental studies indicated some differences in the vibrational spectra but conclusive results could not be extracted, since the samples presented mixed phases and amorphous material. Finally, Davydov *et. al.* successfully synthesized almost pure samples of rhombohedral (2-D), tetragonal (2-D) and orthorhombic (1-D) polymerized phases²¹. The experimental paths used to obtain such phases are presented in figure 1.5. They compared experimental XRD patterns of the samples obtained with XRD simulated patterns of the structures proposed by Nuñez-Regueiro, and the results showed a good agreement for all diffraction peaks.

1.1.3 Superhard Phases of Polymerized C_{60} Molecules

Experimental studies failed in finding a sample with a bulk modulus higher than that of diamond, at least until 1995. In that year, Blank *et. al.* reported that by heating fullerite at high non-hydrostatic pressure, it was possible to obtain an ultrahard material (harder than diamond)²². They worked with a shear diamond anvil cell and created a phase able to scratch the device's walls, made of diamond. In this work the authors even stated: "Ordinary measurement methods of the hardness by indentation of a diamond tip (Knoop method) were not usable, because the diamond tip did not produce traces on the polished surface of hard bulk samples". They obtained such phase using pressures ranging from 9.5 to 13 GPa at temperatures from 620 K up to 1830 K. Their XRD patterns and Raman studies shown that the cages were not collapsed, but the new structure was a random network of sp^2 and sp^3 hybridized bonds formed by C_{60} linked without an orientational order. They also found a Raman band in a zone characteristic for four membered rings, giving some support of the [2+2] cycloaddition. After that, several experimental studies were performed looking for such ultrahard carbon phase². Unfortunately, only Blank's group has been able to produce such a material.

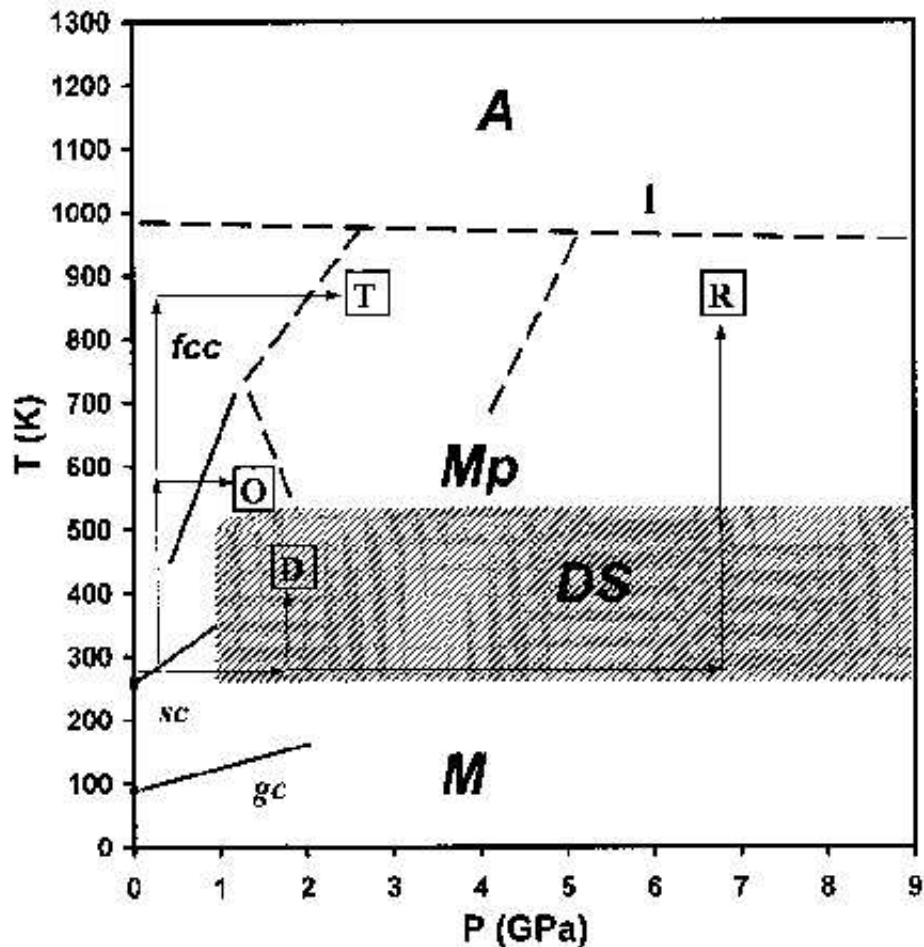


Figure 1.5: Treatment paths for obtaining almost pure Orthorhombic 1D, Tetragonal 2D and Rhombohedral 2D polymeric C_{60} phases. Image from Davidov *et. al.*, Phys. Rev. B **61**, 11936 (2000)

Five years later Chernozatonskii, Serebryanaya and Mavrin reported a superhard phase²³ made when applying pressures of 13 GPa. at 820K, similar to the experiment reported by Blank *et. al.*, and calculated a bulk modulus close to 800 GPa using a theoretical acoustic method. They proposed a body-centered-orthorhombic (bco) arrangement of C_{60} molecules covalently linked by [2+2] cycloadditions and some different covalent intermolecular links, such as the [3+3] cycloaddition and four membered common rings. They provided atomic coordinates in a I_{mmm} crystal structure with nine independent atoms based on the theoretical analysis of the diffraction patterns. Perottoni and Jornada performed theoretical calculations of

Chernozatonskii's structure using first principles calculations²⁴, finding a bulk modulus of 302 GPa and a shear modulus of 301 GPa. Therefore, they demonstrated that the structure proposed by Chernozatonskii is in fact very hard but not harder than diamond. Nowadays, controversy about the existence of an ultrahard polymerized C_{60} phase still remains.

Other theoretical studies were performed in order to study the electronic and mechanical properties of 3-D polymerized C_{60} structures. In this context, Okada, Saito and Oshiyama proposed a structure that could result by applying uniaxial pressure on the C_{60} tetragonal phase²⁵. They calculated that such structure has a bulk modulus of 47 GPa, so the phase is not a candidate for a superhard material. Instead they found that the structure could be candidate for a superconductor material because of its high DOS at the Fermi level. Burgos *et. al.* studied, using *ab initio* density functional methods, two polymeric C_{60} phases exhibiting a bcc arrangement and a bco arrangement²⁶. They found a bulk modulus near 300 GPa and a shear modulus close to 240 GPa. They also proposed that such phases could be synthesized using HPHT on the C_{60} orthorhombic phase. Berber, Osawa and Tománek have recently calculated the electronic and mechanical properties of 12 polymerized phases looking for a structure harder than diamond²⁷. They used different intermolecular links and different lattices (fcc, simple cubic, bcc and bco) in order to construct such phases. They found that structures using a bcc arrangement were stiffer than the others but they did not found any phase harder than diamond, although the hardest structure presented a bulk modulus of 370 GPa.

It is very likely that the values reported by Blank were overestimated due to measurement errors. Therefore, it is possible that an ultrahard phase has not been yet synthesized. However, this work has attracted the attention of several researches, and the quest of low density ultrahard carbon materials is currently underway. It must be mentioned that experimental research on fullerites under HPHT treatments has been difficult due to the difficulty in producing a pure polymerized phase. As discussed earlier, clear differences in the synthesized material are observed between

hydrostatic and non-hydrostatic pressure. The first one produces polymeric crystalline fullerene structures and the second one generates structures with a high proportion of amorphous carbon exhibiting an increased high hardness and high flexural stress. Talyzin *et. al.* reported that the produced samples depend strongly on the synthetic path used and does not depend only on the Pressure-Temperature conditions²⁸. Therefore, one could obtain different phases for the same final P-T conditions. These differences, during the synthesis of the polymerized phases, could explain the disagreements observed in the experimental results.

1.1.4 Intermolecular Bonding Schemes Between C_{60} Molecules

Some studies have suggested that different intermolecular connections might occur in polymerized C_{60} structures. Marques *et. al.* made an experiment applying uniaxial pressure (13 GPa) and heating (820 K) on fullerite. They found Debye-Sherrer ellipses in the XRD pattern, showing that anisotropic deformation were retained at ambient conditions²⁹. These authors reported that the cages were preserved, but presented a statical rotational disorder and also the structure was composed mainly of sp^3 bonds. The XRD pattern could be indexed as a polycrystalline fcc phase of cages with a great radial distortion, suggesting that such structures could support great uniaxial stress. All results mentioned above, and the results of synchrotron studies in addition to simulations considering 3-D models reported by Marques *et. al.* suggested that other links besides [2+2] cycloadditions could be present in the polymerized C_{60} phase. A recent study by Mezouar *et.al.* reported that 3-D structures formed by non-hydrostatic compression are the most stable form of polymerized fullerenes, preserving their structure even under 35 GPa³⁰. These authors also reported that the radial and axial compressibility were different, indicating that two different intermolecular bonding schemes were occurring.

The presence of intermolecular bonding schemes different from [2+2] cycloaddition might be not restricted to 3-D polymerized C_{60} structures. As mentioned earlier, most studies on polymerized C_{60} structures have considered [2+2] cycloaddition

links. This is an energetically favorable connection as can be observed from theoretical studies of C_{60} dimers (using Density Functional Theory (DFT)^{31,32}, tight-binding schemes (TB)³³ and other potentials³⁴). From the experimental standpoint, the principal evidence for [2+2] cycloadditions comes from NMR^{18,35,36}, and XRD^{15,21}; all of them obtained by comparing the experiments with simulated data of the proposed structures. However, it must be noted that the theoretical studies mentioned above did not consider dynamical changes of temperature and crystalline environment. One should emphasize that other stable bonding schemes could be present in the polymerized C_{60} structures that have not been taken into account, and these models could also approximate the experimental data. Another reason for considering different intermolecular links is that polymerized structures with C_{60} cages arranged in the same crystalline packing way, could exhibit metallic or semiconductor behavior depending on how C_{60} molecules are linked²⁰. Some theoretical studies have considered different intermolecular bonding schemes^{23–27} (see some of them in figures 1.6 to 1.8) but there are still different possibilities that have not been explored.

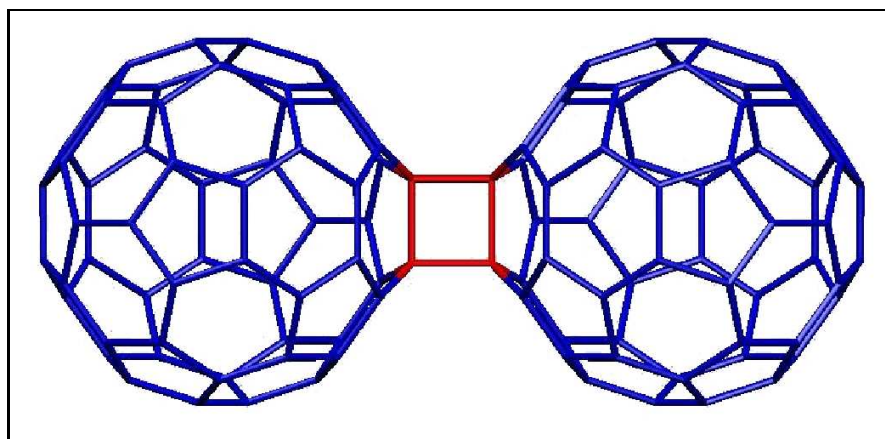


Figure 1.6: The 2+2 cycloaddition between single bonds

1.2 Motivation

Experimental and theoretical studies of polymerized C_{60} have been discussed in the previous sections. It is noted that molecular dynamics simulations have mainly

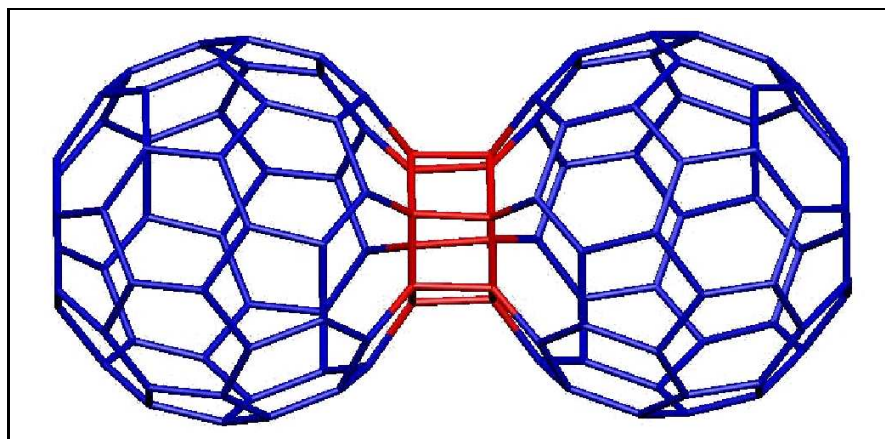


Figure 1.7: “6+6 cycloaddition” resulted by joining hexagons

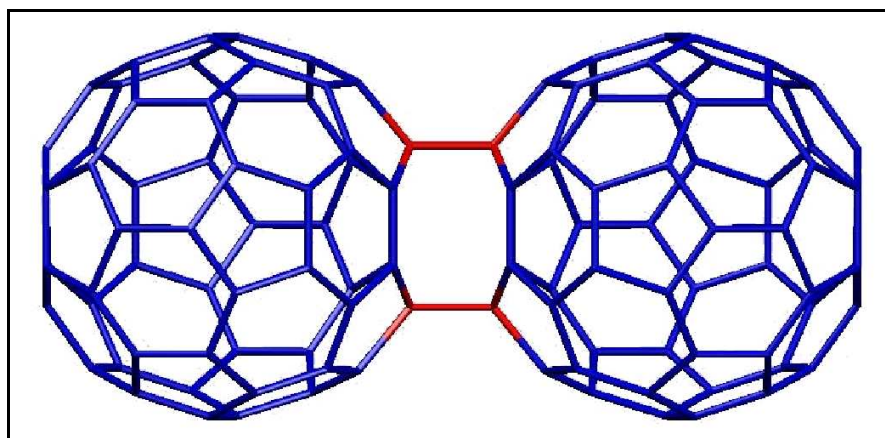


Figure 1.8: 4+4 cycloaddition between hexagons

been performed using already polymerized cages as the starting configurations. In addition, previous works involve mainly the relaxation of structures using a conjugate gradient method, displacing the atoms in such a way that the total force felt by the atoms is decreased. Therefore, pressure and temperature effects during the binding process have been neglected. Further theoretical calculations on different bonding types need to be considered. It is noteworthy that high temperatures and pressures may induce the formation of different connections among fullerenes, apart from [2+2] cycloadditions. It is clear that new insights related to C_{60} intermolecular bonding formation could be obtained by performing molecular dynamics simulations that consider temperature and pressure effects. Similarly, the crystalline orientation effects of the cages should be considered during polymerization.

Hard and (possibly) ultrahard C_{60} polymers are formed due to stress induced by non-hydrostatic pressure. Because of the preferential direction of stress, different intermolecular links could appear in different directions. In addition, a strong deformation of the C_{60} cages is preserved even after applying and releasing the pressure. It should be pointed out that theoretical studies have failed to find a carbon structure, made of polymerized C_{60} molecules, with a hardness higher than that of diamond. However, novel theoretical structures could be proposed using intermolecular links found by MDS in C_{60} crystals under HPHT treatments. These studies should provide crucial information able to find carbon structures with extremely high mechanical properties. Even if an ultrahard phase is never found experimentally, theoretically stable structures could motivate further experimental synthesis research because of their potential applications. The finding of novel intermolecular bonding schemes could also help us to predict systems exhibiting novel electronic properties. It may also be possible to predict other polymerized phases that behave as superconductors, such as has been proposed by Okada et. al.²⁵

1.3 Aims of this work

We are interested in understanding the intermolecular bonding formation in C_{60} crystalline structures at high temperature and under high pressure using MDS. Such studies will provide us with tools able to propose new carbon materials with extremely high bulk modulus, and intriguing electronic properties. Therefore, we could be able to establish relationships between intermolecular bonding and structural properties. These models may exhibit similar XRD patterns when compared to those reported experimentally in the literature. The specific objectives of the present work are:

1. The systematic study of C_{60} polymerization process occurring at high temperature and under high pressure using classical MDS.
2. The dynamic characterization of these polymerized systems.

3. The study of the stability considering [2+2] cycloadditions occurring between double bonds in C_{60} polymerized phases.
4. To suggest novel polymeric C_{60} structures and evaluate their structural stability.
5. The study of different intermolecular connections in C_{60} polymerized crystalline structures by calculating electronic and mechanical properties.
6. The simulation of XRD patterns of the proposed polymerized structures in order to compare them with experimental patterns presented in literature.

REFERENCES

1. H. W. Kroto, J. R. Heath, S. C. O'Brien, R. F. Curl, R. E. Smalley, *Nature* **318**, 162 (1985)
2. B. Sundqvist, *Advances in Physics (Review)* **48**, 1 (1999)
3. W. Kräestchmer, L. D. Lamb, K. Fostiropoulos and D. Huffman, *Nature* **347**, 354 (1990)
4. P. A. Heiney, J. E. Fischer, A. R. McGhie, W. J. Romanow, A. M. Denenstein, J. P. McCauley Jr. and A. B. Smith III, *Phys. Rev. Lett* **66**, 2911 (1991)
5. W. I. F. David, R. M. Ibberson, J. C. Matthewman, K. Prassides, T. J. S. Dennis, J. P. Hare, H. W. Kroto, R. Taylor and D. R. M. Walton, *Nature* **353**, 147 (1991)
6. R. S. Ruoff and A. L. Ruoff, *Nature* **350**, 664 (1991)
7. R. S. Ruoff and A. L. Ruoff, *Appl. Phys. Lett.* **59**, 1553 (1991)
8. M. O'keeffe, *Nature* **352**, 674 (1991)
9. S. J. Duclos, K. Brister, R. C. Haddon, A. R. Kortan and F. A. Thiel, *Nature* **351**, 380 (1991)
10. F. Moshary, N. H. Chen and I. F. Silvera, *Phys. Rev. Lett.* **69**, 466 (1992)
11. J. L. Hodeau, J. M. Tonnerre, B. Bouchet-Fabre, M. Nuñez-Regueiro, J. J. Capponi and M. Perroux, *Phys. Rev. B* **50**, 10311 (1994)
12. A. M. Rao, P. Zhou, K. Wang, G. T. Hager, J. M. Holden, Y. Wang, W. T. Lee, X. Bi, P. C. Eklund, D. S. Cornett, M. A. Duncan and I. J. Amster, *Science* **259**, 955 (1993)
13. R. Morrison, B. Thorton and R. Neilson, *Química*, 5a. Edición, Editorial Pearson Education, México 1998

14. Y. Iwasa, T. Arima, R. M. Fleming, T. Siegrist, O. Zhou, R. C. Haddon, L. J. Rothberg, K. B. Lyons, H. L. Carter Jr., A. F. Hebard, R. Tycko, G. Dabbagh, J. J. Krajewski, G. A. Thomas and T. Yagi, *Science* **264**, 1570 (1994)
15. M. Nuñez-Regueiro, L. Marques, J. L. Hodeau, O. Béthoux and M. Perroux, *Phys. Rev. Lett.* **74**, 278 (1995)
16. C. H. Xu and G. E. Scuseria, *Phys. Rev. Lett.* **74**, 274 (1995)
17. A. M. Rao, P. C. Eklund, U. D. Venkateswaran, J. Tucker, M. A. Duncan, G. M. Bendele, P. W. Stephens, J. L. Hodeau, L. Marques, M. Nuñez-Regueiro, I. O. Bashkin, E. G. Ponyatovsky and A. P. Morovsky, *Appl. Phys. A* **64**, 231 (1997)
18. P.A. Peerson, U. Edlund, P. Jacobson, D. Johnels, A. Soldatov and B. Sundqvist, *Chem. Phys. Lett.* **258**, 540 (1996)
19. V. V. Belavin, L. G. Bulusheva, A. V. Okotrub and D. Tománek, *J. Phy. Chem. Solids* **61**, 1901 (2000)
20. A. V. Okotrub, V. V. Belavin, L. G. Bulusheva, V. A. Davydov, T. L. Makarova and D. Tománek, *J. Chem. Phys.* **115**, 5637 (2001)
21. V. A. Davydov, L. S. Kashevarova, A. V. Rakhmanina, V. M. Senyavin, R. Céolin, H. Szwarc, H. Allouchi and V. Agafonov, *Phys. Rev. B* **61**, 11936 (2000)
22. V. Blank, S. G. Buga, N. R. Serebryanaya, V. N. Denisov, G. A. Dubitsky, A. N. Ivlev, B. N. Mavrin and M. Y. Popov, *Phys. Lett. A* **205**, 208 (1995)
23. L. A. Chernozatonskii, N. R. Serebryanaya and B. N. Mavrin, *Chem. Phys. Lett.* **316**, 199 (2000)
24. C. A. Perottoni and J. A. H. da Jornada, *Phys. Rev. B* **65**, 224208 (2002)
25. S. Okada, S. Saito and A. Oshiyama, *Phys. Rev. Lett.* **83**, 1986 (1999)

26. E. Burgos, E. Halac, R. Weht, H. Bonadeo, E. Artacho and P. Ordejón, *Phys. Rev. Lett.* **85**, 2328 (2000)
27. S. Berber, E. Osawa and D. Tománek, *Phys. Rev. B* **70**, 085417 (2004)
28. A. V. Talyzin, L. S. Dubrovinsky, M. Oden, T. Le Bihan and U. Jansson, *Phys. Rev. B* **66**, 165409 (2002)
29. L. Marques, M. Mezouar, J. L. Hodeau, M. Nuñez-Regueiro, N. R. Serebryanaya, V. A. Ivdenko, V. Blank and G. A. Dubitsky, *Science* **283**, 1720 (1999)
30. M. Mezouar, L. Marques, J. L. Hodeau, V. Pischeda and M. Nuñez-Regueiro, *Phys. Rev. B* **68**, 193414 (2003)
31. G. B. Adams, J. B. Page, O. F. Sankey and M. O'keeffe, *Phys. Rev. B* **50**, 17471 (1994)
32. N. Matsuzawa, M. Ata, D. A. Dixon and G. Fitzgerald, *J. Phys. Chem.* **98**, 2555 (1994)
33. M. Menon, K. R. Subbaswamy and M. Sawtarie, *Phys. Rev. B* **49**, 13966 (1994)
34. S. Stafström and J. Fagerström, *Appl. Phys. A* **64**, 307 (1997)
35. C. Goze, F. Rachdi, L. Hajji, M. Nuñez-Regueiro, L. Marques, J. L. Hodeau and M. Mehring, *Phys. Rev. B* **54**, R3676 (1996)
36. F. Rachdi, C. Goze, L. Hajji, K. F. Thier, G. Zimmer, M. Mehring and M. Nuñez-Regueiro, *Appl. Phys. A* **64**, 295 (1997)

Chapter 2

Theoretical Background

2.1 Molecular Dynamics Simulations

2.1.1 Why Molecular Dynamics Simulations?

Theoretical Physics is aimed for explaining and predicting natural phenomena. This could be achieved either by means of approximated representations of the phenomenon or by using specific theoretical basis. Experiments in Physics also provide us with relevant information related to a specific phenomena. Nowadays, these data are more precise and try to confirm theoretical results of novel physical systems. It is clear that the relationship between theory and experiment provides clearer answers in our search for scientific knowledge. At present, scientists require the use of computer algorithms in order to perform calculations needed for obtaining and interpreting valuable experimental data.

Among the most important theoretical physics applications we could cite computer simulations. The later are performed in order to aid the understanding of a variety of systems, by means of models that could reproduce experimental observations. We carry out experimental simulations by examining the (idealized) system directly. It could be thought as a virtual laboratory. Such characteristics turn simulations into a fundamental tool in scientific research, because it is possible to carry out theoretical research, that in some cases could save time by avoiding trial-and-

error experiments of real systems. In addition, it is possible to simulate extreme and/or very controlled conditions, usually impossible to obtain experimentally. It is even possible to study systems that do not exist in nature. Simulations also provide a way for test the current theory, and could also show which are the limits where these models are reliable.

Molecular Dynamics Simulations (MDS) constitute a special kind of computer simulations that provide an insight on the molecular scale, both in time and space, and allow us to observe displacements of individual atoms in our computer screen. The evolution of any system could be observed in time; as short as femtoseconds. MDS applications are found in several fields such as Physics, Chemistry, Molecular Biology, Materials Science and Engineering. In this way, MDS are naturally being applied in the area of Nanoscience and Nanotechnology, which results from an overlapping of the fields mentioned above. Those simulations have proved to be useful in a great variety of systems and situations such as phase transitions, complex fluids, polymers, solids, biomolecules, etc.¹

However, MDS are limited by the theory level and considerations involved in the problem. In practice, it is always limited to the approximations used. In addition, computers are limited both in speed and information management capacity. The later also constitutes a drawback when predicting properties and geometries of nano-structured systems. Some of the best theoretical tools available, like Density Functional Theory (DFT), can only be applied to systems containing a few hundred atoms, due to the expensive computation effort. Although, some advances have been recently achieved due to the growing computational power of machines in order to perform an incredible amount of mathematic operations per second. In general, MDS constitute a suitable and powerful tool able to help us understanding atomic arrangements. However, they exhibit limitations.

2.1.2 Classical Molecular Dynamics Simulations: Fundamentals

Generalities

The core of Classical Molecular Dynamics Simulations (MDS) is the numerical solution of an N-body problem. From a classical point of view, particles are atoms regarded as spherical objects, with properties that can vary in a continuous form. Wave behavior and quantized energy are not considered for particles, as the quantum mechanical approach would demand. Instead, it is supposed that the past and the future of a system of particles are perfectly defined by the equations of motion and some initial conditions; such as positions and velocities at time $t = 0$. The system's evolution can be calculated based on Classical Mechanics formalisms such as Newton's equations or the Lagrangian or Hamiltonian formalisms (see ref[2]). However, in practice, the evolution of a specific system can not be exactly calculated because the data involved can only be stored and managed by computers with a limited precision. In addition, the simulated time must be regarded in timesteps instead of a continuum. If two simulations are performed with identical conditions but with a different precision, it is known that individual atomic positions and velocities would become uncorrelated as the simulation time develops, i. e. the two simulations will converge at totally different points in the phase space^{1,2}. Therefore one may ask: how can we trust such a method if the specific final state is so variable?

MDS are not aimed to reproduce the precise evolution paths of real molecular systems. In fact, this is impossible, due to the information storage limits and also due to the uncertainty principle. Instead, MDS provide qualitative information of molecular behavior and quantitative information based on statistical sampling. The heart of such power is the *ergodic hypothesis* that " . . . relates the ensemble average to measurements carried out for a single equilibrium system during the course of its natural evolution - both kinds of measurement should produce the same result"¹. In addition, there is no meaningful physical quantity that depends on just a single trajectory; all realistic measurements involve average values. Therefore, by using

statistical mechanics and assuming ergodicity, the thermodynamic properties of a system can be obtained by MDS, and the results can be compared with experimental data. However, the strength of MDS is that detailed trajectory histories are available, so that not only the meaningful quantities in a statistical mechanical framework can be calculated, but also other relevant values (such as correlations).

At the simplest level of theory, the interactions occur between pairs of atoms, being a combination between a repulsive interaction at short range and an attractive interaction with long range effects (e.g. Lennard-Jones potential). Given such interactions, it is possible to calculate a total potential $\mathbf{u}(\mathbf{r})$ that could be experienced for each atom by adding each contribution. In the Newtonian scheme, the force corresponding to $\mathbf{u}(\mathbf{r})$ is $\mathbf{F} = -\nabla\mathbf{u}(\mathbf{r})$, and the motion could be derived using the known velocities and positions, so that Newton's second law could be expressed as:

$$m\ddot{\mathbf{x}}_i = \mathbf{F}_i = \sum_{j=1, j \neq i}^{N_a} \mathbf{f}_{ij} \quad (2.1)$$

where the sum is over all N_a atoms excluding i (itself), \mathbf{f}_{ij} is the force due to pair interactions and m is the atomic mass¹. Calculations of atomic movements are performed by iterations; adequate times are required to ensure that the statistical behavior does not depend on the initial conditions. Through iterative steps, the calculations of averages of different properties could be performed. Although the basic scheme of MDS is simple, the implementation is not trivial. Complications may arise from the need of a reliable and useful calculation. Therefore, different issues must be considered in a MDS: a good numerical stability, simulation speed, reproducibility of results and appropriate potential schemes. Some general considerations that help us to address such issues are presented below.

¹Lagrangian and Hamiltonian formulations are more general than Newtonian formulation. They are used too for calculating atoms's motion in MDS. Selection between different formulations depends on numerical calculations and theoretical manipulations.

In Molecular Dynamics programs, physical quantities must be expressed in reduced or dimensionless units. In this way, computation can be performed with values close to unity instead of extremely small values that are present when normal units are taken into account. Another benefit is that the equations of motion are simplified when dimensionless units are used because some of the parameters defining the model are absorbed into the units. For example, in a homogeneous system, if mass is absorbed into the units, Newton's second law is reduced to $\ddot{\mathbf{r}} = \mathbf{F}$. The switch to such units removes any risk of encountering values lying outside the range that is available by the computer hardware. Subsequently, replacements such as $\mathbf{r} \rightarrow \mathbf{r}'\sigma$ can be performed, in which \mathbf{r}' is the transformed value (dimensionless) and σ is the new unit used. In addition, values in atomic units, like Hartrees for energy, are also suitable for calculations in MDS scales.

An infinite system could be modeled by using periodic boundary conditions (see figure 2.1). This is equivalent to fill the space with identical copies of a cell. The cell size must be large enough in order to ensure that an atom in the cell does not interact with its image in other neighboring cell. The cell size has also to exceed the range of any significant correlation. Cell size is very important but cell shape could also be crucial. When liquids or gases are being simulated, the cell shape could be cubic in order to simplify the simulation, but in most crystalline structures, it is convenient that the cell is defined by a non-orthogonal set of vectors. Then, the size and shape of the cell must be selected accordingly, by simplifying our system, thus avoiding unphysical effects in the output data.

Most of the computer time in MDS is spent on interaction calculations. When a pair-interaction-like calculation considers all pairs that can be formed with all atoms in the system, the calculation effort grows as $O(N_a^2)$. Therefore, multiple efforts have been dedicated to find effective methods able to reduce the amount of computation time required for a system containing a large number of atoms. *Cell subdivision method* is useful in reducing the effort and computation time needed. The simulation box is divided into cells with a cell size close to the maximum in-

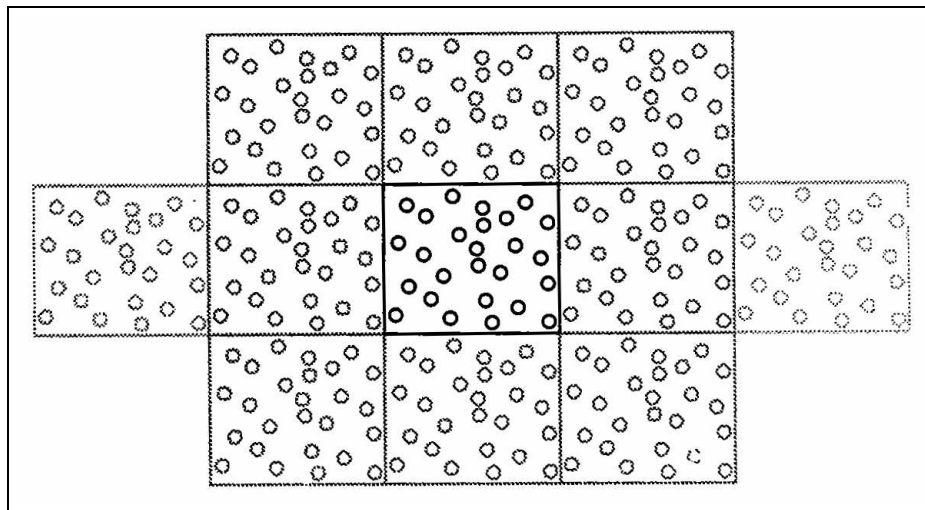


Figure 2.1: Periodic conditions scheme for a two dimensional space. Figure from the D. C. Rapaport's book *The art of molecular dynamics simulations*. The central square is the simulation box. All other squares are mirror images from the first, generated by translation. The atoms are represented here by small circles.

interaction distance defined in the calculation, then each atom is assigned to a cell. This allows us to reduce the calculation time by evaluating only atoms that are on neighboring cells (or in the same cell), avoiding wasteful calculations between atoms that are far away. This method is useful only if the simulation box is large enough to contain non-neighbor cells. Another useful method is the *Neighbor-list*. Here, for every atom, a list of atoms inside a sphere of radius R_n is obtained, with $R_n > R_i$, where R_i is the maximum interaction length. Then, after a few timesteps, it is possible to evaluate the interactions for a specific atom only for the atoms that belong to its neighbor list. The lists must be updated again after additional timesteps in order to ensure that all possible interactions are considered. Usually, R_n is at least 1.5 times the typical interaction distance.

A Molecular Dynamics algorithm must be tested in order to verify its reliability, being the energy and momentum conservation the most obvious parameters. When obtaining a high degree of accuracy in the atomic trajectories, the result may not be a realistic nor a practical goal. Therefore, the criteria for selecting a suitable numerical method focuses on energy conservation and on the ability to reproduce certain time-

and space-dependent correlations to a sufficient degree of accuracy. Some methods for integrating the equations of motion have shown excellent properties in energy conservation; like the *Verlet algorithm*, that uses the equation

$$\mathbf{x}(t + \mathbf{h}) = 2\mathbf{x}(t) - \mathbf{x}(t - \mathbf{h}) + \frac{\mathbf{f}(t)}{m}\mathbf{h}^2 \quad (2.2)$$

where the dependence of velocity has been avoided using a Taylor expansion, but it is implicit in the difference between $\mathbf{x}(t)$ and $\mathbf{x}(t - \mathbf{h})$. Other methods are available, like the *Predictor-corrector methods* that have shown to be better suited to more complex systems, such as rigid bodies or constrained dynamics. The length of the time step is determined by the time scale of the phenomena that are studied. It must be small enough in order to obtain the real picture of the physical phenomena and large enough to save computational time.

The easiest ensemble to simulate in MDS is the microcanonical scheme. In such ensemble the number of particles, volume and energy are the preserved properties rather than temperature and pressure. The system's temperature could be evaluated by means of kinetic energy, and the pressure value could arise from the virial theorem. However, experiments are performed at constant temperature and sometimes at constant pressure. Thus, simulations of canonical ensemble (NVT) or isothermal-isobaric ensemble (NPT) are more suitable for obtaining data that could be compared with the experimental results. An easy way to keep the temperature at the desired value is the *velocity rescaling*, which consists in adjusting by the same factor all atoms's velocities, in such a way that the new kinetic energy corresponds to the desired temperature. However, this process affects the kinetic part of the energy, and therefore energy conservation could be obtained far away of a given limit. Mathematical methods for simulating non-microcanonical ensembles will be discussed below.

A Typical Program

In this section it will be presented the general structure and characteristics presented by MDS programs; the scheme presented comes from D. C. Rapaport's Book *The Art Of Molecular Dynamics Simulation*¹.

The structure of MDS programs is mainly modular, and it allows to preserve an organized code structure, thus making easier the programing task when particular changes are required. Below is presented the structure that could be the main body of a typical MDS program (written in Fortran), the names of functions are self-explanatory:

```
program MDSimulation

use module_a
use module_b
use module_c

call GetNameList ()
call PrintNameList ()
call SetParams ()
call SetupJob ()

do
    call SingleStep ()
        if ( (stepCount >= stepLimit).OR.(other_condition) ) exit
end do

end program
```

The first four subroutines describe the initialization phase in which parameters and additional data are read or initialized, and storage arrays allocated. Subsequently, the code enters in a loop that will terminate when a specified limit is

reached or some other specific logical condition changes its value. The latter could be performed either by the program or by the user. The shared values, parameters or variables can be accessible to the subroutines using the modular structure or by specifying them in the parenthesis zone, after the subroutine name.

All the work needed for initializing the computation is concentrated in the subroutine *SetupJob* shown below. Initial coordinates can be specified in the input files and initial velocities could be initialized by *InitVels* using a Maxwell's distribution.

```
subroutine SetupJob ()

call AllocArrays ()
call InitCoords ()
call InitVels ()
call AccumProps ()
stepCount = 0

end subroutine
```

The subroutine *SingleStep* calls to subroutines that will deal with the force evaluation, integration of the equations of motion, quantification of various properties and adjustments required by the periodic boundaries.

```
subroutine SingleStep ()

stepCount = stepCount + 1
timeNow = stepCount * deltaT

call ComputeForces ()
call LeapFrogStep ()
call ApplyBoundaryCond ()
call EvalProps ()
call AccumProps ()
```

```
if ( mod(stepCount,stepAvg) == 0 ) then
    call AccumProps ()
    call PrintSummary ()
    call AccumProps ()
end if

end subroutine
```

It has been shown a general structure of a MDS program. However, there are many specific subroutines that could be included, and many different forms for programming in order to perform enhanced simulations. Nevertheless, there are elements that are nowadays common to MD simulations of various kinds:

- Parameters input with completeness and consistency checks.
- Runtime array allocation, with sizes determined by the system.
- Initialization of variables.
- The main loop. Which cycles through the force computations and trajectory integration, and performs data collection at specific intervals.
- The processing and statistical analysis of various kinds of measurement values.
- Storage of accumulated results and condensed configurational snapshots for later analysis.
- Run termination based on various convergence criteria.
- Checkpoint (or saving) the current computational state of a long simulation run, both as a safety measure, and also to allow the run to be interrupted and continued at a later time.

2.1.3 Simulating non-microcanonical ensembles

Simulations at constant temperature: Nosé-Hoover thermostat

Simulations made with the standard Newton, Lagrange or Hamilton equations preserve the energy. That is, energy is constant throughout the system evolution. In addition, the volume and the number of particles are maintained constant. If we assume ergodicity, then the measurements obtained in conventional MDS are equivalent to those of the microcanonical (NVE) ensemble. However, as mentioned previously, experiments are performed at constant temperature, so the canonical ensemble (NVT) must be simulated; if constant pressure is also imposed then the system should consider the isothermal-isobaric ensemble (NPT). Strict approaches aimed to generate such ensembles must have the *symplectic property*, that is, the measure of the phase space must be invariant (see ref[3,4] for further explanation). This ensures that the error in our sampling of the phase space is bounded; therefore, the system will exhibit a reasonable long-time statistical behavior of dynamics.

In this context, several approaches have been proposed, the pioneer is the Andersen thermostat⁵. In this scheme a coupling between the system and a heat bath is simulated by stochastic impulsive forces that act on randomly selected particles. There is a probability of selecting one particle at each timestep; in a timestep one particle could be selected or not. The final velocity of the particle is obtained from a Maxwell-Boltzmann distribution. The strong coupling is determined by a frequency ν , in such a way that the probability of a particle to be selected in a time step of length Δt is $\nu \Delta t$. Andersen thermostat is successful in generating a canonical distribution and any thermodynamical property could be calculated. However, the simulated impulses from the bath to the particle break the smooth evolution of the system in time; therefore, the information about dynamical properties of the system turn to be unreliable.

In ref[5], Andersen also presented the *extended Lagrangian* approach. This means the Lagrangian of the system contains additional artificial coordinates and veloci-

ties. Based on this idea, Nosé showed that one could also simulate MDS at constant temperature^{6,7}. The formal scheme is known as the *Nosé thermostat*. The one presented in this work has been taken from Frenkel and Smit's book entitled *Understanding Molecular Simulation*².

In order to construct isothermal MDS, Nosé introduced an additional coordinate (\mathbf{s}) and its corresponding kinetic energy in the Lagrangian of a classical N-body system:

$$\mathcal{L}_{\text{Nosé}} = \sum_{i=1}^N \frac{m_i}{2} s^2 \dot{\mathbf{r}}_i^2 - \mathcal{U}(\mathbf{r}^N) + \frac{Q}{2} \dot{\mathbf{s}}^2 - \frac{L}{\beta} \ln \mathbf{s}, \quad (2.3)$$

where L is a parameter that will be fixed later. Q is an effective "mass" associated to \mathbf{s} . The conjugate momenta to \mathbf{r}_i and \mathbf{s} follow directly:

$$\mathbf{p}_i \equiv \frac{\partial \mathcal{L}}{\partial \dot{\mathbf{r}}_i} = m_i s^2 \dot{\mathbf{r}}_i \quad (2.4)$$

$$p_s \equiv \frac{\partial \mathcal{L}}{\partial \dot{\mathbf{s}}} = Q \dot{\mathbf{s}} \quad (2.5)$$

The extended Hamiltonian for N particles is now written as:

$$\mathcal{H}_{\text{Nosé}} = \sum_{i=1}^N \frac{\mathbf{p}_i^2}{2m_i s^2} + \mathcal{U}(\mathbf{r}^N) + \frac{p_s^2}{2Q} + L \frac{\ln \mathbf{s}}{\beta} \quad (2.6)$$

The variable \mathbf{s} helps to keep constant the temperature but also has an effect on the real size of the simulated timestep; \mathbf{s} could be regarded as a time scale in such a way that the real timestep sampled is not constant.

The extended system generates a microcanonical ensemble of $6N+2$ degrees of freedom. If the energy is the only conservation law, the partition function of the ensemble is given by:

$$Q_{\text{Nose}} = \frac{1}{N!} \int dp_s ds dp^N r^N \delta(E - \mathcal{H}_{\text{Nose}}) \quad (2.7)$$

With the choice of $L=3N+1$ and two integration steps, the partition function reduces to the canonical one:

$$Q_{\text{Nose}} = C \frac{1}{N!} \int dp'^N r^N \exp[-\beta \mathcal{H}(\mathbf{p}', \mathbf{r})] \quad (2.8)$$

where

$$\mathbf{p}' = \mathbf{p}/s \quad \text{and} \quad \mathcal{H}(\mathbf{p}', \mathbf{r}) = \sum_{i=1}^N \frac{\mathbf{p}'_i{}^2}{2m_i} + \mathcal{U}(\mathbf{r}^N) \quad (2.9)$$

The variables \mathbf{p}' are more related to the real observable properties, therefore, it is better to use such variables. Subsequently, Hoover reformulated the scheme^{8,9}, in the sense that the sample timestep is constant and the equations of motion are expressed in terms of the transformed momenta (equation (2.9)). The equations of motion are then expressed by:

$$\dot{\mathbf{r}}_i = \frac{\mathbf{p}'_i}{m_i} \quad (2.10)$$

$$\dot{\mathbf{p}}'_i = -\frac{\partial \mathcal{U}(\mathbf{r}^N)}{\partial \mathbf{r}_i} - \xi \mathbf{p}'_i \quad (2.11)$$

$$\dot{\xi} = \left(\sum_i \mathbf{p}'_i{}^2 / m_i - \frac{L}{\beta} \right) / Q \quad (2.12)$$

where $\xi = \mathbf{p}_s / Q$, and $\mathbf{p}' = \mathbf{p}/s$, and the extended Hamiltonian is:

$$\mathcal{H}'_{\text{Nose}} = \sum_{i=1}^N \frac{\mathbf{p}'_i{}^2}{2m_i} + \mathcal{U}(\mathbf{r}^N) + \frac{s'^2 \mathbf{p}'_s{}^2}{2Q} + L \frac{\ln s}{\beta} \quad (2.13)$$

\mathcal{E}'_{Nose} is a conserved quantity. However \mathcal{H}'_{Nose} is not a Hamiltonian, because the equations of motion can not be derived from it in a standard way. Nosé—Hoover thermostat scheme works well when there is only one conservation law, but if there are more conservation laws (e.g. fixed center of mass), it must be replaced by a Nosé—Hoover Chain. The latter is created by several coupled Nosé—Hoover thermostats (see ref[4]).

Simulation at constant pressure: NPT ensemble

The introduction of fictitious degrees of freedom into a physical system has proved to be extremely powerful in simulating processes at constant temperature. For the NPT ensemble, a similar formulation to that discussed in the previous section is observed. In this case, the volume of the simulation cell is regarded as a variable quantity, and a fictitious mass is assigned to a "barostat". In the same way, a fictitious coordinate and mass are assigned to a Nosé-Hoover thermostat. With such scheme, it is possible to simulate an iso-shape NPT ensemble; the volume changes, but its cell shape does not vary. This behavior does not present problems when gases or liquids are simulated. However, for crystalline systems, it is important to consider different shapes of the unit cell. In this section, it will also be presented the basics of the formalism for simulating NPT ensemble with a flexible cell (developed by E. Hernandez¹⁰). It results from the combination of the Nosé-Poincaré scheme presented by Bond *et. al.*¹¹ in conjunction with the method proposed by Souza and Martins¹², which uses as fictitious dynamical variables the components of the cell metric tensor.

Firstly, it will be most convenient to use the *lattice coordinates*, \mathbf{q}^i , which provide the position of the atom i relative to the simulation cell. Lattice coordinates are then related to Cartesian via the equation:

$$\mathbf{r}_i = \mathbf{H}\mathbf{q}^i \quad (2.14)$$

where \mathbf{H} is a 3 x 3 matrix formed by the simulation cell vectors \mathbf{a}_α , ($\alpha = 1, 2, 3$) in columns. The calculation of interatomic distances when atomic positions are specified in terms of lattice coordinates is given by:

$$\mathbf{r}_{ij} = \sqrt{(\mathbf{q}^i - \mathbf{q}^j)\mathbf{G}(\mathbf{q}^i - \mathbf{q}^j)} \quad (2.15)$$

where \mathbf{G} is the metric tensor, with elements

$$\mathbf{G}_{\alpha\beta} = \mathbf{a}_\alpha \cdot \mathbf{a}_\beta \quad (2.16)$$

The volume of the simulation cell is also given by the metric tensor as $\mathcal{V}_{\text{cell}} = \sqrt{\det\mathbf{G}}$. Metric tensor \mathbf{G} constitutes a convenient dynamical variable for constant pressure MDS. This is invariant under cell rotations, then the orientation of the cell is irrelevant. It is also easy to set up a fictitious kinetic energy term associated with the metric tensor. Following Souza and Martins, each metric tensor component $\mathbf{G}_{\alpha\beta}$ has a conjugate momentum $\mathbf{P}^{\alpha\beta}$, and the fictitious kinetic energy term associated to the dynamics of the metric tensor is expressed by:

$$K_G = \frac{\mathbf{P}^{\alpha\beta}\mathbf{P}^{\beta\alpha}}{2M_G\det\mathbf{G}} \quad (2.17)$$

where the sum over repeated indices is implied. Here M_G is a fictitious mass, but the total effective mass is $M_G\det\mathbf{G}$, which varies as a function of the cell volume.

In the case of hydrostatic external pressure, the potential energy term associated to the metric dynamics is given by:

$$\mathcal{U} = \mathcal{P}_{\text{ext}}\mathcal{V}_{\text{cell}} = \mathcal{P}_{\text{ext}}\sqrt{\det\mathbf{G}} \quad (2.18)$$

The case of an anisotropic external stress can also be considered, if a potential energy of the form

$$\mathcal{U}_G = \frac{1}{2} \sigma_{ext}^{\beta\alpha} G_{\alpha\beta} \quad (2.19)$$

is included, where $\sigma_{ext}^{\beta\alpha}$ are the components of the external stress in contravariant lattice coordinates.

The previous scheme must be coupled with a scheme for simulating constant temperature in order to perform NPT simulations. Canonical (NVT) MD simulations have been usually undertaken by means of the so called Nosé-Hoover method. However, Bond *et. al.*¹¹, have provided an alternative scheme, which also samples the NVT ensemble, but has the additional advantage of being Hamiltonian in structure. This is achieved by performing a Poncaré transformation on the original Nosé Hamiltonian, which results in

$$\mathbf{H}_{\text{Nosé-Poincaré}} = \mathcal{S}(\mathbf{H}_{\text{Nosé}} - H_0) \quad (2.20)$$

where H_0 is a suitable chosen constant, and $\mathbf{H}_{\text{Nosé}}$ is given by (in Cartesian coordinates)

$$\mathcal{H}_{\text{Nosé}} = \sum_{i=1} \frac{p_i^2}{2m_i S^2} + \mathcal{U}(\mathbf{r}) + \frac{P_s^2}{2M_S} + g k_B T_{ext} \ln S \quad (2.21)$$

Here S is the position variable of the thermostat, a strictly positive quantity, P_s its conjugate momentum, g is the number of degrees of freedom of the physical system (i. e. excluding extended or fictitious dynamical variables), k_B is the Boltzmann constant, and T_{ext} is the temperature of the thermostat.

By combining the Nosé–Poincaré Hamiltonian of Bond and coworkers with the metric tensor constant-pressure scheme of Souza and Martins, one arrives at the following Hamiltonian:

$$\begin{aligned}
 H_{NPT} = S [& \sum_i \frac{p_{i\alpha} p_{i\alpha}}{2m_i S^2} + \mathcal{U}(\mathbf{q}, \mathbf{G}) + \frac{\mathbf{P}^{\alpha\beta} \mathbf{P}^{\beta\alpha}}{2M_G \det \mathbf{G}} + \\
 & \mathcal{P}_{ext} \sqrt{\det \mathbf{G}} + \frac{1}{2} \sigma_{ext}^{\beta\alpha} \mathbf{G}_{\alpha\beta} + \\
 & \frac{\mathbf{P}_s^2}{2M_S} + g k_B T_{ext} \ln S - H_0]
 \end{aligned} \tag{2.22}$$

where $\mathbf{p}_{i\alpha}$ is the covariant α component of the momentum of atom \mathbf{i} . The equations of motion that results from such Hamiltonian can be integrated by any numerical method, for example a *Generalized Leap Frog Scheme*. The resulting numerical procedure, in the case of the *Leap Frog* is symplectic and time-reversible. Selection of the thermostat and barostat masses do not affect the average values found for several properties in the NPT ensemble, provided the dynamics is ergodic. However, the sampling efficiency depend on the chosen values, and therefore this selection must be carefully made.

2.2 Atomic interaction schemes

Accuracy of molecular systems studies relies mainly on the selection of interatomic interaction schemes. On the top of accuracy, are the *ab initio* calculations, based either on Density Functional or Hartree-Fock theory. These approaches are the benchmark for other methods due to the implicit inclusion of quantum mechanical characteristics. However, their applicability is limited to systems containing a few hundreds of atoms due to the long computation time required.

Different schemes from *ab initio* methods have been created in order to study systems with a larger number of atoms or where statistical averages calculations are

considered. Such schemes could be divided in two groups: *empirical* and *semiempirical* potentials. Empirical potentials are the fastest of all and provide an accurate description of some real systems. The atomic interaction described by such schemes depends only on the atomic positions and some parameters. The archetypical Lennard-Jones potential is the most well known example of an empirical potential.

Semiempirical methods lie in the middle of *ab initio* and *empirical* methods. They are also parametrized like *empirical* methods, but also retain part of the quantum-mechanical description. Their computation time is two or three orders of magnitude faster than *ab initio* calculations, but unfortunately also are two or three orders of magnitude slower than *empirical* calculations. A very representative method of *Semiempirical* approaches are Tight-Binding (TB) models, that provide good accuracy in systems where electronic orbitals are highly localized.

System size and accuracy are the parameters that determine the kind of calculation that is more convenient for a given problem. There is still another important property that reduces the options for choosing a specific model, this is *transferability*. The latter is related to the ability of a parametrization to produce accurate results in a range of different environments. *Ab initio* methods are totally transferable because they are not parametrized, but when other methods are used, *transferability* must be verified.

In the following sections, three schemes are presented, two of them are used in order to perform the calculations presented in this work: (1) *Tersoff potential*, an *empirical* potential used to perform calculations in systems where more than two C_{60} molecules are contained in the simulation cell; (2) *Tight-binding models*, which are presented as an introduction for *Non-orthogonal-tight-binding* approaches (3).

2.2.1 Tersoff Classical Potential

Although less accurate than *ab initio* methods, the *empirical* methods are valuable in order to study complex and large systems. In particular, a great interest exists in modeling covalent systems due to their technological applications. One of the most well-known models for such systems is the Tersoff potential, which is able to perform calculations for heteronuclear covalent systems¹³. Such an approach has shown an amazing performance for carbon systems with a large quantity of atoms. It also reproduces the behavior of either diamond or graphite structures with great accuracy. In this scheme, the atomic potential is determined by a single parametrized potential, fitted to elemental data. In addition, only a single additional parameter is determined for each pair of different elements. Then, it is very important to make an accurate parametrization for this heteronuclear parameter. The energy is obtained as a sum of pair-like interactions, where the coefficient of the attractive part is dependent of the local environment. The scheme formulation is given by:

$$\begin{aligned}
 E &= \sum_i E_i = \frac{1}{2} \sum_{i \neq j} V_{ij} & V_{ij} &= f_C(r_{ij}) [f_R(r_{ij}) + b_{ij} f_A(r_{ij})] \\
 f_R(r_{ij}) &= A_{ij} \exp(-\lambda_{ij} r_{ij}) & f_A(r_{ij}) &= -B_{ij} \exp(-\mu_{ij} r_{ij}) \quad (2.23) \\
 f_C(r_{ij}) &= \begin{cases} 1 & r_{ij} < R_{ij} \\ \frac{1}{2} + \frac{1}{2} \cos[\pi(r_{ij} - R_{ij}) / (S_{ij} - R_{ij})] & R_{ij} < r_{ij} < S_{ij} \\ 0 & r_{ij} > S_{ij} \end{cases}
 \end{aligned}$$

where

$$\begin{aligned}
 \lambda_{ij} &= (\lambda_i + \lambda_j) / 2 & \mu_{ij} &= (\mu_i + \mu_j) / 2 & A_{ij} &= (A_i A_j)^{1/2} \\
 B_{ij} &= (B_i B_j)^{1/2} & R_{ij} &= (R_i R_j)^{1/2} & S_{ij} &= (S_i S_j)^{1/2}
 \end{aligned}$$

Here i, j and k label the atoms of the system and r_{ij} is the length of the ij bond. All subscripted parameters, such as λ_i and n_i , depend only on the type of atom (C, Si, Ge). The physical meaning of the main components of the equations are: E is the total energy, V_{ij} is the bond energy, f_R represents a repulsive pair potential, f_A corresponds to an attractive pair potential associated with bonding. The extra term f_C is merely a smooth cutoff function. The main idea of the Tersoff potential is that

the bond order depends upon the local environment. In particular, an atom with numerous neighbors forms weaker bonds than an atom with few neighbors. This is represented by function b_{ij} that is regarded as a monotonically decreasing function of the coordination of atoms i and j , and could be expressed as:

$$b_{ij} = \chi_{ij}(1 + \beta_i^{n_i} \zeta_{ij}^{n_i})^{-1/2n_i} \quad (2.24)$$

where

$$\zeta = \sum_{k \neq i, j} f_C(r_{ik}) \omega_{ik} g(\theta_{ijk})$$

$$g(\theta_{ijk}) = 1 + c_i^2/d_i^2 - c_i^2/[d_i^2 + (h_i - \cos \theta_{ijk})^2] \quad (2.25)$$

Here θ_{ijk} is the bond angle between bonds ij and ik . χ_{ij} is the heteronuclear parameter and must be parametrized with special care. Finally, ζ_{ij} is the function that reduces the bond strength when the number of bonds is increased.

2.2.2 Tight-Binding scheme

The Tersoff Classical Potential has been very useful for predicting various atomic systems, but if a better accuracy is required or quantum mechanical effects are significant, then a *semiempirical potential* is convenient. If the system is small, then it is possible to use *ab initio* calculations within an acceptable time interval. However, for systems with a large number of atoms, and no much charge transfer it is better to use a *semiempirical potential* such as the Tight-binding method (TB). This has been applied successfully to metals, semiconductors, fullerenes, ionic materials, etc.^{14,15}

The TB method starts by writing the eigenstates of the Hamiltonian in an *atomic-like basis set* $\{\Psi_{i\alpha}\}$, and replacing the exact many-body Hamiltonian operator with a parametrized Hamiltonian matrix. The atomic-like basis can be a

set of localized states with the same symmetry properties that the original atomic states. It is convenient to regard only valence and conduction states. The eigenstates (Ψ_i) and the eigenenergies (E_i) of the system could be obtained by solving the characteristic equation,

$$(\mathbf{H} - E_i \mathbf{S}) \Psi_i = 0 \quad (2.26)$$

where \mathbf{H} and \mathbf{S} are the Hamiltonian and overlap matrices respectively in the atomic-like basis set.

Slater and Koster proposed the original scheme of crystalline systems¹⁶. They started with an atomic orbital, $\phi_n(\mathbf{r} - \mathbf{R}_i)$, located on an atom with a vector position \mathbf{R}_i , and with quantum numbers denoted by the subscript n . Then, it can be formed a set of Bloch sums based on the atomic orbitals:

$$\Phi_{n,\vec{k}} = N^{-1/2} \sum_{\mathbf{R}_i} \exp[i\vec{k} \cdot \mathbf{R}_i] \phi_n(\mathbf{r} - \mathbf{R}_i) \quad (2.27)$$

where N is the number of periodic images (it can be infinite in principle). A Bloch sum is formed for each atomic orbital on each atomic site on the periodic unit cell. The eigenstates of the system are formed as a linear combination of the Bloch sums. However, Bloch sums, made of real atomic states, are not orthogonal. Then Slater and Koster used Lödwing functions Ψ_i , that form an atomic-like basis set based in real atomic states and make orthonormal the Bloch sums (see ref[15]). Using algebra, the Hamiltonian matrix elements can be expressed by

$$H_{i\alpha j\beta} = \sum_{\mathbf{R}_i} \exp[i\vec{k} \cdot (\mathbf{R}_j - \mathbf{R}_i)] \times \int \Psi_{i\alpha}^*(\mathbf{r} - \mathbf{R}_i) H \Psi_{j\beta}(\mathbf{r} - \mathbf{R}_j) d\mathbf{r} \quad (2.28)$$

where greek indices represent orbitals and roman indices a lattice position.

The key idea of Slater and Koster approach is to replace the integral with a parameter that depends only upon the inter-nuclear distance $|\mathbf{R}_i - \mathbf{R}_j|$, and the symmetry of the orbitals involved. This could be performed using first the "two centers approximation", that replaces the Hamiltonian potential part, formed by contributions of all atoms for a given potential caused by the two atoms involved (in equation (2.28)). Löwdin functions (Ψ_i) could be expressed as a sum of functions with well defined momenta with respect to the axis joining the atoms. In this way, it is possible to write the value of the integral between these expanded terms as a constant multiplied by an angular term (depending upon the symmetry of the functions and the direction cosines k , l and m of the vector $(\mathbf{R}_i - \mathbf{R}_j)$).

After the expansion, the Hamiltonian matrix elements could be written as

$$H_{i\alpha j\beta} = \sum_{\mathbf{R}_j, \mathbf{J}} \exp[i\vec{k} \cdot (\mathbf{R}_j - \mathbf{R}_i)] h_{\alpha\beta J}(|\mathbf{R}_j - \mathbf{R}_i|) G_{\alpha\beta J}(\vec{k}, l, m) \quad (2.29)$$

where \mathbf{J} denotes the angular momentum, $h_{\alpha\beta J}$ is the constant value given ($|\mathbf{R}_j - \mathbf{R}_i|$) and $G_{\alpha\beta J}(\vec{k}, l, m)$ is the angular dependence. Subsequently, the secular equation (2.26) could be solved for each value of \vec{k} from a selected set, and the densities of states can be calculated. Given the Hamiltonian matrix as a function of \vec{k} , the band structure is obtained by solving the single particle Schrödinger equation. It is clear that TB calculations will be, at most, as reliable as the parametrization used.

Then the approximations considered in the TB model are¹⁶:

- The total energy is divided into the sum of single-electron eigenvalues plus the sum of pair potentials.
- The elements of the Hamiltonian matrix depend only upon the vector between two atoms.

- A minimal set of orthogonal, short-range basis functions, which span the occupied subspace, are assumed to exist.
- Self-consistency is neglected, or approximated by onsite terms.
- A limited set of k-points is used to integrate over the Brillouin zone.
- The density matrix is taken to have a finite range.

In order to perform MDS, it is necessary develop the TB scheme as an atomistic method. It is needed that both band energy and repulsion energy be expressed as functions of the interatomic distance. Chadi¹⁷ proposed that the total energy could be written as

$$\mathbf{E}_{tot} = \mathbf{E}_{band} + \mathbf{E}_{rep} \quad (2.30)$$

with a repulsive energy term written as a sum of pair terms,

$$\mathbf{E}_{rep} = \sum_{i,j} U_{ij} \quad (2.31)$$

and the band structure energy can be calculated after performing the Hamiltonian diagonalitation, by adding the eigenvalues energy of the occupied states. That is,

$$\mathbf{E}_{band} = \sum_{\mathbf{k}} \sum_i \epsilon_i \mathbf{f}_i \mathbf{w}_{\mathbf{k}} \quad (2.32)$$

where \mathbf{f}_i is the occupation of the i^{th} eigenstate, and the $\mathbf{w}_{\mathbf{k}}$ are the weights given to the special k-points where the function will be calculated, so that $\sum_{\mathbf{k}} \mathbf{w}_{\mathbf{k}} = \mathbf{1}$ (see ref[18] for a discussion of special k-point selection). With Chadi's proposal, it is possible to obtain the TB parameters from *ab initio* methods. Finally, forces could be obtained using \mathbf{E}_{rep} and the Hellman-Feynman theorem, which states that $\mathbf{F}_{\lambda} = -\partial \mathbf{E}_{band} / \partial \lambda$, where λ is an atomic coordinate.

2.2.3 Non-orthogonal tight-binding

Conventional Tight-Binding is a very effective scheme, but it lacks of transferability. It is possible that the most important factor is the orthogonality assumed. Then, a natural approach, looking for transferability, is to incorporate the overlap between different basis functions, while retaining the empirical nature of the model. Porezag *et. al.* have used first-principles calculations with an atomic-like basis set to calculate and tabulate the Hamiltonian and overlap matrix elements¹⁹. Such parametrization is the one implemented in the TROCADERO code. The basics of the formalism are presented below.

In the Porezag *et. al.* approach, the tight-binding energy is still written as a sum of a band-structure term and a pair-repulsion term. Slater-type orbitals and spherical harmonics are used to construct an atomic basis:

$$\phi_\nu(\mathbf{r}) = \sum_{n,\alpha,l,m} a_{nm} r^{l+n} e^{-\alpha r} Y_{lm} \left(\frac{\hat{\mathbf{r}}}{r} \right) \quad (2.33)$$

This basis is then used to solve a modified Khon-Sham Hamiltonian equation,

$$\left[-\frac{\hbar^2}{2m_e} \nabla^2 + V_{pa}(\mathbf{r}) \right] \phi_\nu(\mathbf{r}) = \epsilon_\nu^{pa} \phi_\nu(\mathbf{r}) \quad (2.34)$$

where $V_{pa}(\mathbf{r})$ is the pseudo-atom potential

$$V_{pa}(\mathbf{r}) = V_{nucl}(\mathbf{r}) + V_H(\mathbf{r}) + V_{xc}(\mathbf{r}) + \left(\frac{\mathbf{r}}{r_0} \right)^N \quad (2.35)$$

V_{nucl}, V_H and V_{xc} are the nuclear, Hartree and exchange-correlation potentials respectively. The last term has the effect of concentrating the charge density closer to the atomic nucleus. It is performed because more concentrated atomic orbitals are more suitable for bulk calculations.

Once the ϕ_ν have been obtained, the tight-binding parametrization is carried out. The overlap matrix elements are tabulated as a function of the internuclear distance. In order to obtain the Hamiltonian matrix elements, an effective potential V_{eff} is constructed for each structure from the atomic contributions:

$$V_{eff}(\mathbf{r}) = \sum_i V_0(|\mathbf{r} - \mathbf{r}_i|) \quad (2.36)$$

where \mathbf{r}_i is the position of atom i , and $V_0^{(i)}$ is the Khon-Sham potential due to this atom, i.e. V_{pa} but without the term $(\mathbf{r}/r_0)^N$. Using this potential, the Hamiltonian matrix elements are tabulated from

$$\langle \phi_\nu^{(i)} | \mathbf{H} | \phi_\mu^{(j)} \rangle = \begin{cases} \epsilon_\nu^{(i)} & \text{if } \mu = \nu, j = i \\ \langle \phi_\nu^{(i)} | \mathbf{T} + V_0^{(i)} + V_0^{(j)} | \phi_\mu^{(j)} \rangle & \text{if } j \neq i \\ 0 & \text{otherwise} \end{cases} \quad (2.37)$$

where \mathbf{T} is the kinetic-energy operator.

In order to specify the model, the repulsive pair-potential must be determined. This is obtained using

$$V_{rep}(\mathbf{r}) = E_{SC}(\mathbf{r}) - E_{BS}(\mathbf{r}) \quad (2.38)$$

where E_{BS} is the band structure energy at separation \mathbf{r} obtained by diagonalizing the parametrized Hamiltonian, and E_{SC} is the total energy obtained from a self-consistent calculation performed on the same atomic configuration. The repulsive potential is usually fitted for diatomic molecules, but sometimes levels-crossing occur and a different model is required. It can be seen from equation (2.37) that only two centre integrals appear in the formalism. The scheme presented here has

been successfully applied to different systems, such as diamond, graphite or borane structures; showing a good accuracy and transferability^{14,18}.

2.3 The TROCADERO code

2.3.1 Code Structure

In order to perform our MDS, we have used a program called TROCADERO. It has been written using Fortran 90 by Eduardo Hernández from the Institut de Ciència de Materials de Barcelona¹⁴. Such a program was devised based on one observation: traditionally simulation packages are only built around an atomistic model, but it is not necessary. Usually, if one wants to compare results between different methods, it is necessary to use different simulation packages. However, the main structure of the MD simulation programs is independent of the atomistic model used. By making packages using numerous atomistic models, it would be easier to compare these models using the same program, and to use the code for calculating different molecular models. In particular, TROCADERO is capable of performing simulations with different approaches; they can be specified by the user in the input file. This could be performed because the program is organized in such a way that the simulation part of the code is independent of the details of the method employed.

The structure of TROCADERO is modular. A module in Fortran 90 is a collection of structured data declarations and subroutines. Data and procedures in a module are accessible in other sections of the program only by the expression **USE** *module_name*. In order to develop a multiple-algorithm multiple-model code like TROCADERO, each simulation algorithm and each atomistic model have to reside on a different module. Only the main program has a **USE** statement for each one of the different simulation modules and atomic-interaction modules. Although all models are accessible, the main program only calls those selected by the user in the input file. This availability does not imply any extra memory requirements. The variables used by any given model are declared, and are only allocated once the

model has been selected for the simulation. The modular structure allows to modify and extend the program in a straight forward fashion with a minimum disturbance in the pre-existing code.

A scheme of the main program of TROCADERO is presented below:

```
!*****
program trocadero
!*****

!  used modules

    use DFTB_module
    use EP_statistics_module
    use molecular_dynamics_module
    use single_configuration_module
    use structural_relaxation_module
    use structure_module
    use TB_statistics_module
    use Tersoff_module

!*****

!Start

    call read_input( debug, ... )

    ...

! allocate, read and check everything needed for specific models

    if ( calculation_model == model(1) ) then
        call allocate_DFTB( debug )
        call read_input_DFTB( debug )
```

```
    call set_up_DFTB( debug )
    call check_out_DFTB( debug, annealing, relax, static )
else if ( calculation_model == model(2) ) then
    call allocate_Tersoff( debug )
    call read_input_Tersoff( debug )
    call set_up_Tersoff( debug )
    call check_out_Tersoff( debug, annealing, relax, static )
end if

...

if ( dynamics ) then

    if ( calculation_model == model(1) ) then

        call molecular_dynamics( debug,                                &
            average_statistics_TB, evaluate_energy_DFTB,             &
            final_structure_TB, read_restart_dynamics_TB,           &
            reset_averages_TB, statistics_TB, ...)

    else if ( calculation_model == model(2) ) then

        call molecular_dynamics( debug,                                &
            average_statistics_EP, evaluate_energy_Tersoff,         &
            final_structure_EP, read_restart_dynamics_EP,           &
            reset_averages_EP, statistics_EP, ...)

    end if

end if

end if
```

```
...  
  
end program trocadero
```

2.3.2 Capabilities of TROCADERO

All data needed for simulations using TROCADERO can and must appear in the input file. It includes the structural model, the simulation type, the specifications of the system under study, and the parameters needed for the specific models. Identification of each data uses command names in the input file such as `textitnumber_of_time_steps` or `external_pressure`. This structure in the input data provides flexibility to the options that can be available to the user. In particular, the simulation cell can be defined either in a matrix form or in magnitudes and angles. All values must be presented in atomic units.

Different simulation models available are:

- *Single configuration*. Given a structure, the program provides output information of the energy, atomic forces, atomic neighbors and electronic structure.
- *Structural relaxation*. The atoms are moved in the simulation box until a minimal configuration is reached. This model uses a Conjugate gradient scheme.
- *Molecular Dynamics Simulations*. TROCADERO can perform simulations in different ensembles such as microcanonical (NVE), canonical (NVT), isothermal-isobaric (NPT) and isobaric-isoenthalpic (NPH).

In this work, we have used *Single configuration*, *Structural relaxation* and *Molecular Dynamics Simulations* in the (NPT) ensemble. The methodology used for simulating (NPT) ensemble in TROCADERO is that presented in previous sections: a Nose-Hoover thermostat within a Nosé–Poincaré transformation combined with the Souza-Martins scheme for constant pressure considering a flexible simulation cell.

Several atomistic models are available in TROCADERO such as the Glue potential, Tersoff, and Tight-Binding. The last two have been used for the calculations

presented in this work. The Tersoff potential is implemented like in ref[13], with a change in the cutoff function of equation (2.23) because the original potential has a discontinuity in the second derivative¹⁴. The proposed function is a Fermi-like function, in which all derivatives are continuous:

$$f_C(\mathbf{r}_{ij}) = \frac{1}{1 + e^{\alpha(\mathbf{r}_{ij} - \mathbf{r}_{ij}^C)}} \quad (2.39)$$

where \mathbf{r}_{ij}^C is the average between \mathbf{R}_{ij} and \mathbf{S}_{ij} , and α is a single parameter fitted to obtain a function as similar as possible to the original one. The TB scheme implemented in TROCADERO is the non-orthogonal designed and parametrized by Porezag *et. al.*.

TROCADERO has been successfully used for a great variety of systems, mainly carbon nanostructures and related materials¹⁴. It has performed calculations of the Young's modulus of carbon nanotubes²⁰, stability of Fullerene structures²¹, Haeckelites²², Schwartzites²³, growth mechanism for carbon nanotubes in presence of Boron²⁴, etc. Also this has been used for studying BN nanotubes²⁵, SiC semiconductors²⁶ and metallic systems inside carbon structures²⁷. Such results confirms the reliability of TROCADERO in materials modeling simulations.

REFERENCES

1. D. C. Rapaport. *The Art of Molecular Dynamics Simulation*. Cambridge University Press, Cambridge, 1995
2. D. Frenkel and B. Smit. *Understanding Molecular Simulation*. Academic Press, 2002
3. M. E. Tuckerman and G. J. Martyna, J. Phys. Chem. **104**, 159 (2000)
4. M. E. Tuckerman, Yi Liu, G. Ciccotti, G. J. Martyna, Journal of Chemical Physics **115**, 1678 (2001)
5. H. C. Andersen, J. Chem. Phys. **72**, 2384 (1980)
6. S. Nosé, J. Chem. Phys. **81**, 511 (1984)
7. S. Nosé, Mol. Phys. **52**, 255 (1984)
8. W. G. Hoover, Phys. Rev. A **31**, 1695 (1985)
9. W. G. Hoover, Phys. Rev. A **34**, 2499 (1986)
10. E. Hernández, Journal of Chemical Physics **115**, 10282 (2001)
11. S. D. Bond, B. J. Leimkuhler and B. B. Laird, J. Comput. Phys. **151**, 114 (1999)
12. I. Souza and J. L. Martins, Phys. Rev. B **55**, 8733 (1997)
13. J. Tersoff, Phys. Rev. B **39**, 5566 (1989)
14. R. Rurali and E. Hernández, Computational Materials Science **28**, 85 (2003)
15. J. C. Slater and G. F. Koster, Phys. Rev. **94**, 1498 (1954)
16. C. M. Goringe, D. R. Bowler and E. Hernández, Rep. Prog. Phys. **60**, 1447 (1997)
17. D. J. Chadi, Phys. Rev. B , **19**, 2074 (1979)

18. H. J. Monkhorst and J. D. Pack, Phys. Rev. B **13**, 5188 (1976)
19. D. Porezag, T. Frauenheim, Köhler, G. Seifert and R. Kaschner, Phys. Rev. B **51**, 12947 (1995)
20. E. Hernández, C. Goze, P. Bernier, A. Rubio, Phys. Rev. Lett. **80**, 4502 (1998)
21. E. Hernández, P. Ordejón, H. Terrones, Phys. Rev. B **63**, 193403 (2001)
22. H. Terrones, M. Terrones, E. Hernández, N. Grobert, J. C. Charlier, P. M. Ajayan, Phys. Rev. Lett. **84**, 1726 (2000)
23. F. Valencia, A. H. Romero, E. Hernández, M. Terrones, H. Terrones, New Journal of Physics **5**, 123 (2003)
24. E. Hernández, P. Ordejón, I. Boustani, A. Rubio, J. A. Alonso, J. Chem. Phys. **113**, 3814 (2000)
25. D. Sánchez-Portal, E. Hernández, Phys. Rev. B **66**, 235415 (2002)
26. S. A. Shevlin, A. J. Fisher, E. Hernández, Phys. Rev. B **63**, 195306 (2003)
27. F. Banhart, E. Hernández, M. Terrones, Phys. Rev. Lett. **90**, 185502 (2003)

Chapter 3

Molecular Dynamics Studies of C_{60} Under Pressure

In this chapter, Molecular Dynamics Simulations on C_{60} crystals using the NPT ensemble will be discussed. The aim is to understand the intermolecular bonding formation between C_{60} molecules under pressure at different temperatures. The molecular dynamics calculations for this chapter were performed using the TRO-CADERO code, and considering the Tersoff Classical Potential¹ for establishing interactions between carbon atoms.

3.1 Different crystalline arrangements

The first approach considered pressure effects and different orientations of C_{60} molecules in a crystalline environment. The time during simulations lasted 4 picoseconds in timesteps of 0.1 femtosecond. The total simulated time appears to be small, but it is large enough for providing valuable physical information. The intermolecular potential used for these simulations was the Tersoff Classical Potential, presented in the previous chapter. This potential does not consider Van der Waals interactions; however, it is justified to use such a potential because our simulations are performed under pressures in the Gigapascal order. The initial configurations were formed by a supercell constructed for each crystalline system. These supercells consisted of periodic crystals containing C_{60} molecules exhibiting the same orienta-

tions for all starting configurations. At the beginning of each simulation there are not intermolecular links established between the C_{60} molecules. The calculations were performed for C_{60} molecules packed in different ways: pristine fcc, rhombohedral, and tetragonal or orthorhombic. The parameters used in all our calculations are those presented by Nuñez-Regueiro *et. al.*². The temperature of the systems was 300 K in order to observe the dynamics under pressure and other orientation effects.

The initial orientations used in all crystalline systems are presented below. These exhibit different face-to-face atom configuration between neighboring C_{60} molecules (see figure 3.1). In addition to the initial orientations, some preferential orientations were included for the fcc arrangement.

3.1.1 Face Centered Cubic Structure

The C_{60} molecules crystallize in a fcc arrangement at room temperature³. In order to simulate this system, the supercell was formed by a 2*2*2 arrangement of conventional fcc cells, so a total of 32 molecules were used in our simulation box. The parameters used were $a = b = c = 14.17\text{\AA} = 26.786a.u.$ and $\alpha = \beta = \gamma = 90^\circ$. Each vector defining the conventional cell is parallel to a cartesian axis; a with “x” axis, b with “y” axis and c with “z” axis. In addition to the five initial orientations presented above, other two initial orientations were also used for this phase. The orientation (a) in figure 3.2 presents ‘double bonds facing’, between neighboring C_{60} molecules, in the $[011]$ and $[0\bar{1}1]$ directions. The orientation (b) of figure 3.2 presents ‘double bonds facing’ in the $[011]$ and $[101]$ directions. The aim of those preferential orientations is to promote [2+2] cycloadditions between double bonds.

The simulations were performed under different pressures of 5, 10 and 20 GPa for each initial orientation. The simulations using the fcc arrangement presented a great temperature stability as can be observed in figure 3.3, with a variation of approximate ± 15 K during the last simulated picosecond. The phase appears to be preserved throughout the 4 picoseconds in all simulations. However, the intermolec-

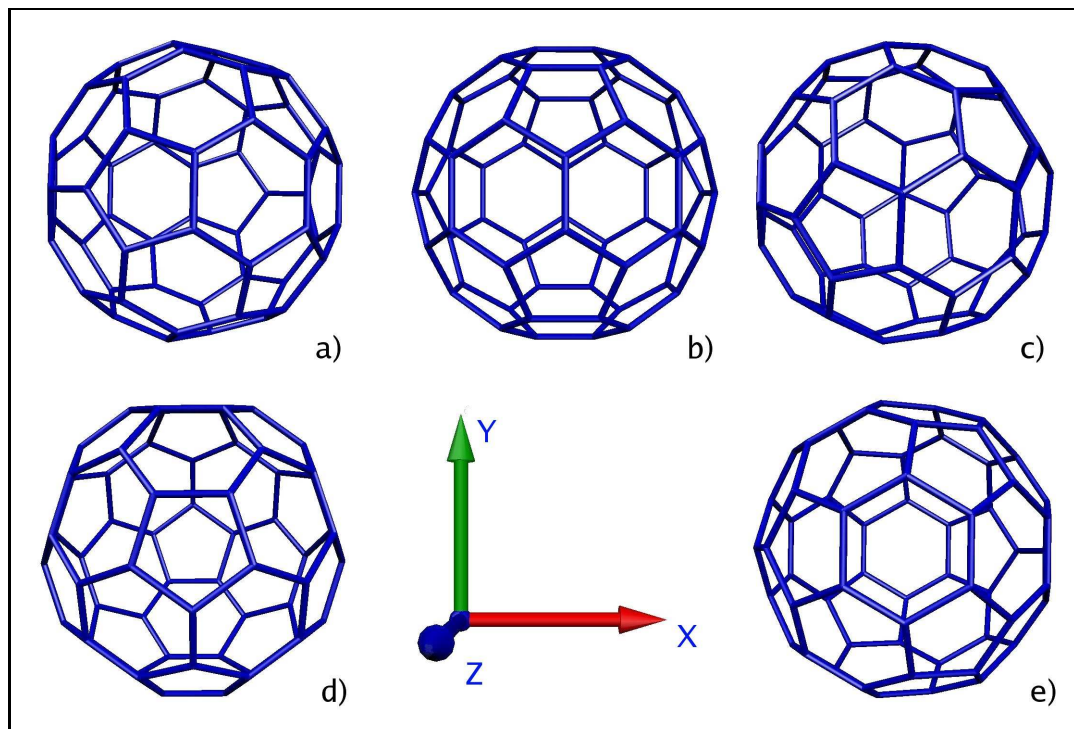


Figure 3.1: Initial orientations of the C_{60} molecules for the room temperature simulations performed in this work: a) The C_{60} molecule possesses two single bonds contained in the yz plane, and the z axis passes throughout the middle of such bonds; b) the molecule has two double bonds contained in the xy plane, another two in the yz plane and other two in the xz plane; c) in this orientation the z axis passes throughout two atoms that are equivalent by inversion symmetry; in addition, two single bonds are contained in the yz plane; d) the z axis passes throughout the centers of two pentagons and the yz plane coincides with a two-symmetry plane of the C_{60} molecule; e) The z axis passes throughout the centers of two hexagons; in addition two opposite atoms of each hexagon are contained in the yz plane.

ular connections found were only a few; the maximum number of intermolecular connections in one simulation was four and, in that specific case, the links were established by one bond. In one particular simulation, we observed an individual two-bond intermolecular connection, formed by joining the extreme atoms of adjacent hexagons from different C_{60} molecules (see figure 1.8).

It has been shown that C_{60} molecules rotate freely in most simulations, as is

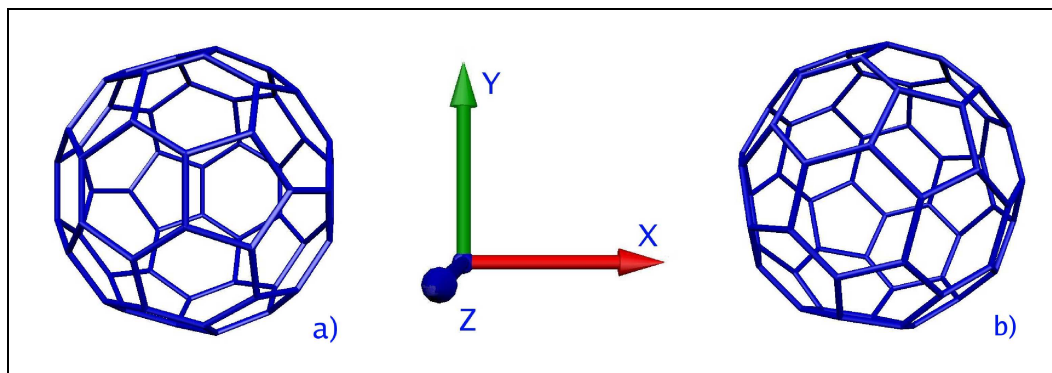


Figure 3.2: Preferred orientations for the fcc phase. Such configurations promote the formation of [2+2] cycloadditions between double bonds in the fcc arrangement.

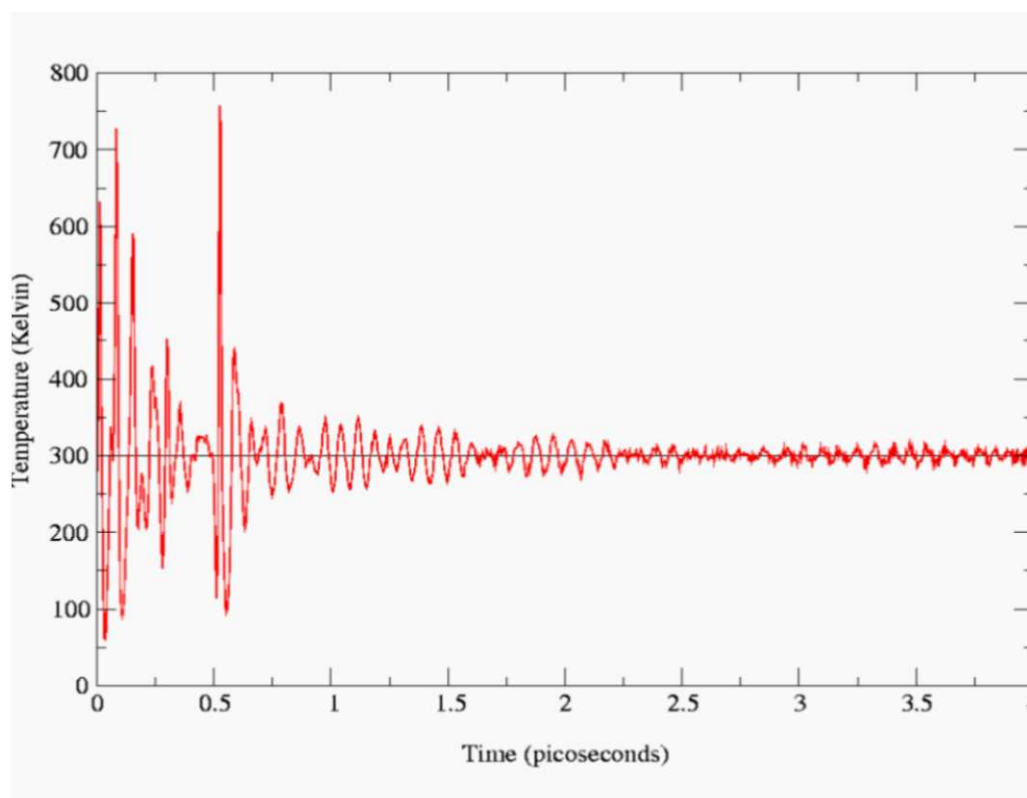


Figure 3.3: Typical thermal stability found in our simulations as a function of time for the fcc arrangement. The set temperature was 300 K.

supposed to occur experimentally at temperatures greater than 249 K⁴. However, simulations carried out under 20 GPa, we observed a 'freezing effect' of the molecules in some occasions. In general, these calculations resulted in C_{60} molecules randomly oriented. However, in one of our simulations an *ordered phase* with freezing effect ap-

peared after 4 picoseconds of calculation. In order to obtain a better understanding, an additional simulation carried out under 25 GPa was performed. Here, it would be possible to observe that others initial configurations result in ordered phases if pressure is increased in small steps, using a longer simulation time. The resulting structure can be compared with that proposed by Guo *et. al.*⁵ (see figures 3.4 and 3.5). It can be noted that the configurations are very similar, but the phase obtained in our work is arranged by planes along the b direction, as can be seen in figure 3.4 c). However, both arrangements are qualitatively similar, because first neighbors face in the same way in both crystal structures. If an ordered phase, similar to that presented here, could be obtained experimentally after applying pressure, it is possible that it would exhibit a combination between the structure reported by Guo *et. al.* and ours. A possible route to obtain this phase is by applying high hydrostatic pressure (20 to 25 GPa), gradually in small steps, at room temperature. The application of non-hydrostatic pressure could result in the destruction of the C_{60} cages when pressures exceed 16 GPa^{6,7}. It is noteworthy that Guo *et. al.* reported a prediction for packing C_{60} molecules, in a fcc lattice at ambient conditions. They observed that facing the hexagons is the preferential state, as can be observed in figures 3.4 and 3.5. Then, such a phase is different to the low temperature simple cubic one, which faces rich-electronic double bonds with low-electronic centers of hexagons or pentagons^{8,9}.

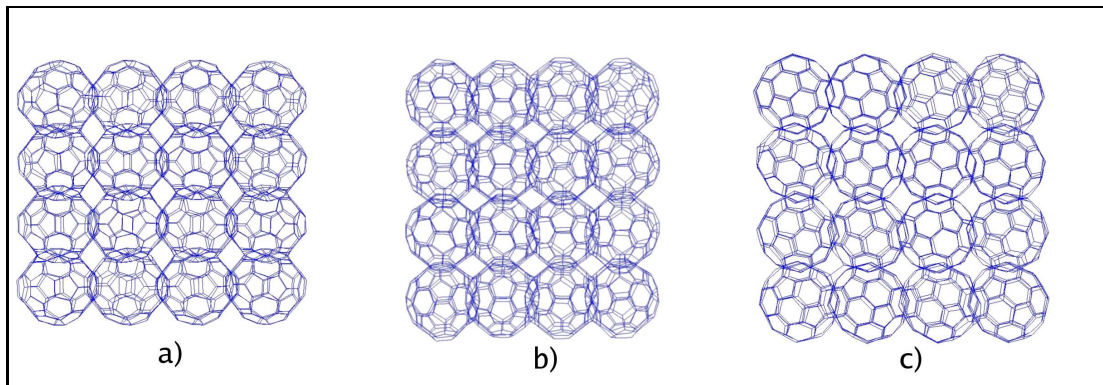


Figure 3.4: Ordered C_{60} crystal obtained after applying pressure. The images are oriented in the same way as in figure 3.5.

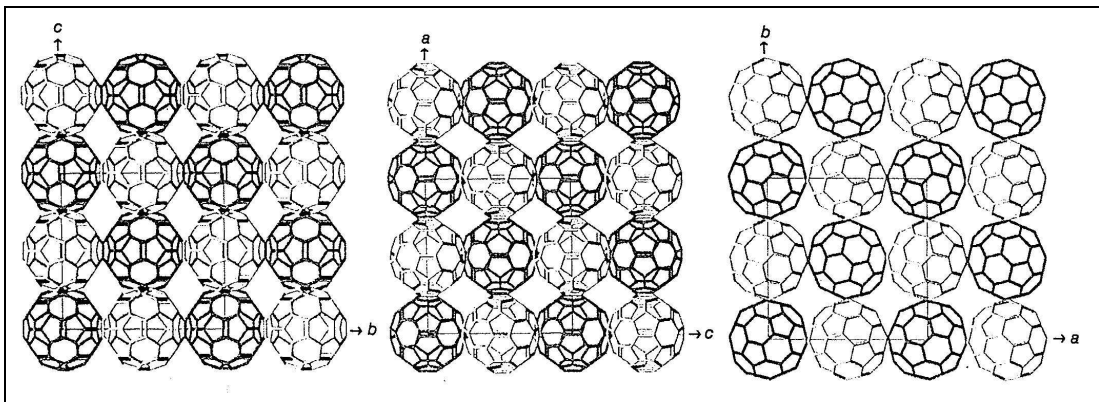


Figure 3.5: Phase ordered proposed by Guo *et. al.* ref[5]. Molecules with different color are at different planes over the c direction.

3.1.2 Rhombohedral Structure

The C_{60} molecules could be 2D-polymerized in a rhombohedral lattice under pressures at 6 GPa and temperatures of 873 K¹⁰ (see figure 1.3). In order to simulate this system, the supercell was created by a 2*2*2 arrangement of conventional cells, so that a total of 24 molecules (non-polymerized) were placed in the simulation box. The conventional cell is depicted in the figure 3.6. In the orientation used in our simulations, vector a was parallel to “x” axis, and vector c to “z” axis. The parameters used are those presented by M. Nuñez-Regueiro *et. al.*² for the polymerized phase, $a = b = 9.19\text{Å} = 17.37$ a.u. and $c = 24.50\text{Å} = 46.31$ a.u., $\alpha = \beta = 90^\circ$ and $\gamma = 60^\circ$. We performed 15 simulations: five initial orientations under three different pressures(5, 10 and 20 GPa).

The pressure provoked the reduction of the cell size and a closer packing of the C_{60} molecules. As in the fcc simulations, there were few intermolecular connections established between C_{60} molecules, less than four in each simulation run. Only one cycloaddition containing two intermolecular bonds was observed, and it occurred at 20 GPa. This cycloaddition involved atoms that are not directly connected in the same C_{60} molecule (see figure 3.7). To the best of our knowledge this connection has not been reported hitherto, although it is very similar to the one used by Berber *et. al.* for calculating the mechanical properties of polymerized C_{60} cages¹¹.

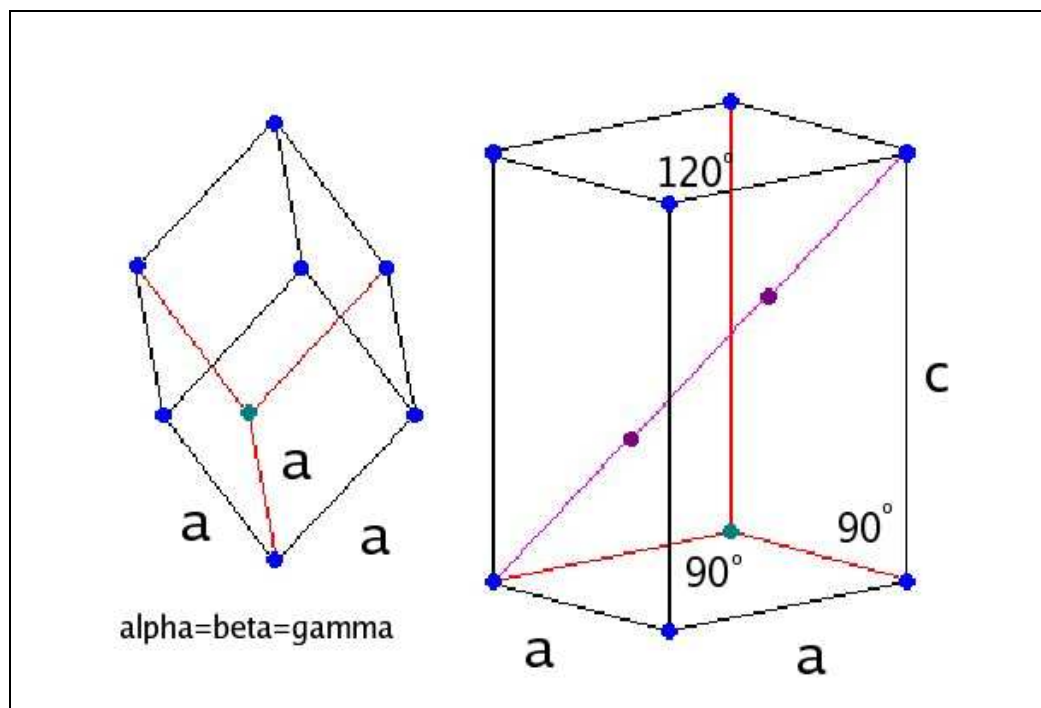


Figure 3.6: On the left is the unitary cell for the rhombohedral lattice. On the right is the conventional cell for the rhombohedral lattice. For the simulations performed in this chapter the origin is set on the left-down point, so that the angle γ had a value of 60° . Image from <http://www.uwgb.edu/dutchs/symmetry/rhombo-lattice.htm>

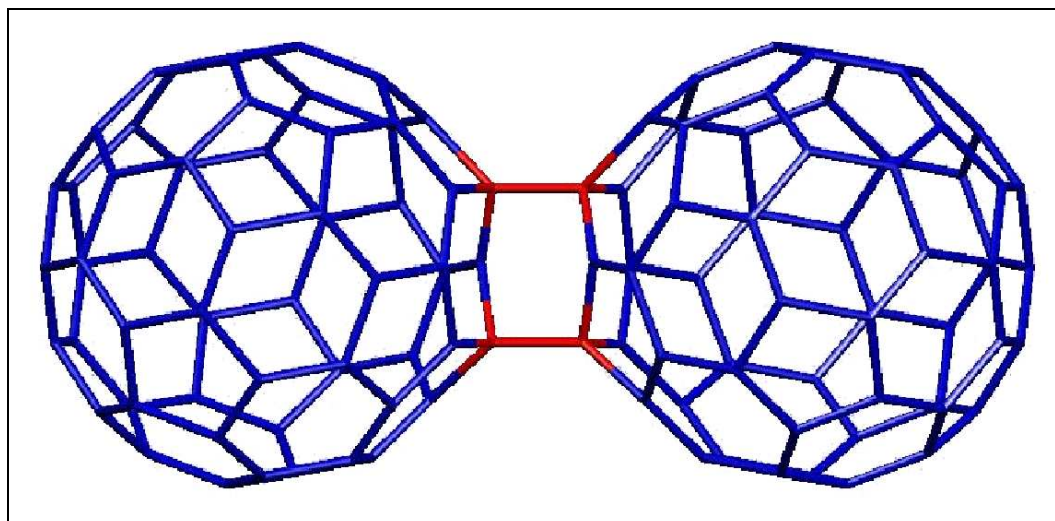


Figure 3.7: First new cycloaddition found in this work. It appeared in a simulation carried out at 20 Gpa using a rhombohedral lattice.

The molecules preserved the free cage rotation, even at 20 GPa; no ordered phases were observed. The temperature was stable, as can be witnessed in figure 3.8. However, it is less stable than that obtained for the fcc case.

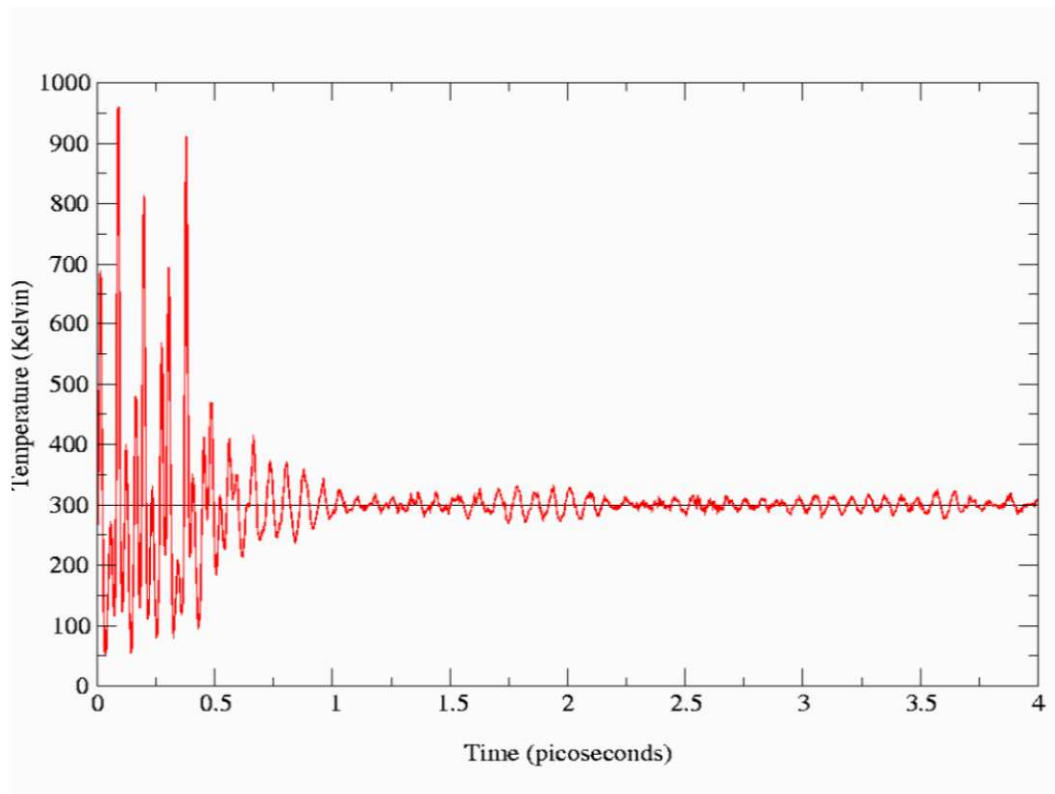


Figure 3.8: Typical temperature stability for C_{60} cages in a rhombohedral arrangement. The temperature was set to 300 K.

3.1.3 Tetragonal Structure

The arrangements of the C_{60} molecules (if they were not connected by bonds) in the fcc, rhombohedral, tetragonal and orthorhombic phases are not very different, as can be seen in figure 1.4. We have chosen the tetragonal and orthorhombic phases, specified by the parameters reported by Nuñez-Regueiro *et. al.*²; but considering an individual C_{60} molecule centred in the (0, 0, 0) point of the cell, instead of having two C_{60} molecules in the cell; as in the polymerized phases, one in (0, 0, 0) and the other in (0.5, 0.5, 0.5) (fractional coordinates). Then, we worked with the orthorhombic and tetragonal phases that are less dense than the orthorhombic and

tetragonal C_{60} polymerized phases.

The supercell for the simulations considered a $3*3*3$ arrangement of unit cells, then 27 molecules were placed in the simulation box. The parameters used here were $\mathbf{a} = \mathbf{b} = 9.09\text{\AA} = 17.183$ a.u. and $\mathbf{c} = 14.95\text{\AA} = 28.261$ a.u., and $\alpha = \beta = \gamma = 90^\circ$. The vectors \mathbf{a}, \mathbf{b} and \mathbf{c} are parallel to axis “x”, “y” and “z” respectively.

Simulations under 5, 10 and 20 GPa were performed for each initial orientation. All simulations at 10 and 20 GPa resulted in catastrophic values. In such a way that simulations did not complete the planned simulation time (a ‘fortran stop’ message appeared on the screen). This could be caused by the initial crystal structure, which is far away from the equilibrium configuration for a non-polymerized C_{60} structure. In addition, at high pressures the dynamics could affect considerably the fictitious coordinates and momenta of the metric tensor (see equation 2.22). The simulations carried out under 5 GPa were able to complete the simulation time after 4 picoseconds, but the stability was extremely poor.

The cell shape changed considerably and the cell volume decreased. This resulted in a phase exhibiting a higher density than that of the initial configuration. Different simulations resulted in different cell’s parameters, but time was not long enough for establishing a phase transformation into a fcc or a rhombohedral arrangement. The simulation carried out at 5 GPa. showed one cycloaddition between double bonds.

3.1.4 Orthorhombic Structure

As in the tetragonal case, the supercell was formed by a $3*3*3$ arrangement of unit cells, so that 27 molecules were fixed in the simulation box. The parameters considered were $\mathbf{a} = 9.26\text{\AA} = 17.5$ a.u., $\mathbf{b} = 9.88\text{\AA} = 18.677$ a.u. and $\mathbf{c} = 14.22\text{\AA} = 26.88$ a.u., and $\alpha = \beta = \gamma = 90^\circ$.

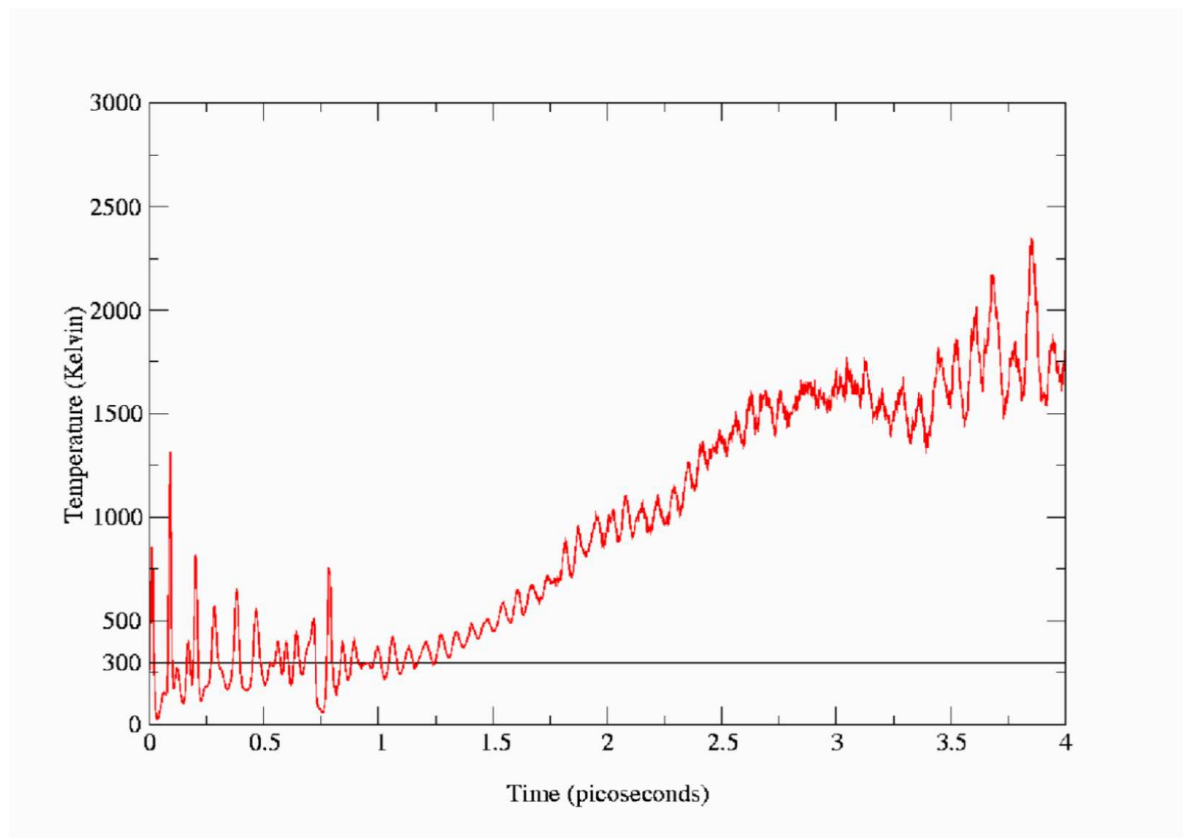


Figure 3.9: Typical temperature behavior for the tetragonal arrangement used. The desired temperature was set to 300 K and the applied pressure was 5 GPa.

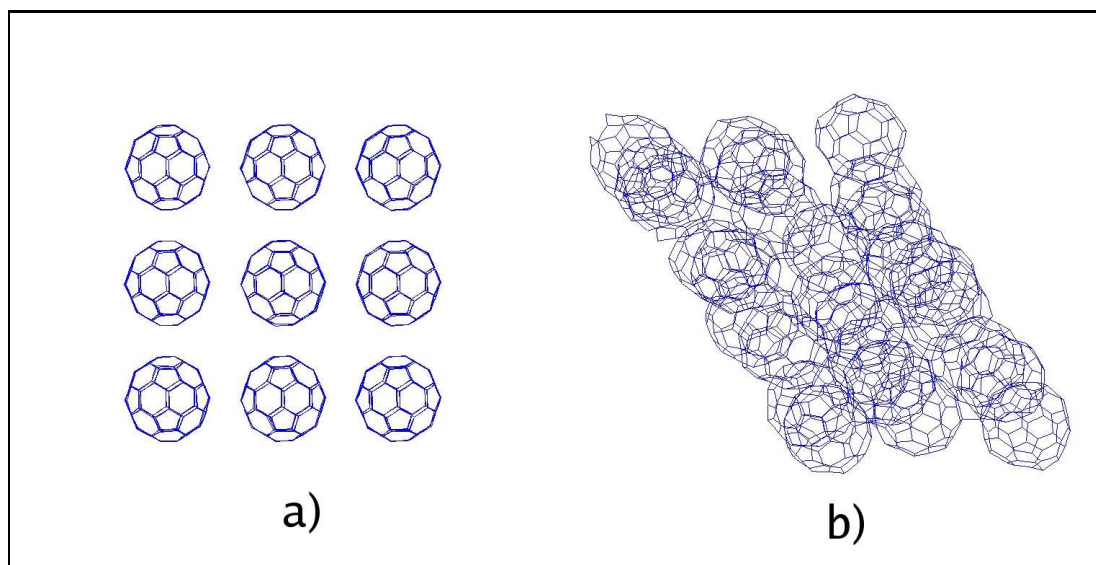


Figure 3.10: Phase transition observed from the tetragonal configuration (a) to a closer packing (b) obtained after applying a pressure of 5 GPa.

We observed once more, a numerical collapse for the simulations carried out under 10 and 20 GPa. In addition, the phase transition occurs faster and the system is less stable. Additional simulations were performed at 6, 7, 8, and 9 GPa. These simulations showed that 5 GPa was the maximum pressure that could be applied without suffering from a numerical or structural collapse (breaking of C_{60} molecules). Simulations without velocity rescaling resulted in numerical collapses at 6 GPa. Calculations using velocity rescaling quickly broke the C_{60} cages at all pressures. For simulations carried out at 5 GPa, the system resulted in a denser phase, but the temperature stability indicates that a structural collapse was about to occur. One intermolecular connection considering two bonds was formed in one simulation, but this also involved the breaking of the C_{60} cage.

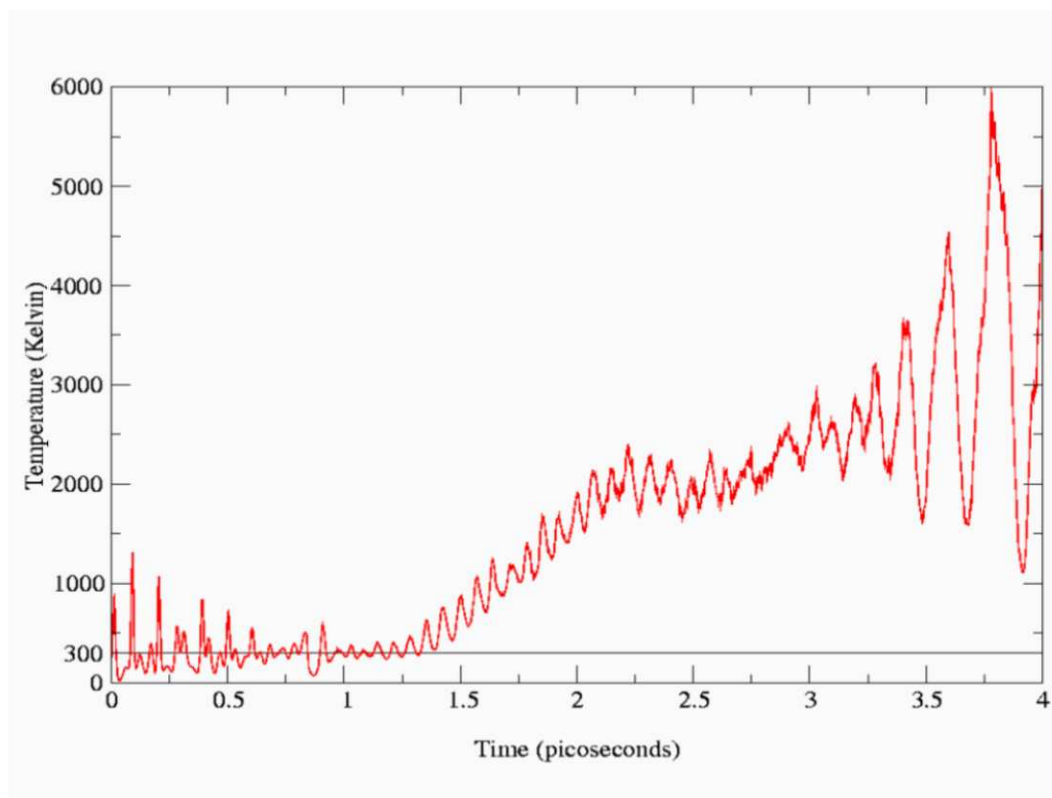


Figure 3.11: Typical temperature behavior experienced by the orthorhombic arrangement. The temperature was set to 300 K.

3.1.5 Brief discussion

It has been found an ordered phase after applying high pressures. This phase could now be treated at high temperatures so that a novel polymerized structure is created. It must be noted that our ordered phase was found after considering several initial C_{60} orientations in our MD calculations. In addition, the use of a conventional cell was important; if an odd number of molecules had been considered in our simulation box, the ordered structure (of even nature) could not be found.

The simulations carried out with an orthorhombic, or tetragonal arrangements, had an initial configuration, which was very far away from the equilibrium. These results demonstrated that the TROCADERO code is sensible to the initial configuration. However, the code is very stable for structures near the equilibrium. The tetragonal and orthorhombic structures used in our calculation had an extremely lowly density and were tested under extremely high pressures. Therefore, the artificial coordinates and momenta of the metric tensor were required to change abruptly. Therefore, the TROCADERO code failed in some of our simulations, but this could be sorted out by considering crystalline structures near the equilibrium.

3.2 Temperature and pressure Effects

The polymerization process of C_{60} molecules occurs when both temperature and pressure are applied. Then, several simulations at different pressures and temperatures have been performed in order to study how the intermolecular bonds are established. First a simulation, looking for a fcc configuration of C_{60} molecules randomly oriented, was performed. The conditions used here were room temperature and a pressure of 0.0 GPa; the simulation time lasted 4 picoseconds. The initial structure was a supercell of $3*3*4$ unitary cells of the fcc arrangement. Therefore, 36 molecules were placed in the simulation box. The final configuration of such a simulation was used as the starting structure of a series of simulations carried out at different pressures and temperatures.

Sixty-four simulations were performed in order to study the effect of using different combinations of temperatures and pressures. The temperatures were ranged from 600 K up to 1300 K in 100 K steps, and different pressures were applied from 2 GPa to 16 GPa in 2 GPa steps. All of them used the same starting configuration of 36 C_{60} molecules.

3.2.1 Intermolecular connections between C_{60} molecules

These *intermolecular connections* could be described as the covalent links established between neighboring C_{60} cages. From now on, it will be used the convention for naming intermolecular connections specified in Appendix A. The table related to different intermolecular connections found in our 64 simulations mentioned previously are presented in Appendix B. Molecular models of the most important links will be presented on chapter 4.

The most common connections for two adjacent C_{60} molecules reported in literature are 6565, 65652, 6666 and 14h14h. From the tables, it is clear that these connections are mainly absent in our simulations. This could be explained by the high temperatures, which allows the stabilization of various configurations that are not of minimal energy. We found a common characteristic in most of our connections: the carbon atoms from the same C_{60} involved in the intermolecular bonds are not connected between them by a covalent bond, *i. e.* they are not first neighbors. An intermolecular connection formed in this way will be called *second neighbor connection* or SN connection. The angles formed by the bonds on these connections are closer to those of 120° formed by sp^2 hybridized bonds in the graphite and those of 109° formed by sp^3 hybridized bonds in diamond. Graphite or diamond-like angles could represent less stress at the atom involved directly in the intermolecular bond than that of 90° angles of the [2+2] cycloaddition. However, it could increase the total stress of the structure due to an increase in curvature. Then, it is possible (and logic) that other intermolecular connections, different from [2+2] cycloaddi-

tion, could be observed experimentally in the polymerized C_{60} structures, at least under high pressures and high temperatures.

From the atomic coordinates obtained at different time frames of our MD calculations, it is noted that, once an intermolecular link is created, the first neighbors of the atom involved in the covalent bond become restricted. This is because the atom involved in the link exhibits an sp^3 hybridization and tries to keep all its bonds in a tetragonal fashion. However, the second neighbors possess more mobility. This rises the probability for the second neighbors to be involved in an additional intermolecular connection. However, these results should be considered with caution because an empirical potential has been applied in our calculations. It is noteworthy that these simulations were capable to show Stone-Wales-type transformations in two of the sixty-four calculations performed.

Although the information obtained is limited from an statistical point of view, it is clear that some C_{60} connections appeared several times. The most important C_{60} - C_{60} links, with more that 20 repetitions were: 13h13ha (24), 13h13hb (27), 13h13h2a (29), 13h13h2b (37), 13h13p (79), 13h13p2 (141), 13h14h (23), 13h14h2 (23) and 13p13p2 (52). All of them are SN connections. Interestingly, these connections represent a family of connections that have not been proposed earlier (except the 13h13h2a which was proposed by Berber *et. al.*¹¹). It can also be seen that the unit 13p (see appendix A) appears in a great number of intermolecular connections. At this point, it is not clear why this specific connection is present in our calculations. However, the deformation of pentagons could result in additional structural stress due to an increase in curvature. Thus, it is possible that such connections do not survive after releasing the pressure.

We also found intermolecular links that involve three or four intermolecular bonds. An important point is that they are also SN connections. Such connections could be more stable than the SN links considering only two intermolecular bonds. They also could exhibit intriguing electronic and mechanical properties.

	2GPa	4GPa	6GPa	8GPa	10GPa	12GPa	14GPa	16GPa
600 K	24 - 0	37 - 0	49 - 0	59 - 0	80 - 0	91 - 0	78 - 2	95 - 0
700 K	28 - 1	44 - 0	61 - 0	76 - 1	83 - 0	92 - 1	97 - 3	93 - 0
800 K	28 - 1	35 - 1	45 - 1	72 - 0	85 - 2	94 - 3	98 - 5	96 - 9
900 K	19 - 1	26 - 0	51 - 2	67 - 3	95 - 3	91 - 4	94 - 2	100 - 10
1000 K	16 - 2	27 - 2	51 - 3	66 - 6	79 - 11	82 - 10	89 - 11	77 - 21
1100 K	15 - 5	50 - 4	43 - 5	76 - 10	71 - 10	69 - 23	83 - 19	83 - 27
1200 K	14 - 2	32 - 10	43 - 11	72 - 13	70 - 20	81 - 26	76 - 35	70 - 32
1300 K	15 - 9	34 - 14	54 - 18	64 - 21	65 - 38	74 - 28	78 - 39	69 - 46

Table 3.1: Number of intermolecular links formed. Each square corresponds to one of the 64 simulations. On the left of each square is the number of intermolecular bonds formed by one bond. On the right of each square is the number of intermolecular bonds formed by two or more bonds.

In the table 3.1 all the intermolecular connections are counted, excepting those that involve the breaking of two or more of the original \mathbf{C}_{60} bonds. In all the simulations, various intermolecular covalent links established by only one bond are found, in such a way that the final structures were highly polymerized. However, they are not considered on the tables of Appendix B. By increasing the pressure and temperature the polymerization process is enhanced among the \mathbf{C}_{60} cages. The maximum values considered in our simulations are already higher by several hundred degrees and several GigaPascals when compared to the experimental values for polymerization processes presented by Davidov *et. al.*¹⁰.

Nine additional simulations were performed at high temperature and high pressure, considering the combinations of 12, 14 and 16 GPa and 1100, 1200, 1300 K. A conventional fcc \mathbf{C}_{60} cell was used, then the simulation box contained 240 atoms. The simulated time lasted 10 picoseconds. Simulations with 36 molecules in the simulation box have shown that most of the intermolecular connections found after

20 picoseconds were already formed at 10 picoseconds. These calculations resulted in the following connections: 13h13h2b, 13h13p, 13h13p2, 13p14h, 13p13p2, 13h652 and 3link3. We also found various links established by one intermolecular bond. This demonstrates that the reduction of molecules in the simulation box keeps the main characteristics of the connection behavior. However, it is clear that the reduction of the cell size also leads to a reduction of possible system configurations and connections.

Additional simulations carried out at 25 GPa and 1000 K shown that the number of intermolecular connections with three and four bonds are increased. In fact, the number of such connections is close to the fourth part of the total number of connections established. We envisage intriguing electronic properties of these novel molecular connections.

3.2.2 Dynamical characterization

The initial structure used for the 64 simulations was similar to those found naturally. The only significant difference could be the distances between neighboring C_{60} molecules, because the Van der Waals forces are not considered by the TRO-CADERO code. However, these forces could be neglected due to the large applied pressures. When the pressures are in the GPa range, the C_{60} molecules get closer, in such a way that the short range forces become more important than the long range interactions. Therefore, the use of a code without considering Van der Waals interactions is justified and our obtained results are reliable within this code limitation.

Figure 3.12 depicts a good temperature stability for the most extreme situation: pressures of 16 GPa and temperatures of 1300 K. The equilibrium value coincides with the set temperature. Fluctuations of ± 50 K occurs after the third picosecond and this situation is maintained during the simulated time (20 picoseconds). This result supports the reliability of the code for systems that do not need an extremely fast change in the shape or size of the simulation box.

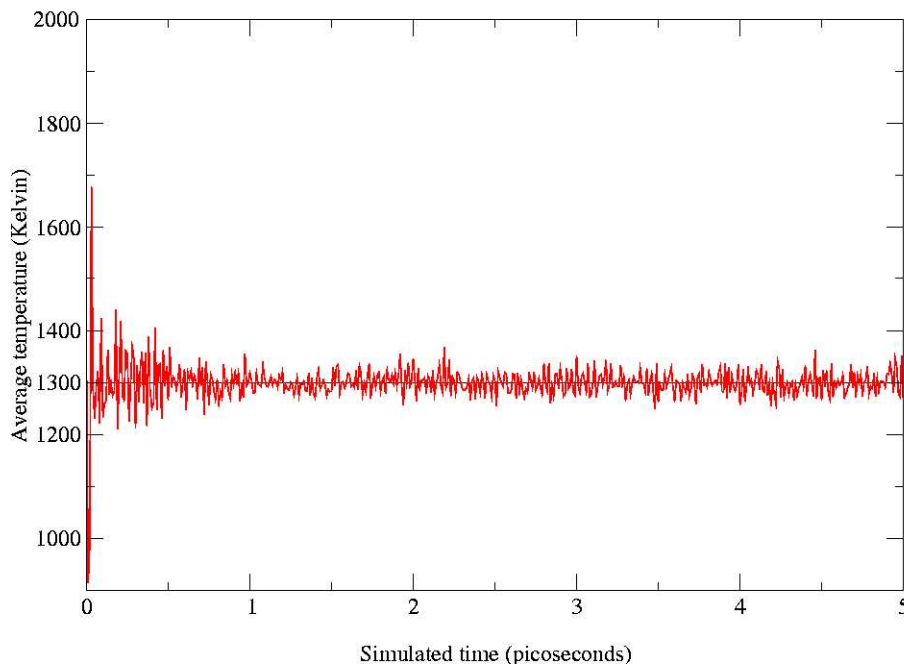


Figure 3.12: Temperature stability for a C_{60} crystal under 16 GPa and 1300 K. It shows a reliable stability for most extremal conditions. Fluctuations are well bounded after the third picosecond.

The average volume *vs* average pressure for the highest and the lowest simulated temperature at different pressures is depicted in figure 3.13. Here, we observe an almost linear behavior. The volume is rather dependent on the pressure than on the temperature. It leads to a very similar line with negative slope for the eight temperature series of simulations (only two lines have been presented in order to obtain a better visualization). These behavior demonstrates the reliability of the code used in our calculations.

The distance between centers of neighboring C_{60} cages in the initial configuration was set to 10.21 Å. This value is slightly greater than the experimental one (10.04 Å). This slight change is due to the presence of Van der Waals forces. For the

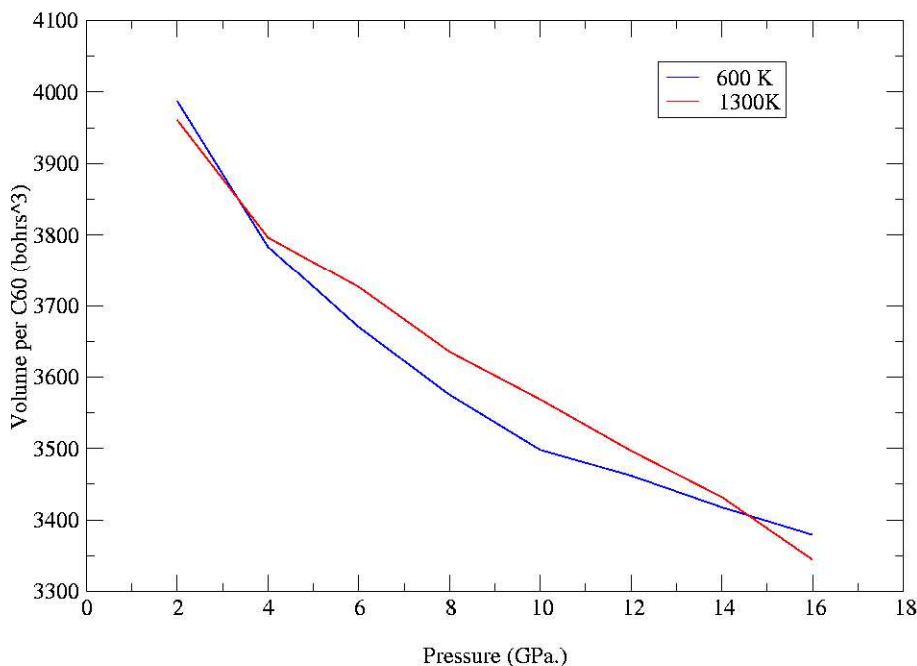


Figure 3.13: Average volume *vs* average pressure behavior observed for C_{60} phases under high temperature and high pressure. The blue line shows the average volume for eight simulations performed at 600 K. The red line shows the average volume for eight simulations carried out at 1300 K.

simulation carried out at 16 GPa and 1300 K, the distance between cages decreased to 8.81 Å. The value is smaller than the experimental data obtained for well known polymerized C_{60} phases because the pressure has not been released at the end of our calculation. In addition, our cages are not elongated in the bonding direction as observed in the orthorhombic, tetragonal and rhombohedral phases, because there are intermolecular bonds established in all directions. The oscillation behavior clearly arises from the repulsive force observed between molecules when they are too close to each other, and from the effect of pressure when they are too far.

The average radius of C_{60} molecules also experienced oscillations. Comparison with the data of figure 3.14 shows that the peaks of the two graphics coincide. Here,

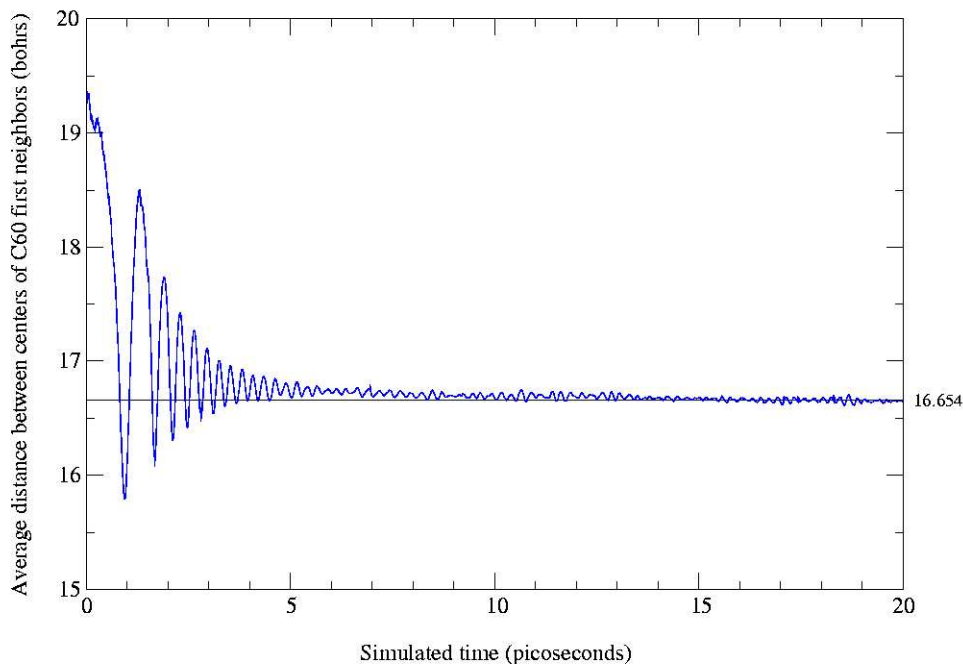


Figure 3.14: Average distance between centers of neighboring C_{60} molecules, calculated at 16 GPa and 1300 K. The equilibrium value is 16.654 bohrs or 8.81 Å.

the main radius is directly related to the structural oscillation. However, the oscillations of less amplitude must be related to the intermolecular vibrations. The average radius goes to 6.885 bohrs or 3.64 Å. This value is greater than 3.52 Å, which has been reported in the literature⁸. This is because: (a) an empirical potential was considered in our calculations and (b), the temperature simulated is much greater than room temperature (1000 K). Therefore, a higher kinetic energy per atom is induced, so a higher atomic movement is found. The latter leads to a higher molecular radius.

In this section we presented a whole family of novel intermolecular connections, mainly based on SN connections. Such connections could lead to polymerized materials exhibiting unusual mechanical and electronic properties. However, the empirical nature of the potential used must be kept in mind. In addition, we should point out that the final configurations found at high pressure and high temperature could be

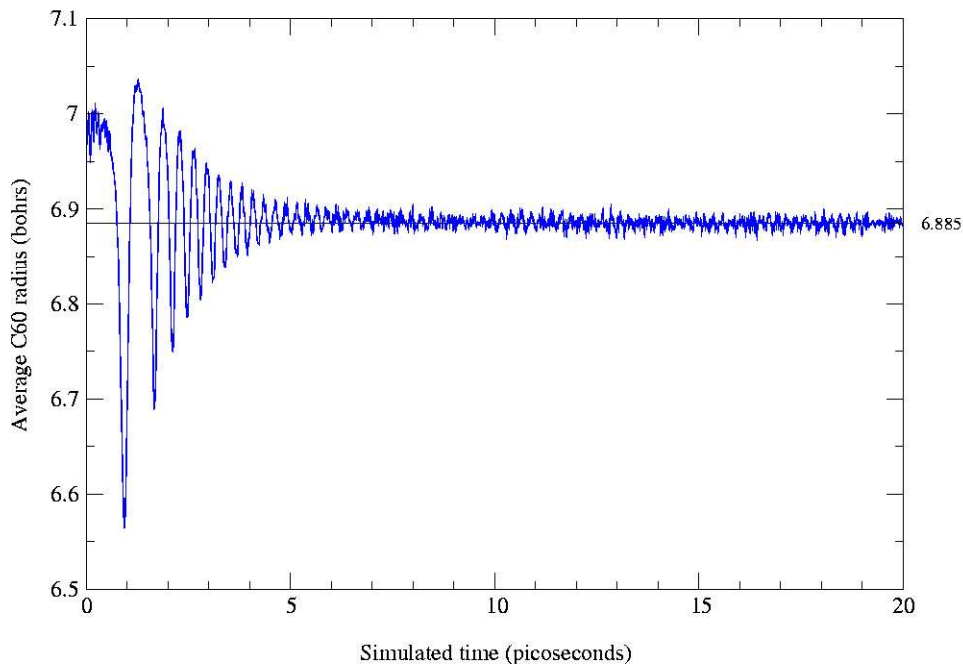


Figure 3.15: Average C_{60} molecule radius at at 16 GPa and 1300 K. The equilibrium value is 6.885 bohrs or 3.64Å.

necessary to preserve these connections. The next chapter will discuss simulations that will clarify this issue. The fact that the initial configuration was not far away from the final configuration indicates that the code conditions seem to be adequate. Such results reinforces the reliability of the TROCADERO code. In addition, the behavior of the average C_{60} radius and the average first neighbor distance have been shown and discussed.

3.3 Additional Simulations

It has been mentioned in chapter one that different structures could result from experiments using C_{60} molecules treated under the same temperature and pressure conditions. It has been proposed that this is due to the fact that different paths are followed in order to reach the same pressure-temperature point¹². Therefore,

nine additional simulations were performed in order to confirm the effect of different paths. The simulation box was a conventional fullerite fcc cell under periodic conditions. The initial configuration considered four C_{60} molecules oriented in a random way. We simulated three different paths:

1. PT path. First, the desired pressure is applied at room temperature for 10 picoseconds. Subsequently, both the desired pressure and the desired temperature are applied for additional 10 picoseconds.
2. TP path. First, the desired temperature is reached at 0 GPa for 10 picoseconds. After that, both the desired pressure and desired temperature are applied for additional 10 picoseconds.
3. TyP path. Both desired pressure and desired temperature are applied for 20 picoseconds.

The simulation conditions were: 1.2 GPa and 573 K, 2.2 GPa and 873 K, and 6.0 GPa with 873 K. Calculations carried out at 573 K presented structures almost without intermolecular links. Simulations at 873 K resulted in structures exhibiting various intermolecular links established by only one bond. Intermolecular connections with two or more bonds were not found. None of the formed structures following PT and TyP paths showed any significant change in the simulation box. Only the TP simulations showed some distortion in the crystalline arrangement. However, it comes from the fact that the simulation code does not consider Van der Waals interactions, so the high temperature provoked that the C_{60} molecules do not keep the crystalline arrangement and started to separate, as in a solid-gas transition.

We failed to find the phase transitions of the C_{60} crystal due to several reasons. First, the simulated time; the experimental time used for obtaining the polymeric phases is several thousands of seconds long. The second factor is the cell used. The number of initial molecules and the shape of the initial simulation box could make harder or impossible to simulate some phase transitions. Think about the importance of such conditions in order to find the simple cubic phase reported by Heiney *et. al.*: without an even number of C_{60} molecules in the simulation box, it

would be impossible to find such a phase. The third factor is the lack of Van der Waals interactions in the potential used. Nevertheless, their inclusion in a potential could be difficult for the empirical potential used. Remember that fullerite at room temperature is kept by Van der Waals forces, the twelve first neighbors are at the same distance for a given C_{60} molecule and the molecules rotate freely. Then, the electronic density must have a high symmetry, and it must be more dependent on the structural geometry than on the molecular geometry and atomic positions. The fluctuations in the Van der Waals forces would require *ab initio* methods rather than empirical potentials such as the Tersoff one.

REFERENCES

1. J. Tersoff, Phys. Rev. B **39**, 5566 (1989)
2. M. Nuñez-Regueiro, L. Marques, J. L. Hodeau, O. Béthoux and M. Perroux, Phys. Rev. Lett. **74**, 278 (1995)
3. W. Kräestchmer, L. D. Lamb, K. Fostiropoulos and D. Huffman, Nature **347**, 354 (1990)
4. P. A. Heiney, J. E. Fischer, A. R. McGhie, W. J. Romanow, A. M. Denenstein, J. P. McCauley Jr. and A. B. Smith III, Phys. Rev. Lett **66**, 2911 (1991)
5. Y. Guo, N. Karawasa and W. A. Goddard III, Nature **351**, 464 (1991)
6. S. J. Duclos, K. Brister, R. C. Haddon, A. R. Kortan and F. A. Thiel, Nature **351**, 380 (1991)
7. F. Moshary, N. H. Chen and I. F. Silvera, Phys. Rev. Lett. **69**, 466 (1992)
8. B. Sundqvist, Advances in Physics (Review) **48**, 1 (1999)
9. W. I. F. David, R. M. Ibberson, J. C. Matthewman, K. Prassides, T. J. S. Dennis, J. P. Hare, H. W. Kroto, R. Taylor and D. R. M. Walton, Nature **353**, 147 (1991)
10. V. A. Davydov, L. S. Kashevarova, A. V. Rakhmanina, V. M. Senyavin, R. Céolin, H. Szwarc, H. Allouchi and V. Agafonov, Phys. Rev. B **61**, 11936 (2000)
11. S. Berber, E. Osawa and D. Tománek, Phys. Rev. B **70**, 085417 (2004)
12. A. V. Talyzin, L. S. Dubrovinsky, M. Oden, T. Le Bihan and U. Jansson, Phys. Rev. B **66**, 165409 (2002)

Chapter 4

Statical studies

In the previous chapter we discussed a new family of intermolecular connections between C_{60} molecules that could appear in polymerized structures when the system is treated at High Pressure and High Temperature (HPHT). However, complementary work is required in order to know: (i) if such intermolecular connections could be found experimentally when the pressure is released, and (ii) the mechanical and electronic properties of the resulting polymerized structures. Therefore, a different methodology, which is not based on the empirical classical potentials must be used to calculate the electronic properties of the novel systems. In this chapter, most of the simulations have been performed using a non-orthogonal tight-binding scheme, as discussed in chapter two, and available in the TROCADERO code. The main simulation mode of TROCADERO used in the following work is *relaxation*. It is based on a conjugate gradients scheme, that reduces in an efficient way the total force experienced by the atoms when displacing them slightly to minimize the average forces. Note that all the structures discussed in the following sections are local minima in space.

4.1 C_{60} Dimers

As explained previously, some intermolecular connections appeared numerous times in our Molecular Dynamics Simulations when applying high pressures and high temperatures. In order to evaluate the stability of those configurations, we have studied,

as a first step, the structural stability of various intermolecular connections established between two C_{60} molecules (dimers). This study could provide us important information related to the structural stability of these systems in non-crystalline configurations. The connections used for structural relaxations were (see Appendix A): 13h13ha, 13h13hb, 13h13h2a, 13h13h2b, 13h13p, 13h13p2, 13h14h, 13h14h2, 13p13p2, 6565, 6666, 6566, 14h14h, 3link1, 3link2, 4link(dd), 4link(sd) and 4link(ss). The first nine are the most common intermolecular connections found in our HPHT simulations. Connections 6565, 6566, 6666 and 14h14h are usually found in literature, and we have studied them in order to compare their stability. The 3link and 4link structures were added because they could be considered as novel and important intermolecular connections involving more than two intermolecular bonds. The (dd) notation is used when a double bond is facing a double bond of its C_{60} neighbor. The (sd) label implies that a C_{60} molecule faces a single bond with a double bond of its C_{60} neighbor. Finally, (ss) is the notation for the single-single bond case.

Figure 4.1 depicts the most statistically representative intermolecular connections found in our MD simulations of fullerite under HPHT. From now on, we call them *Common connections*. Several dimers were constructed with these links, in such a way that the C_{60} cages were not disrupted. As a first step, dimers were relaxed using the Tersoff Classical Potential, in order to minimize the structural strain. It is noteworthy that all structures keep connected with the starting intermolecular connection after this first relaxation. However, the local minima in space do not strictly match for different interatomic potentials. Then, we explored various points near to the local minima obtained with the Tersoff Potential using a tight-binding relaxation calculation. This search helps us to obtain different structural configurations of C_{60} dimers. Several configurations were obtained using the Tersoff Potential, and their respective coordinates were scaled by multiplying them times 0.90, 0.95, 1.00, 1.05. In this way, we had five structures for each intermolecular connection. Subsequently, such dimers were relaxed within a tight-binding approach. The same process was applied for the eighteen intermolecular connections mentioned at the beginning of this section.

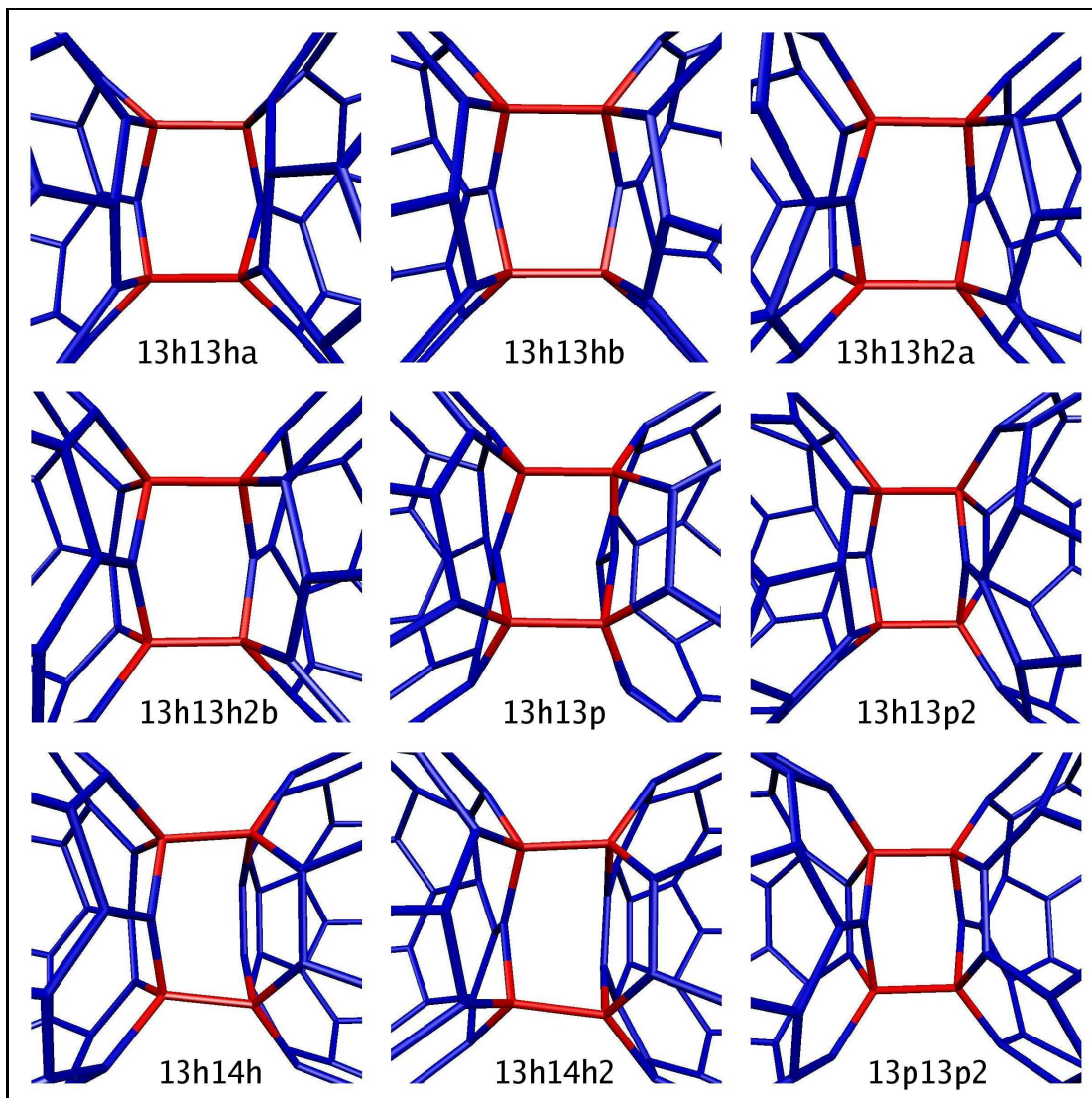


Figure 4.1: The most common interconnections found in HPHT simulations.

Clear differences were observed between the converged structures using the Tersoff Classical Potential and the non-orthogonal tight-binding potential of TROCADERO. Only one of the nine common connections survived after tight-binding relaxation, the others resulted in 6566 and 6666 connections or in two isolated C_{60} molecules. This is because the Tersoff Potential does not consider charge transfers. The 13h13ha intermolecular connection could transform into a 6566 configuration or into two isolated C_{60} molecules. 13h13hb could be converted into a 6666 dimer configuration or into a "3 bonds" dimer configuration (see figure 4.2). Only the 13h14h intermolecular connection is preserved after geometrical relaxation using the tight-

binding approach. However, for the other four scaled configurations exhibiting the 13h14h connection, the final geometries correspond to two isolated C_{60} molecules non-connected. As discussed previously, the other six popular connections lead only to non-linked C_{60} molecules.

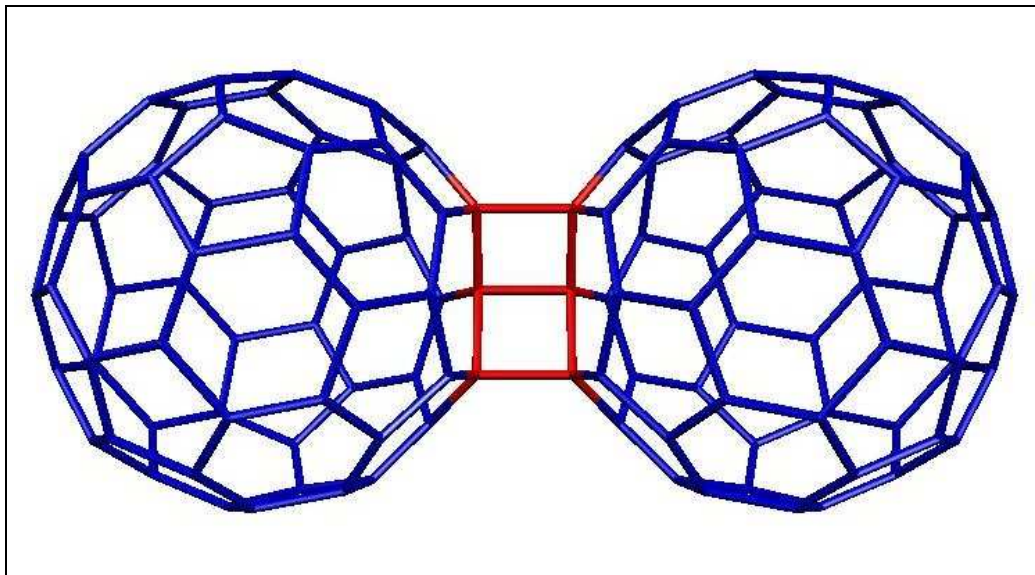


Figure 4.2: Dimer using a 3-bonds intermolecular connection. This resulted by relaxing a dimer connected with the 13h13hb intermolecular link.

All dimers discussed previously in literature remain dimerized after relaxation, and preserved the starting configuration. They correspond to 6565^{1,2}, 6566¹, 6666¹⁻⁶ and 14h14h^{5,7}. The relaxed intermolecular bonds in the 6565 connection exhibit bond lengths of 1.598 Å; an extended bond when compared with the value corresponding to polymerized rhombohedral C_{60} using the 6565 connection (1.582 Å¹). The bond length of the intermolecular bonds for the created using 6666 connections is 1.589 Å. The reported values for such bonds are: 1.51 Å², 1.588 Å⁴, 1.546 Å⁵ and 1.55 Å⁶. The best agreement is observed with the value reported by Adams *et. al.*, who used local-orbital first-principles molecular-dynamical relaxations⁴. For the 14h14h interconnection the bond length corresponded to 1.61 Å, a value which is in good agreement with the calculated value of 1.604 Å using *ab initio* methods⁵.

The dimers related with a 3link1 connection resulted in a dimer linked by a 6666

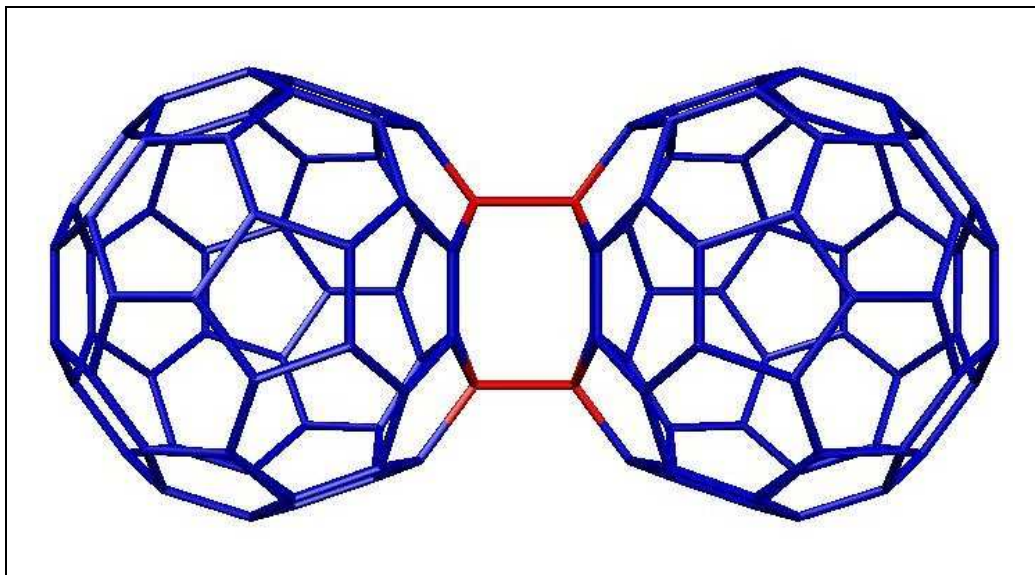


Figure 4.3: Dimer connected by the 14h14h link.

connection after tight-binding relaxation. For the 3link2 connection, the final configuration corresponded to a 6566 connection. On the other hand, the 4link connections (ss) and (dd) remained linked with the starting connection after tight-binding relaxation. In the case of the 4link (sd) connections, the fully relaxed structure corresponded to two isolated C_{60} molecules. These results could be explained by the competition established between the bonding energy and the structural strain. For example, for 3link connections the strain is greater than the bonding force experienced in the three intermolecular bonds. For the 4link connections (ss) and (dd), the binding force from the four bonds could be strong enough to preserve the dimer, even with a high structural strain (see the energy table below). For the dimers joined using a 4link (sd) connection, the loss of symmetry produces a larger strain.

It has been found that the *common connections* do not keep connected after tight-binding relaxation, except for the 13h14h. It is possible that a crystalline environment or an extreme polymerization degree is required in order to find such connections experimentally. In this section, stable dimers using 4link connections were also presented. However, it is very difficult to obtain dimers joined using such connections, because the 4link links require a high polymerization degree to appear (see Appendix B) and this makes difficult the presence of dimers.

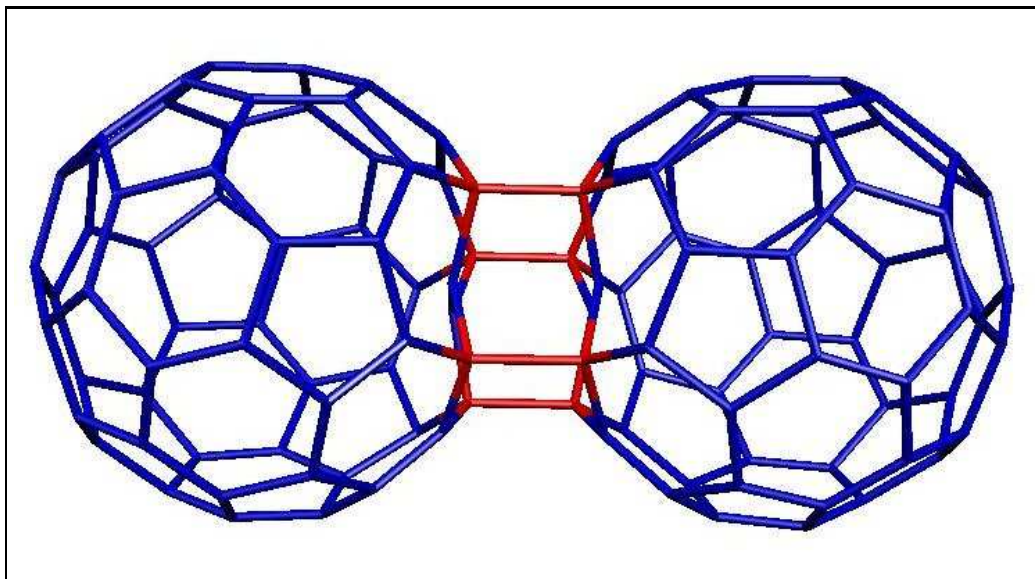


Figure 4.4: Dimer linked by the 4link(sd) connection. The structure exhibits structural strain but the four intermolecular bonds keep the dimer together.

In table 4.1 the energies of the different relaxed dimers are summarized. The ‘non-connected’ row has the energy for two isolated C_{60} molecules. The one-bond row shows the energy for two C_{60} molecules joined by one intermolecular bond (without relaxation), exhibiting a bond length of 1.6 Å. Such a distance was chosen because it is close to those found for the intermolecular connections 6565,6566, 6666 and 14h14h. The 6666 connection is the only one with energy below the level of isolated C_{60} molecules, as reported previously^{2,4}. It is clear that the connections that involve the 66 unit possess a lower total energy, so the participation of double bonds in intermolecular connections is favored. Once a bond has been established between two C_{60} molecules, almost all the most stable configurations involve a 66 unit. In addition, all SN connections exhibit a higher energy than the single-bond connection.

As a result of our simulations, four new meta-stable dimers could be reported: 3bonds, 13h14h, 4link (ss) and 4link (dd). The first two have an energy lower than a dimer reported previously: the 14h14h. Two 4link connections were found to be stable. Of course, their synthesis could be very difficult. However, a stability study of dimers is important as a first step to evaluate the feasibility of the SN connections,

Intermolecular connection	Energy(eV)	Energy per atom (eV/at)
6666	0.000	0.000
isolated C_{60} s	0.408	0.003
6566	0.842	0.007
6565	1.682	0.014
3bonds	3.020	0.025
single-bond	3.814	0.032
13h14h	4.184	0.035
14h14h	4.885	0.041
4link (dd)	7.083	0.059
4link (ss)	7.317	0.061

Table 4.1: Total energies for relaxed dimers.

and compare these results with other connections such as the [2+2] cycloaddition.

4.2 A formation mechanism for the rhombohedral, tetragonal and orthorhombic C_{60} polymerized phases

It has been previously mentioned in chapter 3 that additional simulations were performed under isobaric-isothermal conditions. During these simulations, various intermolecular connections formed by a single bond were observed. The final configurations of such calculations were relaxed using a tight-binding approach, but without changing the shape or size of the simulation box. In all cases, the structures obtained after relaxation were highly polymerized. However, such polymerization mainly consisted on intermolecular connections formed by one single intermolecular bond. If the performed simulations are close to reality, then it is suggested that the 6666 intermolecular connections found in the orthorhombic, tetragonal and rhom-

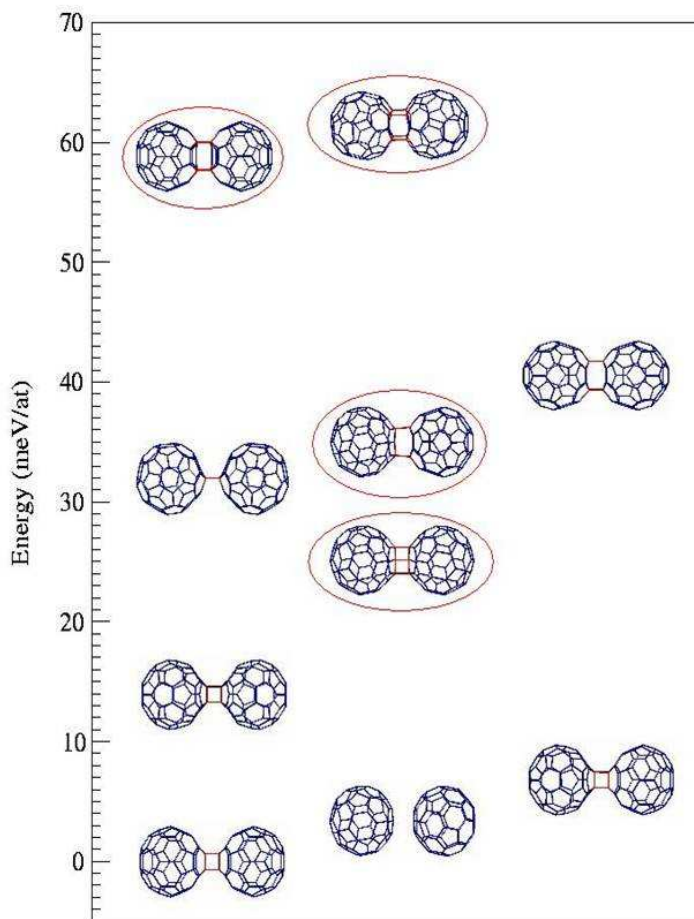


Figure 4.5: Metastable dimers found. They are ordered by energy, using as reference the energy for the dimer connected by [2+2] cycloaddition between double bonds. The dimers inside a red ellipse have not been reported before.

bohedral phases are formed after or during the temperature and pressure release. Such a possibility suggests a formation mechanism for these three different phases, by means of the average “coordination number” of the C_{60} molecules. In this context, one should remember the experimental paths proposed by Davidov *et. al.*⁸ in order to obtain the C_{60} polymerized phases (see figure 1.5). They corresponded to 1.2 Gpa and 573 K for the orthorhombic phase, 2.2 Gpa and 873 K for the tetragonal phase and 6 Gpa and 873 K for the rhombohedral phase. Based on the polymerization trends of the simulations of chapter 3 (see table 3.1), it can be assumed that at the moment before quenching and releasing the pressure, a sample treated by

the rhombohedral path has a higher polymerization degree than a sample prepared by following the orthorhombic path. How can this fact help us to understand the formation of the different phases? The answer is explained below.

Consider a polymerized C_{60} structure, in which intermolecular connections are formed mainly by establishing only a single intermolecular bond. Here, each C_{60} molecule could participate in several intermolecular connections (the maximum is twelve, the number of neighbors in the fcc arrangement). If the average number of intermolecular connections per C_{60} is large enough (maybe from six up to nine are good numbers), then it is very possible to find regions in the solid that are locally 2-D polymerized instead of 3-D polymerized. In these regions, the structural oscillations exhibit a higher component in the orthogonal direction to the 2-D polymerized plane. Such oscillations would stretch the intermolecular bonds in neighboring regions; mainly those bonds that are more orthogonal to the plane. Subsequently, such displacements lead to the growth of the 2-D polymerized region by breaking preferential bonds. As time passes by, this process also promotes the formation of planes parallel to the first one. A scheme of such a process for 1-D regions in a 2-D polymerized lattice is presented in figure 4.6.

The breaking of bonds and the formation of [2+2] cycloadditions in the proposed formation mechanism is now supported. If we assume that the general geometrical trends from the dimers energies are preserved (see previous section), it can be concluded that once an intermolecular connection of a single intermolecular bond has been formed, the most probable final state of such connection involves the breaking of the bond or, alternatively, the formation of an [2+2] cycloaddition between double bonds. The bond rupture must be more probable in the stretched regions, as shown in figure 4.6. In addition, the formation of polymerized planes or chains favors the formation of the [2+2] cycloaddition, because a coordinated reorientation of the C_{60} molecules is easily achieved. This phenomenon could make more stable the 1-D and 2-D polymerized regions by establishing [2+2] cycloadditions. The proposed depolymerization process from 3-D polymerized structures to 2-D or 1-D

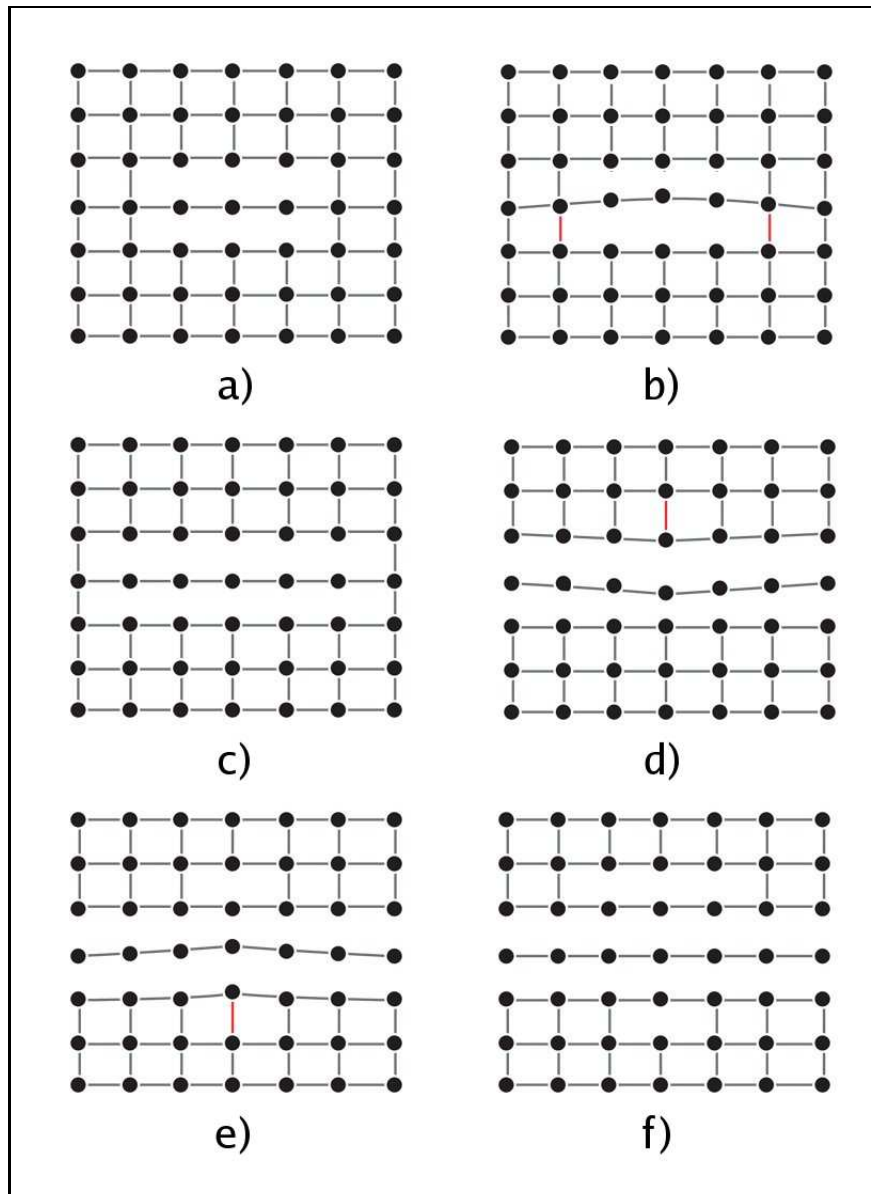


Figure 4.6: Scheme of the proposed formation mechanism. The points represent the C_{60} molecules. The lines represent intermolecular connections, they could be formed by one or several intermolecular bonds. The red lines represent stretched intermolecular connections. The square lattice is used for simplicity. a) The structure is a 2-D polymerized structure with a 1-D polymerized region. b) The structural oscillations in the 1-D region stretches the closer intermolecular connections. c) At this point, the 1-D regions becomes larger. d) The molecules closer to the 1-D region have more freedom and stretches specific bonds, thus weakening some links. e) Additional intermolecular connections break. f) New 1-d regions arise.

polymerized systems is thought to occur mainly after temperature quenching, while pressure is being released. By the proposed process it is not required that the structure has locally 1-D or 2-D polymerized regions before quenching the temperature and releasing the pressure, and they could be formed by the natural breaking of the intermolecular connections of single intermolecular bonds.

The difference between the formation of rhombohedral and tetragonal phases could be explained by the average number of intermolecular connections. If such a number is high, then it is more feasible that, in the 2-D polymerized regions, the C_{60} molecules be connected with six neighbors. If the number is lower, then it is more possible that the C_{60} molecules be connected with four neighbors instead of six in the 2-D polymerized regions. Remember that such 2-D regions could be formed when the pressure is released. Therefore, a higher polymerization degree in the 3-D structure leads to 2-D regions. For the orthorhombic phase, the average number of intermolecular connections is the lowest; in such a way that the formation of 1-D polymerized regions is more probable than the formation of 2-D regions. This phenomenon would lead to a crystalline structure, formed by chains, following a similar process as that discussed previously.

If the proposed formation mechanism is occurring experimentally, then it is possible to conclude that the existence of rhombohedral, tetragonal and orthorhombic phases are mainly due to the C_{60} symmetry and the fcc arrangement of the fullerite.

In particular, the proposed mechanism for the formation of the rhombohedral, tetragonal and orthorhombic phases could be summarized as follows. By means of HPHT treatments of fullerite, a polymerized C_{60} structure could be obtained. The polymerization degree depends on the pressure-temperature path followed. When the temperature and pressure are released, local 2-D or 1-D polymerized regions are formed from the 3-D polymerized structure by breaking the most stretched intermolecular bonds. Such effects are promoted by thermally activated oscillations. The specific increment of molecular freedom earned during this process promotes

the formation of (or separation in) new planes and chains. This separation process allows the molecules to rotate, thus forming [2+2] cycloadditions between double bonds as the preferential intermolecular connection. The final polymeric structure is finally obtained as a function of the average number of intermolecular connections per C_{60} molecule. This scenario is not valid for very high polymerized structures, such as those obtained when using pressures larger than 10 GPa^{9–11}, where the 3-D polymerization is preserved even after releasing the pressure and quenching the temperature.

An important issue that has not clearly been addressed in the literature, is the effect of the specific pressure-temperature path followed in order to obtain C_{60} polymerized structures. Therefore, we now address one specific case. Davydov *et. al.* proved the existence of the tetragonal C_{60} polymerized phase following different pressure-temperature paths. These authors characterized the phases using XRD and Raman spectroscopy¹². The followed paths are shown in the figure 4.7, the products of the HPHT treatments were preserved after quenching the system down to room temperature under a fixed pressure. Subsequently, the samples were studied at ambient conditions. It was observed that the amount of tetragonal phase for the first, second and third paths, was about 90, 65 and 15 per cent respectively (total treatment time: a second). In all cases, an increase of the total treatment time resulted in a greater amount of the tetragonal phase content, and less rhombohedral phase. In particular, for the third synthesis path, the amount of tetragonal phase raised to 40 per cent after a total time treatment of 10 000 seconds.

Davidov *et. al.* also proposed a possible conversion mechanisms of the monomeric states of C_{60} to the polymerized ones. The prerequisite for obtaining a polymerized phase is a molecular orientational order, induced by the pressure, so that double bonds in adjacent C_{60} molecules are parallel, thus favoring [2+2] cycloaddition. Thus, the tetragonal phase could be obtain in two steps: in the first, a molecular precursor is formed by the orientation of C_{60} molecules commensurate with the tetragonal polymerized phase; the second step is the polymerization of such precu-

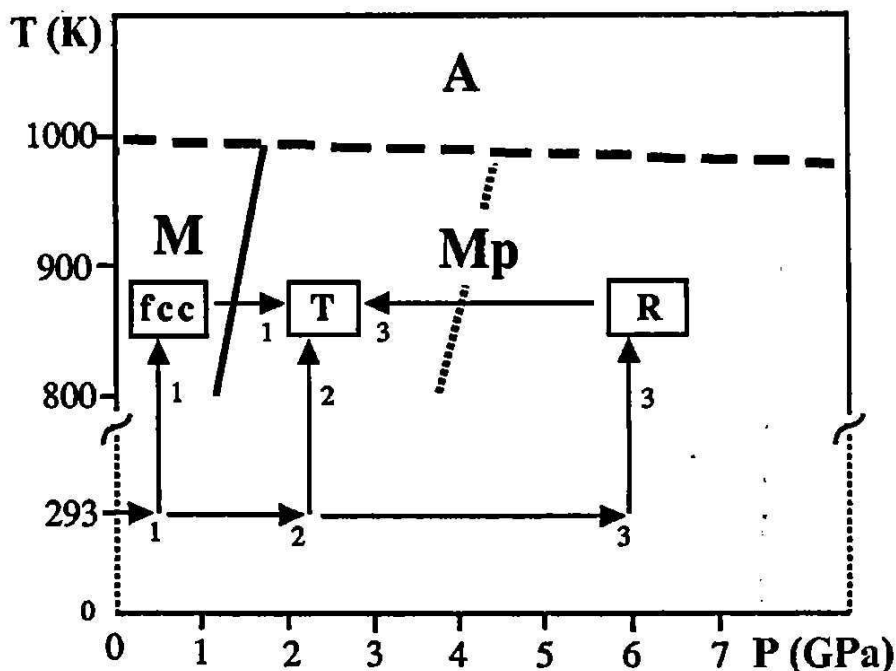


Figure 4.7: Different paths for the synthesis of the tetragonal C_{60} polymerized phase. R denotes the point for obtaining of the rhombohedral phase. T is for the point where tetragonal phase is obtained. Image from Davydov *et. al.*, Phys. Rev. B **58**, 14786 (1998)

sor. This proposed mechanism still requires an extra conversion step involving high activation energies in order to transform the rhombohedral phase into the tetragonal one for the path three¹². Such a transformation would demand the breaking of various [2+2] cycloadditions¹.

In our proposed mechanism, several experimental transformations are explained. By the trends presented in chapter 3, it can be seen that path 1 produces the structure with the lowest *average number of intermolecular connections per C_{60} molecule* (ANICCM), path 2 follows, and path 3 has the higher ANICCM. In path 2, more bonding formation occurs because, when pressure is applied, the non-connected

¹Such a conversion requires the breaking of a high percentage of intermolecular bonds in the rhombohedral phase because the polymerization occurs on different planes (see figure 1.4)

molecules could be brought closer than those already polymerized molecules in path 1 (where temperature was applied first). The subsequent increase in the temperature promotes a higher polymerization rate than that shown in path 1. In this way, the proportion of tetragonal phase and rhombohedral phase found in the sample, could be explained by the probability of finding 2-D polymerized defects with a local ANICCM with a value of four (our tetragonal precursor) or six (our rhombohedral precursor). In path 3, a large amount of 2-D polymerized regions with a local ANICCM of six could be formed. It could occur when the treatment goes from the 873 K and 6 GPa point (R) to the 873 K and 2.2 GPa point (T). This is a partial pressure-release process. It could explain the large proportion of rhombohedral phase observed in the experiments when path 3 is followed. The percentage of tetragonal and rhombohedral phases reported by Davidov and coworkers for the three paths, appears to be in good agreement with our proposed mechanism. The increment of the observed proportion of tetragonal phase, due to a long treatment time in paths 2 and 3, could be explained by the fact that the pressure and the temperature applied must lead to the ‘natural’ ANICCM of the T point. This could be achieved by breaking some rhombohedral regions, but mainly by changing the ANICCM of high polymerized regions that in other way would be converted in rhombohedral regions. The proposed mechanism considers that a hydrostatic pressure has been applied, as in the experimental synthesis^{3,11}.

The main advantages of our proposed mechanism are:

- An initial orientational order of C_{60} molecules is not required. Instead, the formation of [2+2] cycloadditions during the formation of 1-D and 2-D regions, promotes the formation of new cycloadditions due to the C_{60} symmetry and molecular rotations.
- An additional step from the rhombohedral to the tetragonal phase transition, as mentioned by Davydov *et. al.*, is not required.
- The mechanism provides a geometrical reason for the existence of three crystalline C_{60} polymerized phases found experimentally until now.

- The formation mechanism allows the formation of 1-D and 2-D regions oriented in different directions. This is in agreement with the fact that the obtained experimental samples are highly disordered with a small grain size¹³.

The main disadvantage of our proposed mechanism is the need of several assumptions. The first is that the single-bond intermolecular connections are commonly found before releasing the pressure and reducing the temperature. The second assumption is that the local 2-D and 1-D regions are sufficiently stable in their formation process. It is supported by the fact that in such local regions, C_{60} molecules could rotate easily, thus forming locally stable [2+2] cycloadditions. The final assumption is that the ANICCM of an C_{60} polymerized structure under HPHT is mainly determined by the pressure-temperature point, which needs to remain for long periods of time (seconds).

4.3 1-D Polymerized Structures

This section and the following two are devoted to discuss the structural stability of the different intermolecular connections in a crystalline environment. Mechanical and electronic properties as well as simulated XRD data are presented. In this work only have only studied crystalline structures where all C_{60} molecules are equivalent. Note: In the DOS figures the peaks were broadened using a Lorentzian of 0.003 Ha and the line for the Fermi level was set in the value correspondent to the highest point of the HOMO peak. Therefore, it is possible, at the first sight, to assume that the structures studied are metallic. However, it is not true, all of them resulted semiconductors in our calculations and the gap must be considered from HOMO peak to LUMO peak. See the gap value for each structure in the table 4.2

The studied 1-D polymerized structures were formed in a C_{60} orthorhombic polymerized phase. Therefore, the simulation box is an orthorhombic cell containing two (modified) C_{60} molecules, one centered in (0, 0, 0) and the other in (0.5, 0.5, 0.5) (fractional coordinates), but both with the same orientation. The intermolecular

connections are established along the direction of the vector \mathbf{a} . The length of this vector was chosen in such a way that the intermolecular bonds exhibited lengths of 1.4 Å, a value close to the length expected for the relaxed structures (1.4 to 1.6 Å). Subsequently, under periodic conditions, we obtain a crystal, formed by \mathbf{C}_{60} chains, just as the orthorhombic phase (see figure 1.4). The intermolecular connections studied were: 13h13h2, 13p13p2, 14h14h2, 65652, 6666, 4link (ss) and 4link (dd). These are all possible if all molecules are displayed with the same orientation.

The parameter values for the initial configurations were chosen in order to obtain structures closer to those expected after tight-binding relaxation. The parameter \mathbf{a} in the constructed configurations is smaller than the expected for the relaxed structure. The parameter \mathbf{b} was set to 9.831 Å, as reported by Davidov and coworkers⁸. The \mathbf{c} parameter used in the construction step was 16.2 Å. This value is larger than the value of 14.72 Å reported by Davidov and coworkers.

New structures were constructed from those initial configurations as follows. The parameter \mathbf{a} and \mathbf{c} of the simulation box were modified in such a way that \mathbf{a} was multiplied by $1+x$ and \mathbf{c} by $1-x$ ($x = 0.00, 0.01, 0.02, \dots, 0.09, 0.10$). Thus, the \mathbf{C}_{60} cages are modified because the atomic positions are given in fractional coordinates. The reason for using this process is to obtain a \mathbf{c} parameter closer to the experimental value, at the same time that the \mathbf{C}_{60} cages are expanded in the bonding direction and compressed in the \mathbf{c} direction, as expected for the final crystalline structure¹⁵.

All configurations were relaxed with the TROCADERO code using a tight-binding potential and 1 k-point. For most configurations, the results showed isolated \mathbf{C}_{60} molecules. However, for some others the molecules remained connected. If several relaxed configurations used the same intermolecular connection, then the structure with minimal energy was selected. The intermolecular connections that remain after the first relaxation process were 14h14h2, 65652, 6666, 4link (ss) and 4link (dd). For these configurations the \mathbf{c} parameter was set to 14.72 Å, as reported by Davidov *et. al.*, and relaxed once more. Then, the final \mathbf{b} and \mathbf{c} parameters dis-

played the values reported by Davidov and coworkers for the orthorhombic phase. In such directions, the distance between C_{60} molecules is mainly determined by van der Waals interactions. Then, we have set the experimental values because we could not obtain the actual values of the b and c parameters from the tight-binding method. Finally, a search for the optimal a value was performed, in 0.5 per cent steps. Here, the relaxation used an arrangement of $2*2*2$ k-points, selected by the Monkhorst-Pack method¹⁶. A final check of energy convergence was performed with a $8*8*8$ grid of k-points.

The obtained intermolecular bonds were 1.854, 1.592, 1.583, 1.670 and 1.70 Å for the 14h14h2, 65652, 6666, 4link (dd) and 4link (ss) orthorhombic crystals respectively. For the 6666 configuration, Xu and Scuseria calculated using a tight-binding approach, an intermolecular bond length of 1.64 Å, which is close to our value. The 14h14h2 intermolecular connection is not stable for the orthorhombic arrangement in a dynamical process, as could be observed from the intermolecular bond distance. Then, this structure was not considered². The intermolecular bond lengths of the 65652 and 6666 orthorhombic crystals are slightly smaller than the distances reported in this work for dimers. Therefore, the orthorhombic structures could exhibit a better structural stability in comparison with dimers using the same intermolecular connections. Finally, the 4link connections presented an intermolecular bond length slightly larger than that reported in this work for dimers.

One aim of this work is to discuss which (non-previously reported) orthorhombic structures could be present experimentally for the orthorhombic C_{60} polymerized phase. In the figure 4.8 is shown an XRD pattern of the 6666 orthorhombic optimized crystalline structure, obtained using the Cerius2 code¹⁸. All peaks and magnitudes are in good agreement with those ones reported experimentally by Davidov *et. al.*⁸. In figure 4.8, XRD patterns for the other orthorhombic C_{60} structures using different interconnections among the C_{60} molecules are also depicted. The magni-

²The largest known C_{sp^3} - C_{sp^3} bond length in hydrocarbons is 1.72 Å¹⁷

tudes and positions for the 4link connections are clearly different from those of the 6666 structure. However, the data for the 65652 structure exhibit all reflections located at the same positions as those obtained from the 6666 structure. In addition, the magnitudes of the peaks appear not to be significantly different for determining the presence (or absence) of the 65652 structure in the experimental samples of the orthorhombic C_{60} phase. Then, it is required to make careful comparisons between experimental and simulated data using different analytical techniques, e. g. NMR studies, in order to determine if the 65652 connection is observed experimentally.

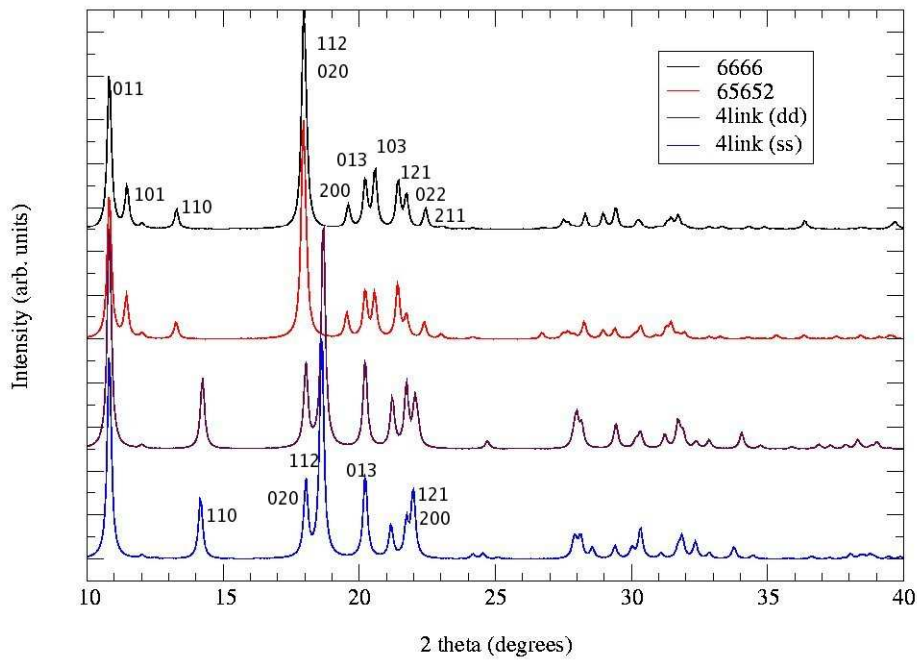


Figure 4.8: Simulated XRD pattern for 1-D polymerized structures using different intermolecular connections.

The density of states of the crystalline systems were calculated using a $8*8*8$ grid of k-points. The 6666 structure reveals a band gap of 1.68 eV. This value is smaller than the value of 2.18 eV, reported by Belavin *et. al.*¹⁹ for the direct gap at the gamma point using tight-binding calculations. This difference could be due to the number of k-points used in the calculation. The gap for the 65652 struc-

ture is 0.92 eV, for the 4link (ss) is 0.01 eV and for the 4link (dd) is 0.79 eV. The band gaps were measured between the delta peaks of the DOS, without broadening, therefore the 4link (ss) structure should be metallic. The 6666 has the largest gap. If graphite and diamond are taken as reference, it could be expected that the gap might be larger if the number of four-coordinated atoms per C_{60} molecule is larger too. The results show that it is not true: the structures with 4link connections have eight four-coordinated atoms per C_{60} and a smaller gap is observed when compared to the 6666 structure, which contains four four-coordinated atoms per C_{60} . It is noteworthy the very different electronic behavior between the structure with 4link (ss) connections and the one using 4link (dd) connections, although the structural differences could be considered small. The first is a metal and the second is a semiconductor.

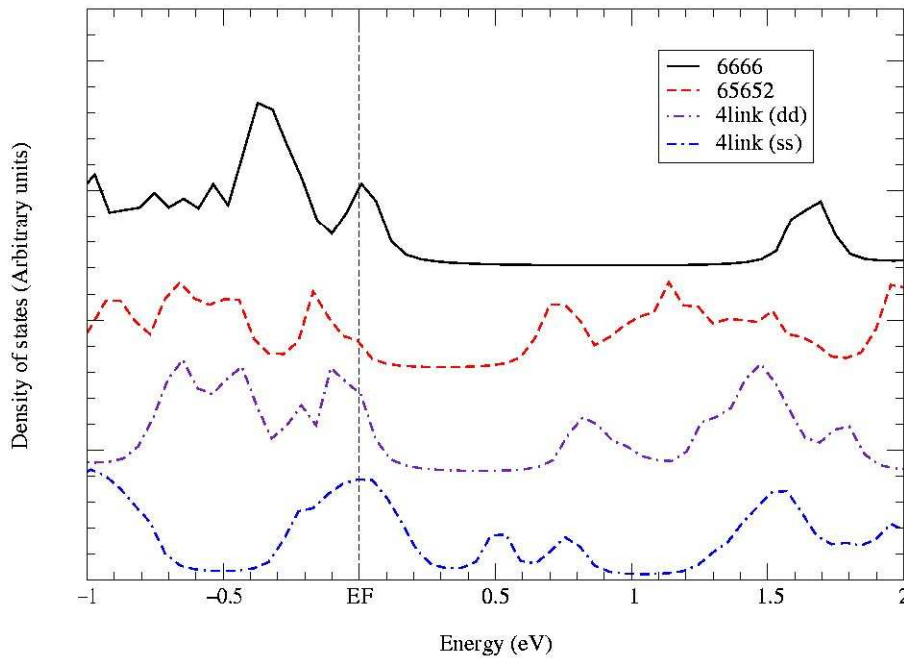


Figure 4.9: Density of states for the C_{60} orthorhombic 1-D polymerized structures using different intermolecular connections.

4.4 2-D Polymerized Structures

The presence of different intermolecular connections could depend on the crystalline environment. In order to confirm this possibility, several configurations were built using almost the same process discussed in the previous section, but now looking for the tetragonal and rhombohedral phases.

4.4.1 Tetragonal Structures

The cell in the tetragonal phase proposed by Nuñez-Regueiro *et. al.*³ has two C_{60} molecules. One in the (0, 0, 0) point and another in the (0.5, 0.5, 0.5) point (fractional coordinates), and the intermolecular connections runs along the directions of vectors \mathbf{a} and \mathbf{b} . The following structures were constructed: (13h13h2,13h13h2), (13h13h2,13p13p2), (13h13h2,65652), (13p13p2,6666), (14h14h2,65652), (14h14h2,6666), (14h14h2, 4link (dd)), (65652,6666), (6666,6666) and (4link (dd),4link (dd)). The first intermolecular connection runs along the \mathbf{a} direction, and the second runs along the \mathbf{b} direction. Other configurations could be constructed, by substituting 6666 and 65652 connections by 4link (dd) and 4link (ss) respectively.

The first configurations had a \mathbf{c} parameter of 16.2 Å, and the intermolecular bonds exhibited a length of 1.4 Å. As explained in the previous section, numerous configurations were obtained from the constructed systems, but in such a way that the C_{60} cages adopted a M&M shape, elongated in the bonding direction and compressed in the direction of vector \mathbf{c} . They were relaxed first using one k-point. Only four combinations remained after tight-binding relaxation: (14h14h2, 4link (dd)), (65652,6666), (6666,6666), and (4link (dd),4link (dd)). Then, the \mathbf{c} parameter was set to 15.02 Å, as reported by Davidov and coworkers⁸, and new relaxations were performed. Finally, a search to obtain optimal \mathbf{a} and \mathbf{b} magnitudes were performed, in steps of 0.5 per cent, by independent variation in \mathbf{a} and \mathbf{b} magnitudes. Those relaxations were carried out using a 2*2*2 k-point grid. For the (14h14h2, 4link (dd)) and (65652,6666) configurations, their simulation boxes were orthorhombic

cells, but very close to a tetragonal cell.

For the (14h14h2, 4link (dd)), the 14h14h2 connection is lost in the search for an optimal \mathbf{a} parameter. For the (65652,6666), the final intermolecular bonds exhibited a bond length of 1.621 Å in the 65652 connections, and 1.615 Å in the 6666 connection. These values are larger than those reported in this work for the 65652 and 6666 connections in orthorhombic structures. For the (6666,6666) configuration the intermolecular bonds possessed a bond length of 1.583 Å, the same value found for the 6666 orthorhombic configuration. For the (4link (dd),4link (dd)) configuration, the bond value obtained was 1.7 Å, which is larger than that reported for the 4link (dd) orthorhombic structure. Thus, for the tetragonal structures discussed here, the mechanical strength of the intermolecular bonds decreases with respect to the orthorhombic structure.

The simulated XRD patterns for the final structures is presented in figure 4.10. The data for the (6666,6666) is in good agreement with the data reported by Davydov *et. al.*⁸, although in our data the peaks located at c. a. 20° are more packed. The data for the (4link (dd),4link (dd)) is clearly different from the (6666,6666) simulation. The reflections for the (6566,6666) and (6666,6666) structures are almost in the same positions for a 2-theta value lower than 32°. From 32° up to 40°, the peaks occurs at different locations. However, the differences could not be clear enough for determining the presence of the (6566,6666) structure experimentally. Therefore, alternative characterization techniques are required in order to confirm such (6566,6666) structures.

The density of states have been calculated using a 8*8*8 k-point grid. The (6666,6666) structure displays a band gap of 1.71 eV. This result is in good agreement with the value of 1.852 eV, reported by Belavin *et. al.*¹⁹. The gap for the (65652,6666) structure is 0.72 eV. It is clear that the 6666 intermolecular connection has an enhanced insulator behavior when compared to the 65652 connection. The gap for the (4link (dd),4link (dd)) structure was 1.28 eV.

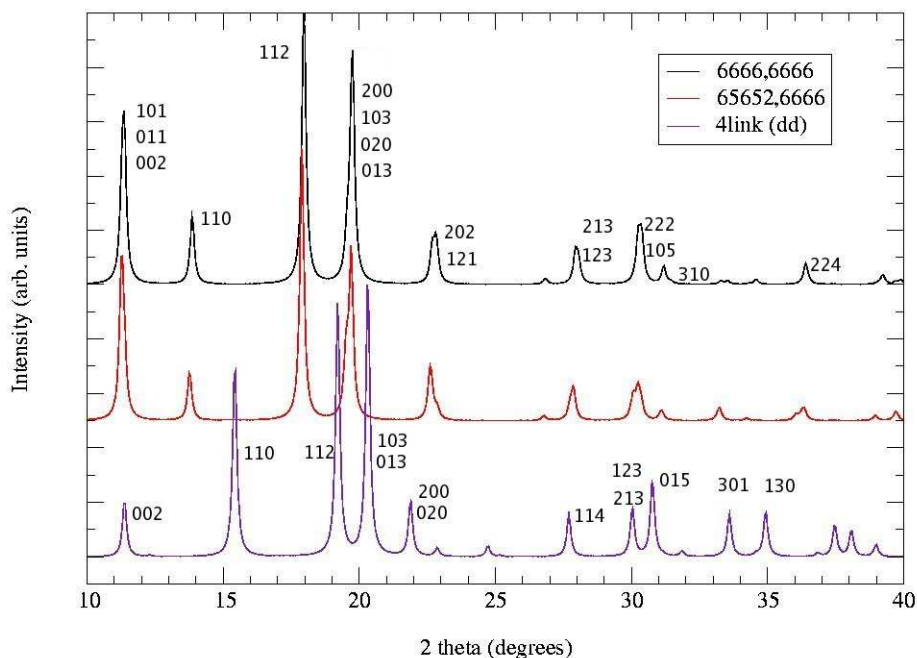


Figure 4.10: Simulated XRD patterns for 2-D polymerized structures using a tetragonal arrangement.

4.4.2 Rhombohedral Structures

Only two rhombohedral structures were studied. We did not find more rhombohedral C_{60} polymerized structures linked by the intermolecular connections presented in Appendix A. The simulation box used was a rhombohedral unit cell with a C_{60} molecule at the point (0, 0, 0) (see figure 3.6). The polymerized planes are oriented parallel to the plane defined by the “x” and “y” axis. One of the structures is the one proposed by Nuñez-Regueiro *et. al.* for the C_{60} rhombohedral phase. It uses [2+2] cycloadditions between double bonds as intermolecular connections, and we called it **drombo**. The other studied structure is constructed by connecting C_{60} molecules with 65652 connections and was originally proposed by Okotrub *et. al.*¹. We will refer to this structure as **srombo**. As in the previous section, a M&M shape for the C_{60} cages was promoted: C_{60} cages elongated in the bonding direction and

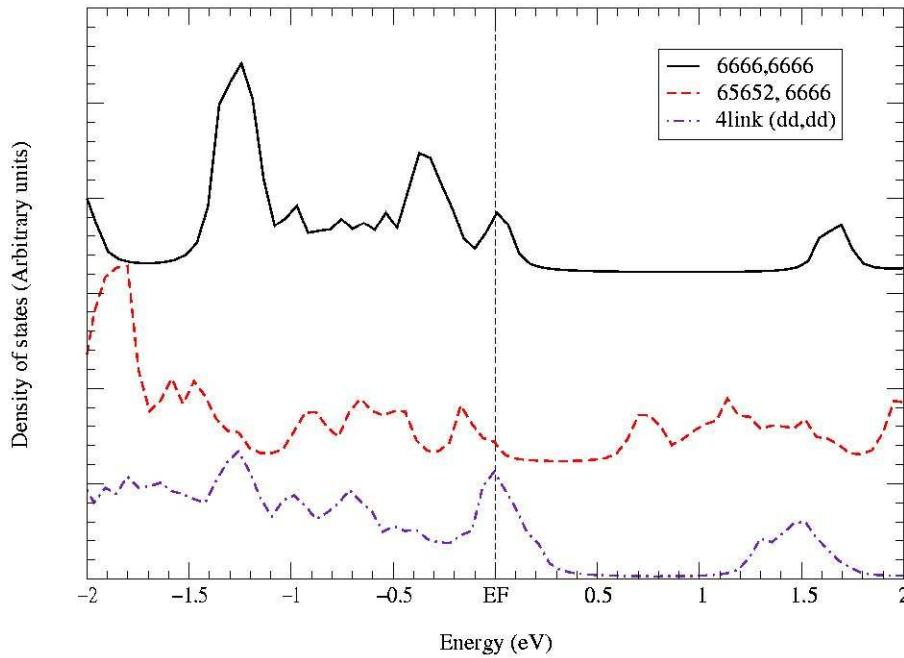


Figure 4.11: Density of states for C_{60} tetragonal 2-D polymerized structures using different intermolecular connections.

compressed in the “z” direction. The optimizations were performed using a $2 \times 2 \times 2$ k-point grid.

Both structures remained after tight-binding relaxation. The drombo intermolecular bonds display a length of 1.585 Å, and for the srombo structure the bond distance value is 1.637 Å. The first value is in good agreement with 1.582 Å, the calculated value obtained by Okotrub and coworkers using an empirical tight-binding Hamiltonian¹. For the srombo structure Okotrub *et. al.* reported 1.594 Å. Our simulated XRD patterns for the srombo and drombo structures are, both of them, in good agreement with the patterns reported by Davidov *et. al.*⁸. It is clear that additional studies must be performed in order to determine if the srombo structure is present in experimental samples.

The density of states were calculated using a $8 \times 8 \times 8$ k-point grid. The calculated

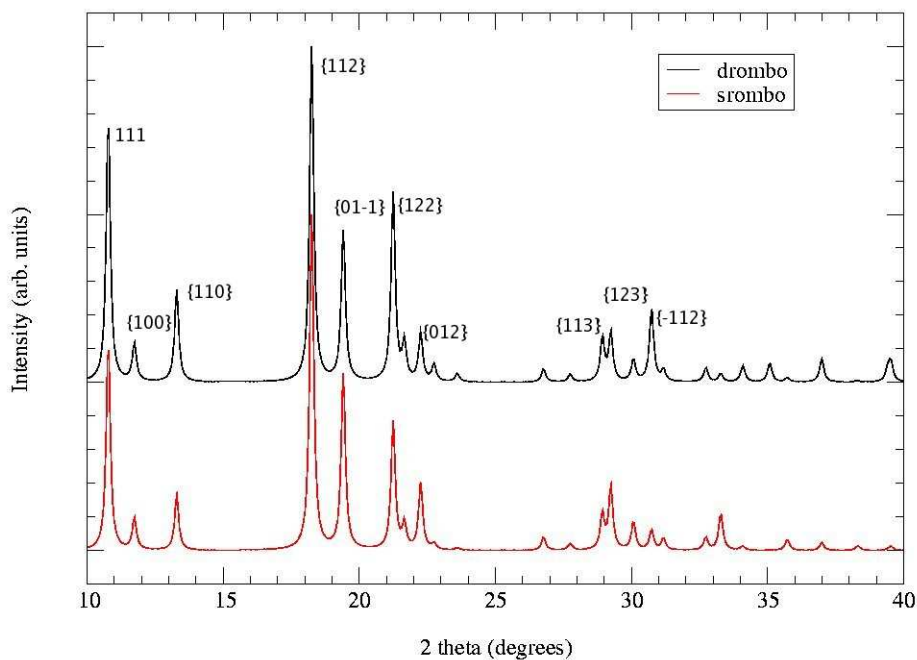


Figure 4.12: Simulated XRD patterns for rhombohedral 2-D polymerized structures using different intermolecular connections.

band gap for the drombo structure is 2.15 eV. Okotrub and coworkers¹ reported an indirect gap of 0.81 eV, and Xu and Scuceria¹⁵ reported 1.0 eV. For the srombo structure a band gap of 1.36 eV was found. These results are not in agreement with those reported by Okotrub describing a metallic behavior. Again, the 6666 connection has an insulator effect when this is compared with other connections.

4.5 3-D Polymerized Structures

Blank and coworkers have reported an ultrahard phase, obtained from fullerite, able to scratch diamond⁹. Theoretical works have not found support for such statement. We present in this section, results from the study of 3-D C_{60} polymerized structures, including the calculation of the bulk modulus. In order to determine the bulk modulus we first optimized the unit cell for each structure, as discussed for the 1-D

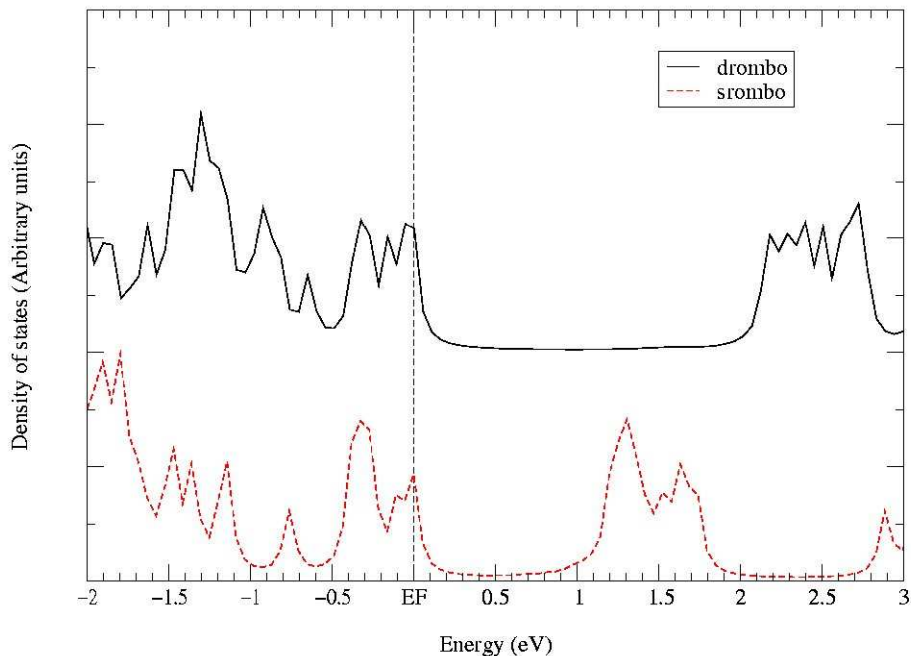


Figure 4.13: Density of states for C_{60} rhombohedral 2-D polymerized structures using different intermolecular connections.

and 2-D structures. Subsequently, we have scaled the unit cell; and we calculated the total energy as a function of the cell size (21 points for each structure). All the atoms have been fully relaxed for each volume, and total energies have been determined for the relaxed structures. The bulk modulus was evaluated using the “EOS” code²⁰ and the Murnaghan equation²¹. This combination give us a bulk modulus value of 484.32 GPa for diamond, which is in good agreement with previous calculations.

4.5.1 Simple Cubic Structures

Two structures with simple cubic arrangement are discussed in this work. The simulation box is cubic and has only one C_{60} molecule. The first structure is connected by [2+2] cycloadditions between double bonds along the three axes, it will be called **cubic [2+2]**. The second one uses 4link (dd) as intermolecular connection along

the three axes, it will be called **cubic (dd)**. The optimization was performed by relaxations and by changing the three parameters at the same time. Other configurations are possible if a 6666 connection is used instead of a 4link (dd), or viceversa. However, the only two structures mentioned above were chosen in this work.

We find that XRD patterns are very different for both structures. They could be used to distinguish them if they are synthesized experimentally. The intermolecular bonds for the cubic (dd) structure exhibit bond lengths of 1.727 Å. It is on the upper limit for a carbon-carbon bond length. Therefore, their structural stability must be very weak under ambient conditions. The cubic [2+2] structure has a band gap of 2.55 eV., such value is in good agreement with the gap of 2.235 eV, reported by Belavin *et. al.*¹⁹; but larger than 1.4 eV, value reported by Berber *et. al.*²². For the cubic (dd) structure the band gap found was 2.32 eV. Their bulk modulus are high, but significantly lower than that of diamond (see table 4.2).

4.5.2 BCO Structures

Berber *et. al.* have shown that bcc and bco arrangements present the higher bulk modulus for C_{60} polymerized structures²². Then, these phases are specially interesting for explaining ultrahard structures. Several initial configurations have been constructed, but many result on structures with broken intermolecular bonds after tight-binding relaxation. However, several interesting configurations survived after relaxing and we have studied them in detail. Here, we will present only five configurations from the almost ten configurations obtained. The reason for this is that some obtained structures reveal very small structural differences between them.

The called **564bc** (in this work) structure has been studied before by Burgos *et. al.*²³ and Perottoni and Jornada²⁴. However these authors used the name of (56-4). This structure is formed by C_{60} molecules in a bco arrangement. The molecule is oriented in such a way that three of the two-symmetry axes are parallel to the “x”, “y” and “z” axis (figure 4.16). The next step is to join the atoms of the hexagons

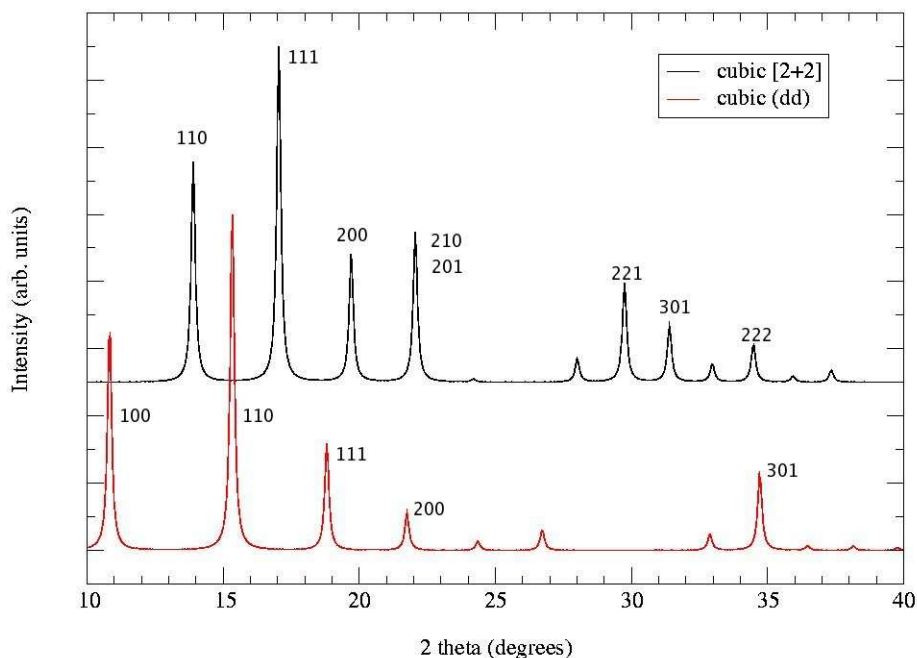


Figure 4.14: Simulated XRD patterns for cubic 3-D polymerized structures using different intermolecular connections.

in the diagonal directions ($[111]$ family) with the nearest atom of the hexagons of other molecules. In this way, only 12 atoms are not four-coordinated. The final step is to connect using $[2+2]$ cycloadditions in the “x” and “y” directions. The final structure contains 56 atoms four-coordinated and 4 atoms three-coordinated per C_{60} molecule. A detail of the structure is presented in figure 4.17. The calculated bulk modulus for this system was 305.78 GPa. This value is in good agreement with those reported in references 19 and 22.

A similar structure is the **bcca**. It is formed by breaking two intermolecular atoms by each of the eight diagonal hexagons of the 564bc structure, as shown in figure 4.18. For the construction, the $[2+2]$ cycloadditions of 564bc structure were broken. The vertical $[2+2]$ cycloadditions of the structure, as shown in figure 4.19, were a result from the tight-binding relaxation process. Then, this structure possesses 28 four-coordinated atoms. The structure exhibits a bulk modulus of 244.72 GPa

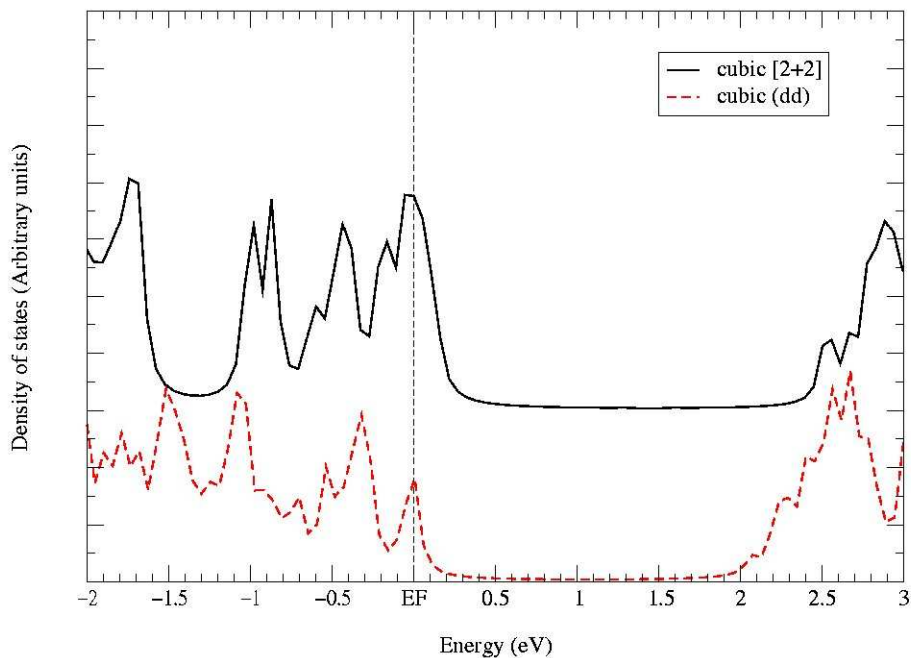


Figure 4.15: Density of states for C_{60} simple cubic 3-D polymerized structures using different intermolecular connections.

and a band gap of 0.22 eV.

Another structure studied is the called **bccb**. It is formed in the same way as the **bcca** structure, by breaking the cycloadditions of the 564bc structure, and breaking two intermolecular connections per hexagon in the diagonal. However, the selected atoms are different as could be seen in figure 4.19. The bulk modulus obtained for this structure was 273.57 GPa and the band gap had a value of 2.93 eV. It is noteworthy the difference between the gap values for the **bcca**, **bccb** and 564bc structures. Perhaps the most important structural factors for the gap value are the [2+2] cycloadditions, and the lack of sphericity of the C_{60} cages for the **bcca** structure.

The called **b0m** structure can not be clearly specified in words (see figure 4.20).

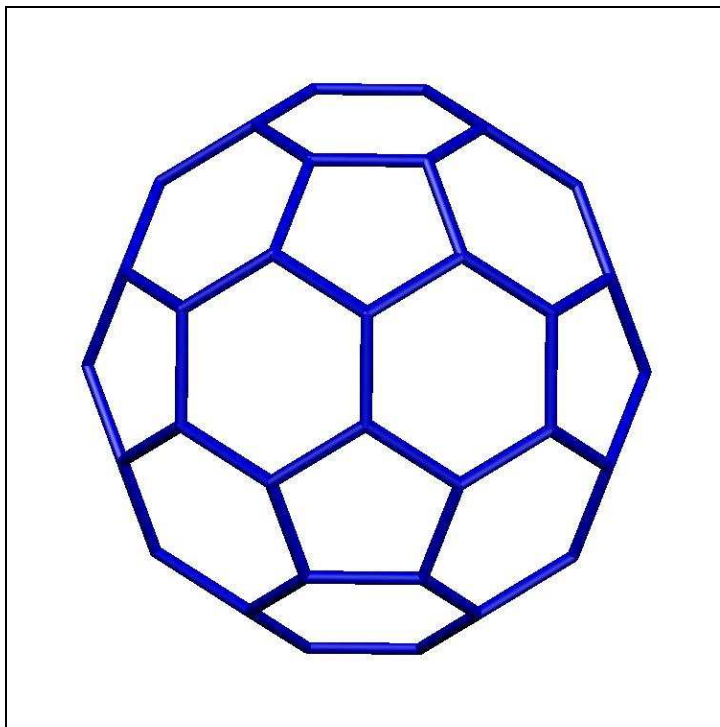


Figure 4.16: Orientation of the molecules in the 564bc structure.

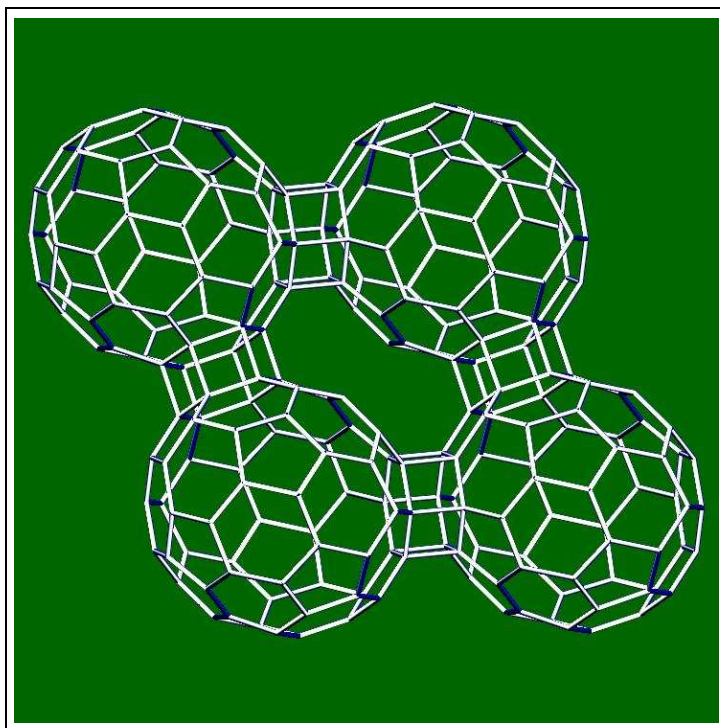


Figure 4.17: Detail of the 564bc structure.

The C_{60} cages are slightly broken and the structure is highly polymerized. An important characteristic of this system is that in such structure, 13p13p2 and 13h13p2

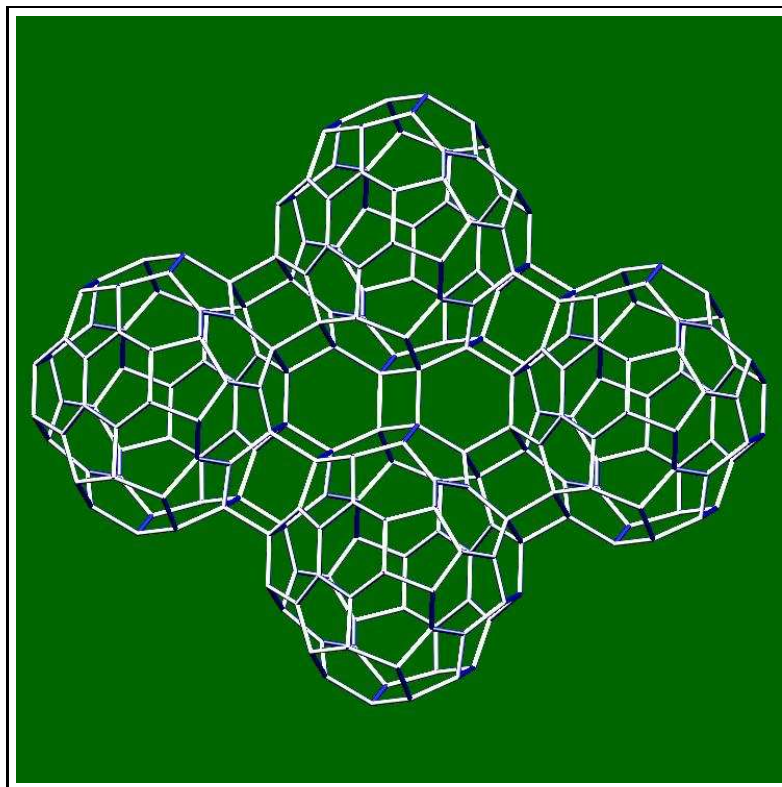


Figure 4.18: Detail of the bcca structure.

intermolecular connections are found. Maybe a basic requirement for the presence of SN connections is the partial breaking of the cages. This structure resulted after a tight-binding relaxation for a very different configuration. The obtained bulk modulus was 133.44 GPa, a very large value for a material. Its band gap correspond to 0.63 eV.

The **bccm** structure resulted from a wrong relaxation procedure, where all the parameters were changed significantly. After that, a carefully search for the optimal parameters was achieved. The main characteristic of this structure is that the cages have been broken. This promotes the connections between the top of the molecule in $(0.5, 0.5, 0.5)$ point with the bottom of the molecule in the $(1, 1, 1)$ point (conventional bcc cell). Then, the structure displays a large proportion of a continuous surface. It resembles carbon Schwarzites proposed by H. Terrones and Mackay²⁵. However, the bccm structure is not a perfect surface and contains several atoms out of it, providing a complex structure. The bulk modulus of this system is 208.92 GPa

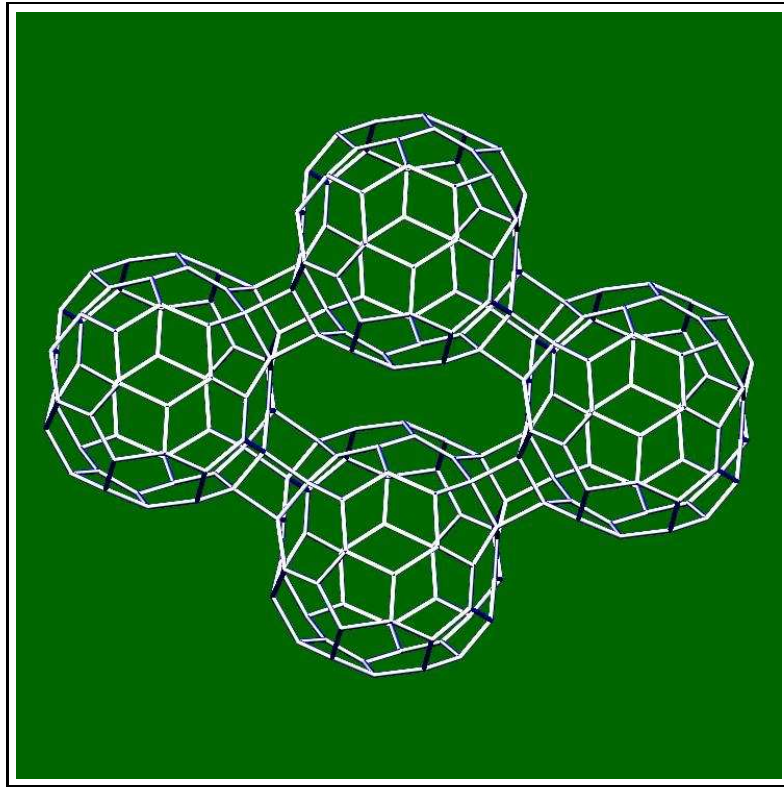


Figure 4.19: Detail of the bccb structure.

and the band gap is 0.28 eV.

The simulated XRD patterns for these structures reveals that all of them would be clearly identified. However, the experimental samples obtained by HPHT temperature do not show orientational order for 3-D polymerized structures²⁶. Then, it is possible that these structures will not be able to be synthesized. The XRD patterns for the 564bc, bcca and bccb structures are depicted in figure 4.21. Figure 4.22 shows that the 564bc and bccb structures are insulators while bcca structure is semiconductor. bccm and b0m structures are also semiconductors. The bcca structure is an interesting one, due to it shows that the deformation of the C_{60} cages could be a promoter of metallic behavior.

For the 3-D polymerized structures presented here, high bulk modulus values resulted. However, an ultrahard phase has not been found. On the electronic side, the properties were very different, as has been seen with the 564bc, bcca and bccb

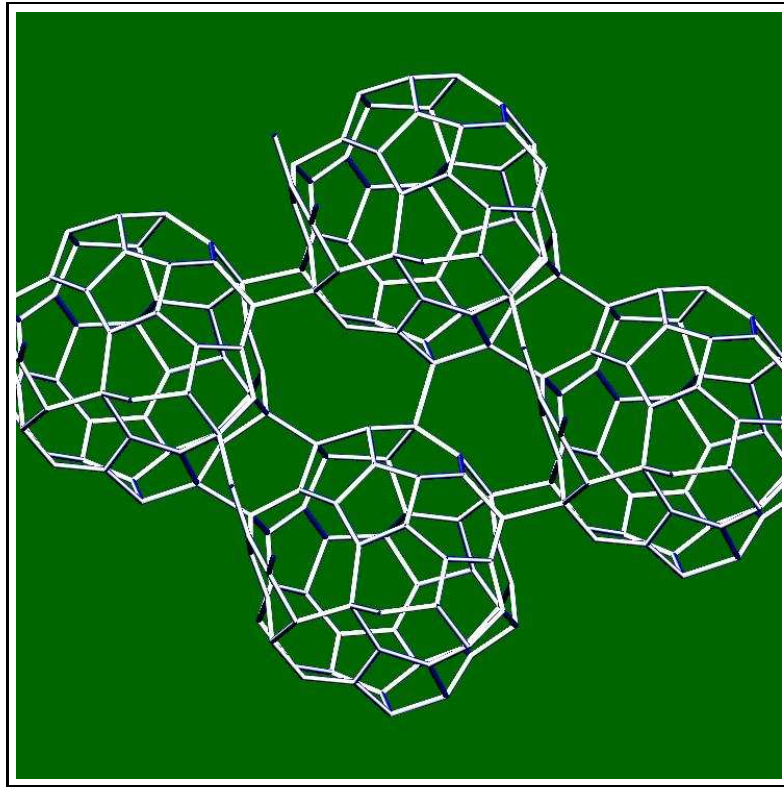


Figure 4.20: Detail of the bccm structure.

structures. A final table with the data of all the presented structures is shown. It is arranged by the comparative energetic stability. It is clear that the 6666 connections are favored in all phases, and after that the 65652 connections are favored. It can also be observed that the bco structures with conserved cages are more stable than those bco structures with broken cages. In addition, it is clear that each 4link connection cost a large (comparatively) amount of energy. If the phases are compared, the bco phase exhibits the worst energetic stability, a fact that has been reported before²².

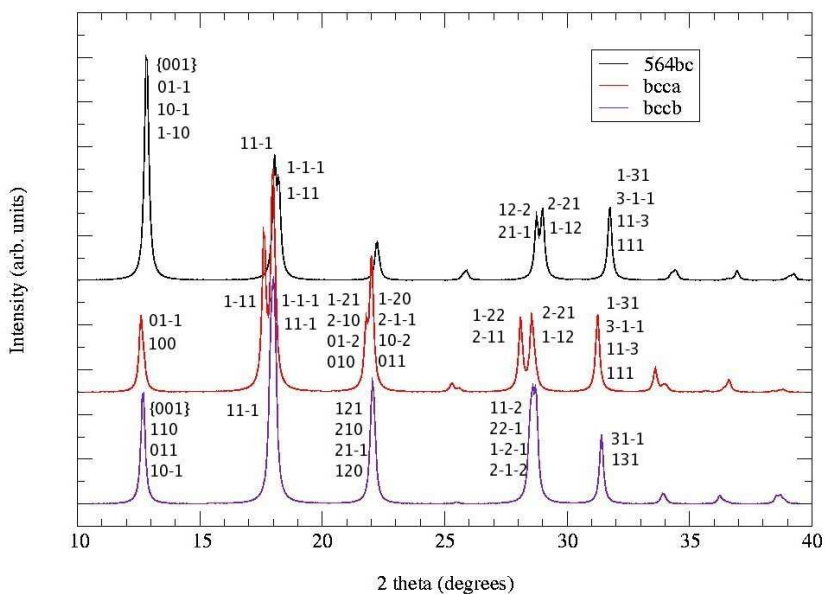


Figure 4.21: Simulated XRD patterns for bco 3-D polymerized structures using different intermolecular connections

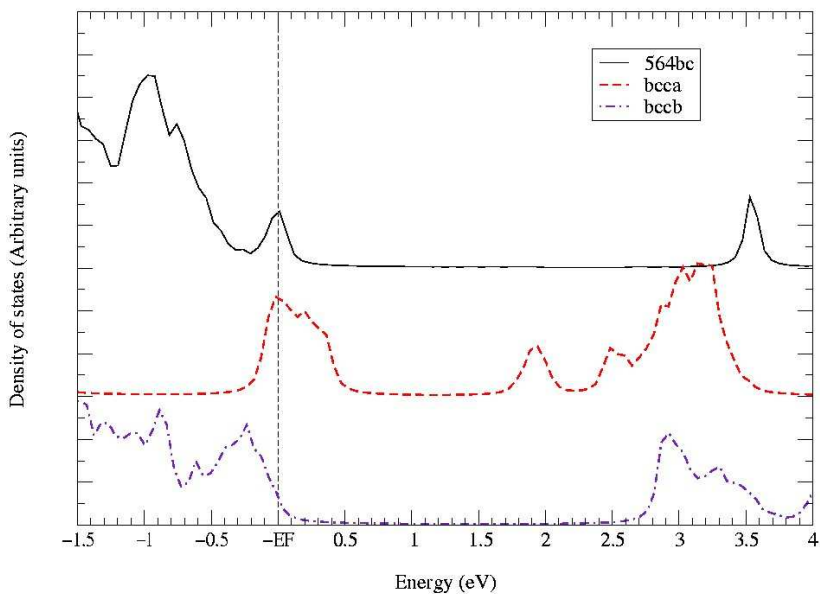


Figure 4.22: Density of states for C_{60} bco 3-D polymerized structures using different intermolecular connections.

Name	Lattice	Energy (eV/at)	Gap (eV)	BM
Cubic [2+2]	Simple cubic	0.0000	2.55	81.08
(6666,6666)	Tetragonal	0.0038	1.71	—
6666	Orthorhombic	0.0077	1.68	—
drombo	Rhombohedral	0.0289	2.15	—
(65652,6666)*	(quasi) Tetragonal	0.0327	0.72	—
65652*	Orthorhombic	0.0347	0.92	—
srombo	Rhomhedral	0.0981	1.36	—
4link (ss)*	Orthorhombic	0.1287	0.01	—
4link (dd)*	Orthorhombic	0.1310	0.79	—
bcca*	BCO	0.1364	0.22	244.72
bccb*	BCO	0.1636	2.93	273.57
564bc	BCO	0.2268	3.58	305.78
4link (dd,dd)*	Tetragonal	0.2343	1.28	—
bccm*	BCO	0.3028	0.28	208.92
b0m*	BCO	0.3032	0.63	133.44
Cubic (dd)*	Simple cubic	0.3443	2.32	116.35
Diamond	FCC	-0.2713	5.51	484.32

Table 4.2: Properties of the structures studied. The “*” denotes novel metastable structures.

REFERENCES

1. A. V. Okotrub, V. V. Belavin, L. G. Bulusheva, V. A. Davydov, T. L. Makarova and D. Tománek, *J. Chem. Phys.* **115**, 5637 (2001)
2. M. Menon, K. R. Subbaswamy and M. Sawtarie, *Phys. Rev. B* **49**, 13966 (1994)
3. M. Nuñez-Regueiro, L. Marques, J. L. Hodeau, O. Béthoux and M. Perroux, *Phys. Rev. Lett.* **74**, 278 (1995)
4. G. B. Adams, J. B. Page, O. F. Sankey and M. O'keeffe, *Phys. Rev. B* **50**, 17471 (1994)
5. N. Matsuzawa, M. Ata, D. A. Dixon and G. Fitzgerald, *J. Phys. Chem.* **98**, 2555 (1994)
6. S. Stafström and J. Fagerström, *Appl. Phys. A* **64**, 307 (1997)
7. L. A. Chernozatonskii, N. R. Serebryanaya and B. N. Mavrin, *Chem. Phys. Lett.* **316**, 199 (2000)
8. V. A. Davydov, L. S. Kashevarova, A. V. Rakhmanina, V. M. Senyavin, R. Céolin, H. Szwarc, H. Allouchi and V. Agafonov, *Phys. Rev. B* **61**, 11936 (2000)
9. V. Blank, S. G. Buga, N. R. Serebryanaya, V. N. Denisov, G. A. Dubitsky, A. N. Ivlev, B. N. Mavrin and M. Y. Popov, *Phys. Lett. A* **205**, 208 (1995)
10. L. Marques, M. Mezouar, J. L. Hodeau, M. Nuñez-Regueiro, N. R. Serebryanaya, V. A. Ivdenko, V. Blank and G. A. Dubitsky, *Science* **283**, 1720 (1999)
11. M. Mezouar, L. Marques, J. L. Hodeau, V. Pischeda and M. Nuñez-Regueiro, *Phys. Rev. B* **68**, 193414 (2003)

12. V. A. Davydov, L. S. Kashevarova, A. V. Rakhmanina, V. Agafonov, H. Al-louchi, R. Ceolin, A. V. Dzyabchenko, V. M. Senyavin and H. Szwarc, *Phys. Rev. B* **58**, 14786 (1998)
13. L. Marques, J. L. Hodeau and M. Nuñez-Regueiro, *Mol. Mat.* **8**, 49 (1996)
14. S. Buga, V. Blank, Å. Fransson, N. Serebryanaya. B. Sundqvist, *J. Phy. Chem. Solids* **63**, 331 (2002)
15. C. H. Xu and G. E. Scuseria, *Phys. Rev. Lett.* **74**, 274 (1995)
16. H. J. Monkhorst and J. D. Pack, *Phys. Rev. B* **13**, 5188 (1976)
17. H. F. Bettinger, P. von R. Schleyer and H. F. S. III, *Chem. Commun. (Cambrige)* **7**, 769 (1998)
18. Cerius² Version 4.6, Copyright ©2001, Accelrys Inc.
19. V. V. Belavin, L. G. Bulusheva, A. V. Okotrub and D. Tománek, *J. Phy. Chem. Solids* **61**, 1901 (2000)
20. Equation of State (EOS), program for fitting total energy data to a model equation of state and extracting various parameters, written by J. K. Dewhurst, Uppsala, Sweden (2002), version 1.0
21. F. D. Murnaghan, *Am. J. Math.* **49**, 235 (1937)
22. S. Berber, E. Osawa and D. Tománek, *Phys. Rev. B* **70**, 085417 (2004)
23. E. Burgos, E. Halac, R. Weht, H. Bonadeo, E. Artacho and P. Ordejón, *Phys. Rev. Lett.* **85**, 2328 (2000)
24. C. A. Perottoni and J. A. H. da Jornada, *Phys. Rev. B* **65**, 224208 (2002)
25. A. L. Mackay and H. Terrones, *Nature* **352**, 762 (1991)
26. A. V. Okotrub, V. V. Belavin, L. G. Bulusheva, V. A. Davydov, T. L. Makarova and D. Tománek, *J. Chem. Phys.* **115**, 5637 (2001)
27. B. Sundqvist, *Advances in Physics (Review)* **48**, 1 (1999)

Chapter 5

Concluding Remarks and future work

5.1 Conclusions and Contributions

The polymerization process of C_{60} molecules under HPHT conditions has been studied using Classical Molecular Dynamics Simulations. In them, several and non previously reported intermolecular connections different from the [2+2] cycloaddition between double bonds, were observed. In the studied pressure-temperature range, the main intermolecular connection is the single-bond connection, and the polymerization degree depends mainly on the applied pressure and temperature. A preferential direction for linking molecules, as expected for the formation of different phases, was not found. Only in one single case, an ordered molecular reorientation occurred. However, such information must be treated carefully, because an empirical potential has been used in order to perform the simulations in order to gain a better understanding of the C_{60} polymerization process, a time demanding simulation using a semi-empirical potential is required.

Although the quenching temperature and the pressure released have not been simulated, an alternative polymerization mechanism has been proposed. In particular, the existence of the rhombohedral, tetragonal and orthorhombic has been explained. The main ideas of these processes was the role of the polymerization de-

gree as a phase selector, and the promotion of the 2-D and 1-D polymerized regions. In order to compare our results with those obtained experimentally, *in situ* XRD data from the different systems needs to be carried out. It is also very likely that the real process be a combination of several mechanisms proposed in literature.

The structural stability of numerous 1-D and 2-D C_{60} polymerized structures has been studied. Several structures using intermolecular connections different from 6666 has been found to be metastables. Their feasibility could be confirmed using XRD simulations. In order to complete the job, it is required to simulate such structures using other techniques, such as NRM. The structural stability promoted by the 6666 connection, reported previously, is supported by our energy calculations. Besides, an insulator behavior has been found to be promoted if the 6666 connection is present. Several 3-D structures were studied. All of them exhibited a bulk modulus lower than that of diamond. In one of the structures, two SN connections were found. Then, the presence of different SN connections could be promoted by enhancing the degree of polymerization and by breaking and reordering the C_{60} cages.

In order to obtain a better picture for the polymerization process, it is required to simulate fullerite under HPHT with at least four C_{60} molecules in the simulation box, using tight-binding methods for several picoseconds. Unfortunately, the computational time required is too large for the process.

5.2 Summary of contributions

- The C_{60} polymerization process, under HPHT treatment, has been studied using Classical Molecular Dynamics.
- A whole family of intermolecular connections has been found to possibly exist in highly polymerized phases.
- A polymerization mechanism has been proposed for the formation of the rhom-

bohedral, tetragonal and orthorhombic phases.

- It has been found by XRD simulations of various structures, that the systems proposed by Nuñez-Regueiro *et. al.* could be the main component of the phases observed experimentally. Additional efforts are required for analyzing the orthorhombic 65652 structure and the quasi-tetragonal (65652,6666) structure. It is noteworthy that no other intermolecular connections could appear in a significant amount.
- The presence of [2+2] cycloadditions established between double bonds (6666 connection) appear to be the main intermolecular connections.
- The promotion of an insulating behavior caused by the presence of 6666 intermolecular connections.
- The structural stability promoted by the 6666 connection, reported previously, is supported.
- New metastable structures were found. It covers from dimers to 3-D C_{60} polymerized structures.

5.3 Future research

There are four ways to complement the work presented in this thesis. The first is to perform simulations using better potentials, different from the Classical Tersoff Potential. It could be extremely demanding in computational effort, but it could also provide a better picture of the C_{60} polymerization process. The second way, is to perform *in situ* experimental studies for the polymerization processes for the rhombohedral, tetragonal and orthorhombic C_{60} phases. These experiments could confirm the mechanism described in this work. The third is to introduce interstitial atoms in the presented bco structures. This could promote a higher hardness due to a higher polymerization in specific sites of the net. The last is to substitute carbon atoms by Boron and/or Nitrogen atoms in the proposed 3-D structures, in order to

increase the bulk modulus. The latter structures may be harder than diamond.

Appendix A

Intermolecular C_{60} links

In this appendix we present the units considered in this work for the formation of intermolecular C_{60} connections. In the figures, the atoms involved in the intermolecular bonds are marked in red.

At the beginning of this work seven units were regarded. All of them involve two atoms per unit. They considered the cases where such two atoms are first or second neighbors. One additional case, where the atoms are third neighbors is also considered.

The units that are easily found in the literature are 65 and 66 units. The 65 represents the unit where the atoms form a single bond in the C_{60} molecule as is shown in the figure A.1. The name comes from the fact that a single bond has a hexagon on one side and a pentagon on the other side. 66 codename is assigned to the double bond case, and the name comes from the fact that a hexagon is found on each side. However, the term *double bond* could be better changed to *bond joining* pentagons from a geometrical rather than electronic point of view.

A bond of a C_{60} molecule could be broken when atoms forming it are involved in intermolecular connections. The units presented below are the same presented above but with broken bonds. The codename go from 65 to 65r and from 66 to 66r. The letter 'r' was originally assigned for the word *roto* is Spanish that means *broken*.

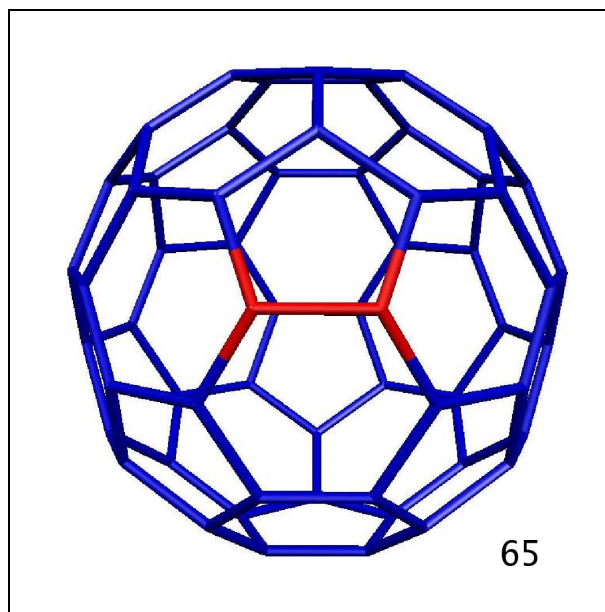


Figure A.1: 65 unit. The single bond in a C_{60} molecule shares a hexagon on one side and a pentagon on the other.

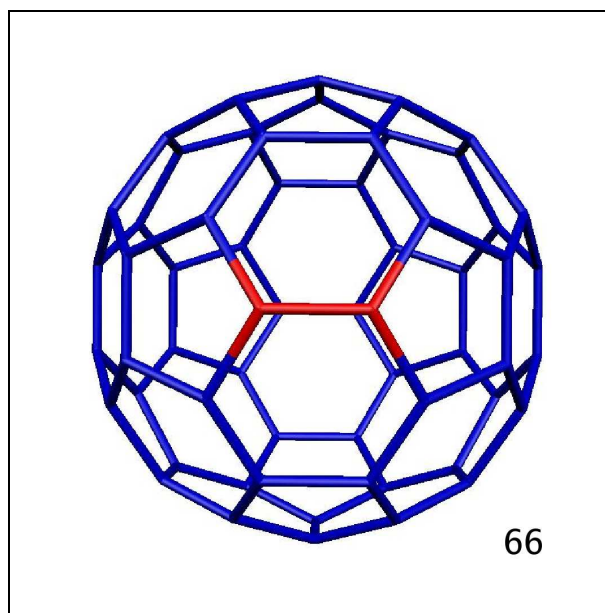


Figure A.2: 66 unit. The double bonds are shared only by hexagons.

However, in English it can be associated with the word *ripped*.

When the atoms involved in the connections are not first neighbors, the code-name is assigned in a way similar to that used for the cycloaddition names. First, one atom involved in the connection is chosen and it is marked with the number 1.

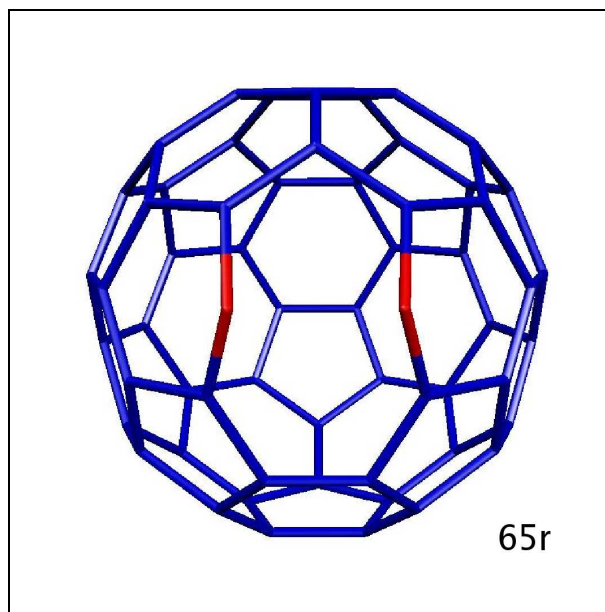


Figure A.3: 65r unit. The single bond has been broken.

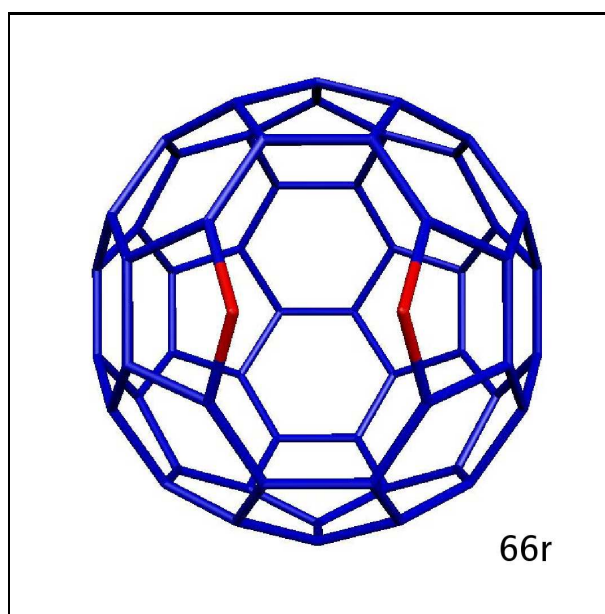


Figure A.4: 66r unit. The double bond has been broken.

Subsequently, the atoms are consecutively numbered until the other atom involved in the connection is reached. The counting must be done by the shorter side on the common ring (hexagon or pentagon). Finally, the unit is named using the numbers of the atoms involved in the intermolecular connection, and followed by one letter: 'p' if the common ring is a pentagon, or 'h' if it is an hexagon. The units 13h, 13p and 14h are depicted below.

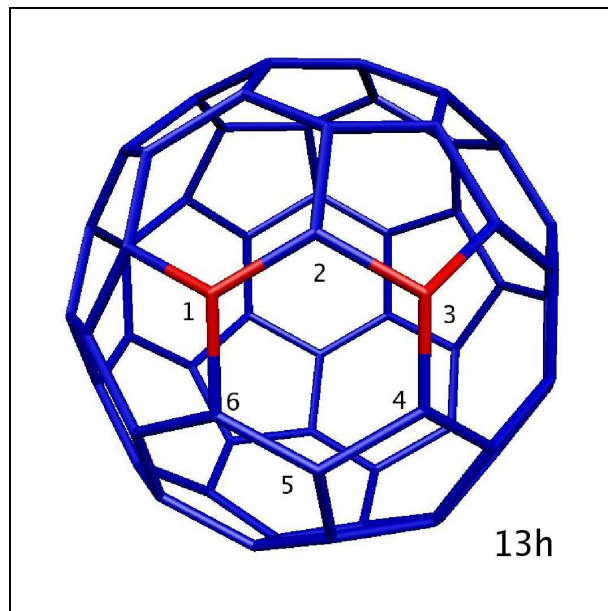


Figure A.5: 13h unit. The atoms involved in the connection are the number “1” and the number “3” within the hexagon.

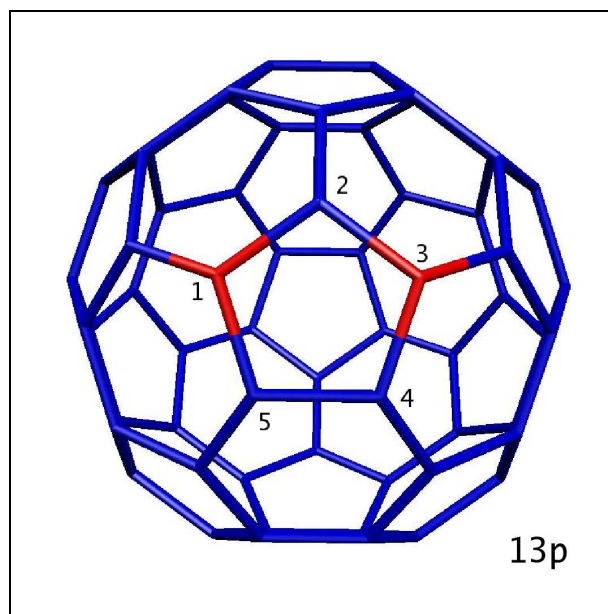


Figure A.6: 13p unit. The atoms involved in the link are the number “1” and the number “3” along the pentagon.

The intermolecular links result by combining the units presented. However, it can be seen from these figures that most of the units are not symmetric with respect

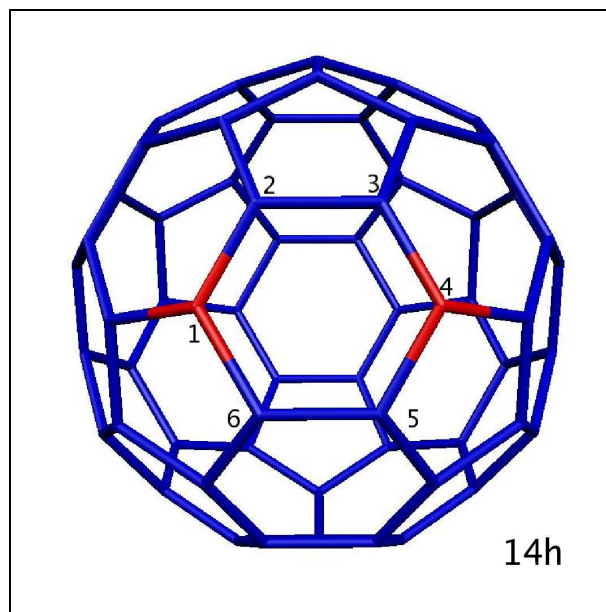


Figure A.7: 14h unit. The atoms involved in the connection are the number “1” and the number “4” along the hexagon.

to the plane; orthogonal to the page, indicated by red atoms. Therefore, most of the units can be combined in two different orientations, in such a way that different geometrical connections could be created using the same pair of units. In order to define names for the connections, we have defined an orientation for each unit as follows. The units are presented in the figures in such a way that the atoms in red are in a horizontal line. Then, following this orientation, all units have now a top and a bottom. The connections are named by joining the codename of the units involved followed by the number “2” if the units are at different orientations (top-bottom). If they are along the same orientation (top-top) no number is added. For an example, units 13h and 13p can form the 13h13p and the 13h13p2 connections. The connections are generated when using a 66 or a 66r unit do not required the number “2”, because these units are symmetric with respect to the plane involved.

This convention is able to provide names for most of the connections that have appeared in our simulations discussed in chapter 3. However, there is another asymmetry. The top of the 13h unit in the figure shows a hexagon on the left and a pentagon on the right. The situation would be different if the atoms in red were number “2” and number “4”. This asymmetry is only important in 13h13h-like

connections, because the other units has reflection symmetry respect to a vertical plane. In order to complete the convention, a letter 'b' is added if the pentagon of a C_{60} is closer to the pentagon of the other C_{60} ; a letter 'a' is added otherwise. Finally, an order is imposed to avoid connections with two names, like 13h13p and 13p13h. The order is: 13h, 13p, 14h, 65, 65r, 66, 66r. Thus, between 13h13p and 13p13h, the right name is 13h13p, because 13h comes first that 13p in the list.

Therefore, the 43 connections that could be formed are: 13h13ha, 13h13hb, 13h13h2a, 13h13h2b, 13h13p, 13h13p2, 13h14h, 13h14h2, 13h65, 13h652, 13h65r, 13h65r2, 13h66, 13h66r, 13p13p, 13p13p2, 13p14h, 13p14h2, 13p65, 13p652, 13p65r, 13p65r2, 13p66, 13p66r, 14h14h, 14h14h2, 14h65, 14h652, 14h65r, 14h65r2, 14h66, 14h66r, 6565, 65652, 6565r, 6565r2, 6566, 6566r, 65r65r, 65r65r2, 6566, 6566r and 6666. The last link is the well known [2+2] cycloaddition between double bonds.

Although at the beginning of this work, only connections considering two bonds were considered, our simulations also generated connections formed by three and four bonds. There are three connections with three intermolecular bonds. The code-names have been chosen for convenience. Two units 3link (see figure A.8) at the same orientation (top-top) form a 3link1 connection. Two units 3link at different orientation form a 3link2 connection. A connection formed by a 3link unit and a 3link "extra" unit (see figure A.9) is called 3link3 connection. It must be noted that this additional 3link unit has 3-symmetry. Connections formed by two units of 3link extra type were not found in our simulations. In addition, intermolecular connections formed using four intermolecular bonds were found in our simulations. A typical unit is shown in figure A.10. All the connections formed by units like this are called 4link connections (see Appendix B).

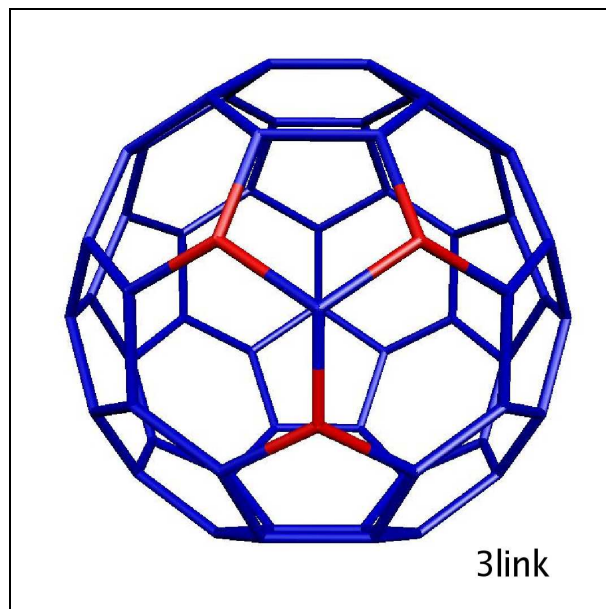


Figure A.8: 3link unit. The unit involves three atoms that are second neighbors with a common first neighbor.

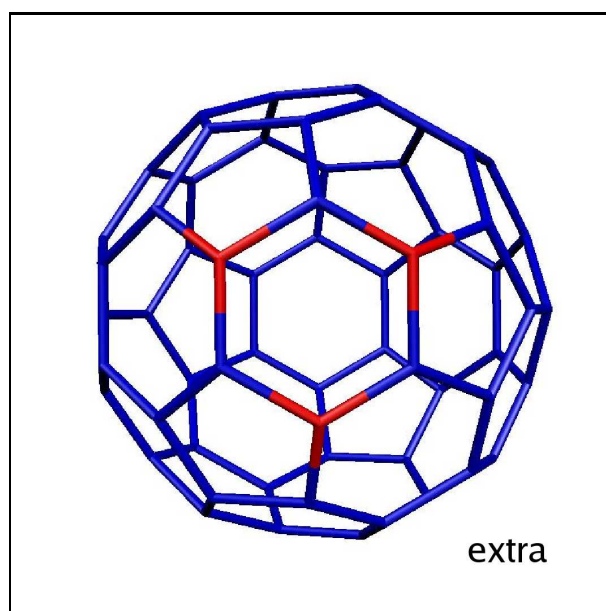


Figure A.9: 3link extra unit. This unit involves three atoms that are second neighbors and belong to the same hexagon.

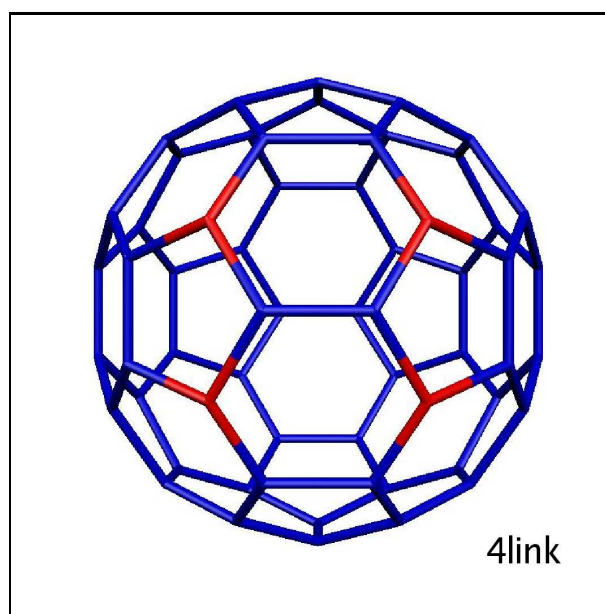


Figure A.10: 4link unit. The four first neighbors of two bonded atoms are involved in the intermolecular connection.

Appendix B

Tables of intermolecular connections appeared in our simulations for systems at high pressure and temperature

In this appendix, we summarize the number of times that different intermolecular connections have been observed in our 64 simulations described in chapter 3. The codes of the left column represent different intermolecular links. The structure can be understood by seeing appendix A. The pressure is indicated on the top left, as well as the temperature. In the tables, we present only the connections that appeared at least once, and we named them using the conventions explained in Appendix A. Some other connections appeared in our simulations, but they have not been considered here.

	600K	700K	800K	900K	1000K	1100K	1200K	1300K
13h13ha		1						
13h13hb								1
13h13h2a								
13h13h2b								
13h13p						1		2
13h13p2					1	1	1	
13h14h								
13h14h2								
13h65								
13h65r								
13h65r2								
13h66								
13p13p								
13p13p2					1	2		1
13p14h								
13p14h2								
13p65r2								
14h14h								
14h14h2								
65652						1		
6565r			1					1
6565r2								1
6566							1	
65r65r								
65r65r2								1
65r66								2
6666r								
3link1				1				
3link2								
3link3								
4link								

Table B.1: Intermolecular connections for the simulations performed under 2 GPa.

	600K	700K	800K	900K	1000K	1100K	1200K	1300K
13h13ha								
13h13hb								
13h13h2a						1		
13h13h2b						1		
13h13p					1		2	3
13h13p2			1		1	1	1	6
13h14h								
13h14h2								1
13h65								
13h65r							1	
13h65r2								
13h66								
13p13p							1	
13p13p2							1	1
13p14h								
13p14h2								
13p65r2								
14h14h								
14h14h2								1
65652								
6565r							2	1
6565r2							1	
6566								
65r65r								
65r65r2						1	1	
65r66								
6666r								
3link1								
3link2								
3link3								
4link								

Table B.2: Intermolecular connections for the simulations performed under 4 GPa.

	600K	700K	800K	900K	1000K	1100K	1200K	1300K
13h13ha					1			1
13h13hb							1	1
13h13h2a						1	1	3
13h13h2b					1	2	3	
13h13p							1	4
13h13p2				1	1		4	1
13h14h								
13h14h2								2
13h65								
13h65r							1	
13h65r2								1
13h66								
13p13p								
13p13p2			1	1		1		1
13p14h								
13p14h2								
13p65r2								
14h14h								
14h14h2								
65652								
6565r								1
6565r2								1
6566								
65r65r								
65r65r2								
65r66						1		
6666r								
3link1								
3link2								
3link3								
4link								

Table B.3: Intermolecular connections for the simulations performed under 6 GPa.

	600K	700K	800K	900K	1000K	1100K	1200K	1300K
13h13ha								1
13h13hb								
13h13h2a						1		
13h13h2b						2		1
13h13p		1		1	1	1		1
13h13p2				1	2	3	6	8
13h14h				1			1	1
13h14h2						1	1	2
13h65								1
13h65r								1
13h65r2								1
13h66								
13p13p							1	1
13p13p2					3		1	
13p14h								
13p14h2						1	1	
13p65r2								1
14h14h								
14h14h2								
65652								
6565r								
6565r2						1		
6566							1	
65r65r								
65r65r2								
65r66								
6666r								1
3link1								
3link2								
3link3							1	
4link								

Table B.4: Intermolecular connections for the simulations performed under 8 GPa.

	600K	700K	800K	900K	1000K	1100K	1200K	1300K
13h13ha							2	2
13h13hb			1		1	1		2
13h13h2a					1	2	1	2
13h13h2b							1	3
13h13p			1	1	2	4	3	2
13h13p2					2	1	7	10
13h14h						1	1	1
13h14h2					1		2	1
13h65								1
13h65r								
13h65r2								1
13h66								1
13p13p				1	2			1
13p13p2				1	1		1	
13p14h								
13p14h2								
13p65r2								
14h14h								1
14h14h2								
65652								
6565r								1
6565r2							1	
6566								
65r65r								
65r65r2								
65r66								1
6666r								
3link1						1		
3link2							1	2
3link3								1
4link					1			

Table B.5: Intermolecular connections for the simulations performed under 10 GPa.

	600K	700K	800K	900K	1000K	1100K	1200K	1300K
13h13ha				1	1	2	2	1
13h13hb			1			2		3
13h13h2a					1	3	3	1
13h13h2b						2	2	
13h13p					2	3	5	5
13h13p2		1	2	1	1	4	6	10
13h14h						1		2
13h14h2						1	1	
13h65								
13h65r								
13h65r2								
13h66							1	
13p13p						2	1	1
13p13p2				1	3	3	1	3
13p14h					1		1	
13p14h2							1	1
13p65r2								
14h14h								
14h14h2								
65652								
6565r				1				1
6565r2							1	
6566								
65r65r								
65r65r2								
65r66								
6666r								
3link1							1	
3link2								
3link3								
4link								

Table B.6: Intermolecular connections for the simulations performed under 12 GPa.

	600K	700K	800K	900K	1000K	1100K	1200K	1300K
13h13ha						1	1	1
13h13hb			1	1		1	2	3
13h13h2a			1		1			
13h13h2b			1	1	1	2	3	2
13h13p		1			1	2	5	3
13h13p2		1	2		4	4	8	9
13h14h						2	1	4
13h14h2		1			2		1	1
13h65								
13h65r							2	1
13h65r2							1	
13h66								
13p13p						1		
13p13p2	1					3	4	2
13p14h					1			1
13p14h2								2
13p65r2							1	1
14h14h								
14h14h2							1	
65652								
6565r	1							1
6565r2							1	1
6566								
65r65r								
65r65r2								
65r66							1	1
6666r								
3link1					1	1	2	1
3link2						1		3
3link3								
4link								

Table B.7: Intermolecular connections for the simulations performed under 14 GPa.

	600K	700K	800K	900K	1000K	1100K	1200K	1300K
13h13ha				1	2		1	2
13h13hb				1		2	1	1
13h13h2a					1	1	1	3
13h13h2b			1	1			5	2
13h13p			3	2	2	6	4	3
13h13p2			4	2	10	4		8
13h14h							5	2
13h14h2					1	1	1	4
13h65								
13h65r				1		1		2
13h65r2								1
13h66							1	2
13p13p				1		1	1	
13p13p2				1	4	1	4	4
13p14h						2	2	
13p14h2							1	
13p65r2						1		
14h14h								
14h14h2								3
65652								
6565r						2		
6565r2							1	1
6566								
65r65r							1	
65r65r2								
65r66						1		
6666r								
3link1								
3link2			1		1	1		
3link3							1	5
4link								1

Table B.8: Intermolecular connections for the simulations performed under 16 GPa.